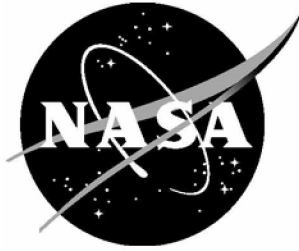


NASA/TP-2009-215956



# Comparison of Transport Codes, HZETRN, HETC and FLUKA, Using 1977 GCR Solar Minimum Spectra

*John H. Heinbockel and Tony C. Slaba  
Old Dominion University, Norfolk, Virginia*

*Ram K. Tripathi, Steve R. Blattnig, and John W. Norbury  
Langley Research Center, Hampton, Virginia*

*Francis F. Badavi  
Christopher Newport University, Newport News, Virginia*

*Lawrence W. Townsend and Thomas Handler  
University of Tennessee, Knoxville, Tennessee*

*Tony A. Gabriel  
Scientific Investigation and Development, Knoxville, Tennessee*

*Lawrence S. Pinsky and Brandon Reddell  
University of Houston, Houston, Texas*

*Aric R. Aumann  
Analytical Services and Materials, Inc., Hampton, Virginia*

---

December 2009

## NASA STI Program . . . in Profile

Since its founding, NASA has been dedicated to the advancement of aeronautics and space science. The NASA scientific and technical information (STI) program plays a key part in helping NASA maintain this important role.

The NASA STI program operates under the auspices of the Agency Chief Information Officer. It collects, organizes, provides for archiving, and disseminates NASA's STI. The NASA STI program provides access to the NASA Aeronautics and Space Database and its public interface, the NASA Technical Report Server, thus providing one of the largest collections of aeronautical and space science STI in the world. Results are published in both non-NASA channels and by NASA in the NASA STI Report Series, which includes the following report types:

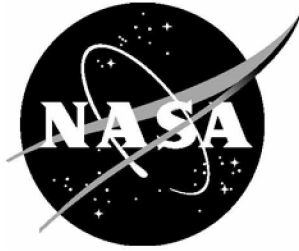
- **TECHNICAL PUBLICATION.** Reports of completed research or a major significant phase of research that present the results of NASA programs and include extensive data or theoretical analysis. Includes compilations of significant scientific and technical data and information deemed to be of continuing reference value. NASA counterpart of peer-reviewed formal professional papers, but having less stringent limitations on manuscript length and extent of graphic presentations.
- **TECHNICAL MEMORANDUM.** Scientific and technical findings that are preliminary or of specialized interest, e.g., quick release reports, working papers, and bibliographies that contain minimal annotation. Does not contain extensive analysis.
- **CONTRACTOR REPORT.** Scientific and technical findings by NASA-sponsored contractors and grantees.
- **CONFERENCE PUBLICATION.** Collected papers from scientific and technical conferences, symposia, seminars, or other meetings sponsored or co-sponsored by NASA.
- **SPECIAL PUBLICATION.** Scientific, technical, or historical information from NASA programs, projects, and missions, often concerned with subjects having substantial public interest.
- **TECHNICAL TRANSLATION.** English-language translations of foreign scientific and technical material pertinent to NASA's mission.

Specialized services also include creating custom thesauri, building customized databases, and organizing and publishing research results.

For more information about the NASA STI program, see the following:

- Access the NASA STI program home page at <http://www.sti.nasa.gov>
- E-mail your question via the Internet to [help@sti.nasa.gov](mailto:help@sti.nasa.gov)
- Fax your question to the NASA STI Help Desk at 443-757-5803
- Phone the NASA STI Help Desk at 443-757-5802
- Write to:  
NASA STI Help Desk  
NASA Center for AeroSpace Information  
7115 Standard Drive  
Hanover, MD 21076-1320

NASA/TP-2009-215956



# Comparison of Transport Codes, HZETRN, HETC and FLUKA, Using 1977 GCR Solar Minimum Spectra

*John H. Heinbockel and Tony C. Slaba  
Old Dominion University, Norfolk, Virginia*

*Ram K. Tripathi, Steve R. Blattnig, and John W. Norbury  
Langley Research Center, Hampton, Virginia*

*Francis F. Badavi  
Christopher Newport University, Newport News, Virginia*

*Lawrence W. Townsend and Thomas Handler  
University of Tennessee, Knoxville, Tennessee*

*Tony A. Gabriel  
Scientific Investigation and Development, Knoxville, Tennessee*

*Lawrence S. Pinsky and Brandon Reddell  
University of Houston, Houston, Texas*

*Aric R. Aumann  
Analytical Services and Materials, Inc., Hampton, Virginia*

National Aeronautics and  
Space Administration

Langley Research Center  
Hampton, Virginia 23681-2199

December 2009

## **Acknowledgments**

This work was supported, in part, by NASA grant NNL06AA14A. The HETC - HEDS data were obtained under NASA contract NNL07AA36C. The FLUKA data were obtained under NASA contract NNL07AA18C.

Available from:

NASA Center for AeroSpace Information  
7115 Standard Drive  
Hanover, MD 21076-1320  
443-757-5802

# Contents

<b>1</b>	<b>Introduction</b>	<b>1</b>
<b>2</b>	<b>Monte Carlo codes</b>	<b>3</b>
2.1	HETC - HEDS . . . . .	3
2.2	FLUKA . . . . .	4
<b>3</b>	<b>Analysis of dose and dose equivalent curves</b>	<b>5</b>
3.1	FLUKA calculation of dose and dose equivalent . . . . .	6
3.1.1	Method 1 . . . . .	6
3.1.2	Method 2 . . . . .	7
3.1.3	Method 3 . . . . .	7
3.2	HETC - HEDS calculation of dose and dose equivalent . . . . .	7
3.3	HZETRN calculation of dose and dose equivalent . . . . .	8
<b>4</b>	<b>Comments on dose and dose equivalent</b>	<b>9</b>
<b>5</b>	<b>Flux calculations</b>	<b>9</b>
<b>6</b>	<b>Additional graphs</b>	<b>10</b>
<b>7</b>	<b>Conclusions</b>	<b>11</b>

## List of Figures

1	Computational Geometry. The prominent GCR incident ions are H, He, C, O, Mg, Si and Fe. . . . .	18
2	Boundary Conditions for Aluminum shield. . . . .	18
3	Dose (upper panel) and Dose Equivalent (lower panel) versus Depth in Water for Hydrogen on Aluminum shield. . . . .	19
4	Same as Figure 3, except for Helium. . . . .	20
5	Same as Figure 3, except for Carbon. . . . .	21
6	Same as Figure 3, except for Oxygen. . . . .	22
7	Same as Figure 3, except for Magnesium. . . . .	23
8	Same as Figure 3, except for Silicon. . . . .	24
9	Same as Figure 3, except for Iron. . . . .	25
10	Quality factor versus LET. . . . .	26
11	Forward Neutron flux for Hydrogen on Aluminum shield. . . . .	27
12	Backward Neutron flux for Hydrogen on Aluminum shield. . . . .	28
13	Total Neutron flux for Hydrogen on Aluminum shield. . . . .	29
14	Proton flux for Hydrogen on Aluminum shield. . . . .	30
15	$^2\text{H}$ flux for Hydrogen on Aluminum shield. . . . .	31
16	Forward Neutron flux for Helium on Aluminum shield. . . . .	32
17	Backward Neutron flux for Helium on Aluminum shield. . . . .	33
18	Total Neutron flux for Helium on Aluminum shield. . . . .	34
19	Proton flux for Helium on Aluminum shield. . . . .	35
20	$^2\text{H}$ flux for Helium on Aluminum shield. . . . .	36
21	$^4\text{He}$ flux for Helium on Aluminum shield. . . . .	37
22	Forward Neutron flux for Carbon on Aluminum shield. . . . .	38
23	Backward Neutron flux for Carbon on Aluminum shield. . . . .	39
24	Total Neutron flux for Carbon on Aluminum shield. . . . .	40
25	Proton flux for Carbon on Aluminum shield. . . . .	41
26	$^2\text{H}$ flux for Carbon on Aluminum shield. . . . .	42
27	$^3\text{H}$ flux for Carbon on Aluminum shield. . . . .	43
28	$^3\text{He}$ flux for Carbon on Aluminum shield. . . . .	44
29	$^4\text{He}$ flux for Carbon on Aluminum shield. . . . .	45
30	Forward Neutron flux for Oxygen on Aluminum shield. . . . .	46
31	Backward Neutron flux for Oxygen on Aluminum shield. . . . .	47
32	Total Neutron flux for Oxygen on Aluminum shield. . . . .	48
33	Proton flux for Oxygen on Aluminum shield. . . . .	49
34	$^2\text{H}$ flux for Oxygen on Aluminum shield. . . . .	50
35	$^3\text{H}$ flux for Oxygen on Aluminum shield. . . . .	51
36	$^3\text{He}$ flux for Oxygen on Aluminum shield. . . . .	52
37	$^4\text{He}$ flux for Oxygen on Aluminum shield. . . . .	53

38	Forward Neutron flux for Magnesium on Aluminum shield. . . . .	54
39	Backward Neutron flux for Magnesium on Aluminum shield. . . . .	55
40	Total Neutron flux for Magnesium on Aluminum shield. . . . .	56
41	Proton flux for Magnesium on Aluminum shield. . . . .	57
42	$^2\text{H}$ flux for Magnesium on Aluminum shield. . . . .	58
43	$^3\text{H}$ flux for Magnesium on Aluminum shield. . . . .	59
44	$^3\text{He}$ flux for Magnesium on Aluminum shield. . . . .	60
45	$^4\text{He}$ flux for Magnesium on Aluminum shield. . . . .	61
46	Forward Neutron flux for Silicon on Aluminum shield. . . . .	62
47	Backward Neutron flux for Silicon on Aluminum shield. . . . .	63
48	Total Neutron flux for Silicon on Aluminum shield. . . . .	64
49	Proton flux for Silicon on Aluminum shield. . . . .	65
50	$^2\text{H}$ flux for Silicon on Aluminum shield. . . . .	66
51	$^3\text{H}$ flux for Silicon on Aluminum shield. . . . .	67
52	$^3\text{He}$ flux for Silicon on Aluminum shield. . . . .	68
53	$^4\text{He}$ flux for Silicon on Aluminum shield. . . . .	69
54	Forward Neutron flux for Iron on Aluminum shield. . . . .	70
55	Backward Neutron flux for Iron on Aluminum shield. . . . .	71
56	Total Neutron flux for Iron on Aluminum shield. . . . .	72
57	Proton flux for Iron on Aluminum shield. . . . .	73
58	$^2\text{H}$ flux for Iron on Aluminum shield. . . . .	74
59	$^3\text{H}$ flux for Iron on Aluminum shield. . . . .	75
60	$^3\text{He}$ flux for Iron on Aluminum shield. . . . .	76
61	$^4\text{He}$ flux for Iron on Aluminum shield. . . . .	77
62	Magnified View of Figure 18 for $30\text{ g/cm}^2$ depth in water. . . . .	78
63	Magnified View of Figure 20 for $30\text{ g/cm}^2$ depth in water. . . . .	78
64	Magnified View of Figure 56 for $0\text{ g/cm}^2$ depth in water. . . . .	79
65	Magnified View of Figure 60 for $30\text{ g/cm}^2$ depth in water. . . . .	79
66	Heavy ion flux associated with Carbon on Aluminum shield. . . . .	80
67	Heavy ion flux associated with Oxygen on Aluminum shield. . . . .	81
68	Heavy ion flux associated with Magnesium on Aluminum shield. . . . .	82
69	Heavy ion flux associated with Iron on Aluminum shield. . . . .	83

## List of Tables

1	Dose rate (Gy/day) RMS differences between codes. . . . .	6
2	Dose Equivalent rate (Sv/day) RMS differences between codes. . . . .	6
3	$F$ values and quantitative comparison of flux graphs. Abbreviations are as follows: forward neutron (f - n), backward neutron (b - n), total neutron (t - n), proton (p). The decimal number after the figure number refers to the value of the water depth in g/cm <sup>2</sup> . For example, 11.0 refers to Figure 11 at a water depth of 0 g/cm <sup>2</sup> , which is the upper left panel of Figure 11.	12
4	Table 3 continued. . . . .	13
5	Average $F$ values. . . . .	14
6	$F$ values heavy ions . . . . .	14

## Nomenclature

g	Unit of gram.
kg	Unit of kilogram ( $10^3$ g).
mg	Unit of milligram ( $10^{-3}$ g).
m	Unit of meter.
$\mu$	Unit of micro meter or micron ( $10^{-6}$ m).
J	Unit of Joule.
eV	Unit of electron volt.
keV	Unit of kilo electron volt ( $10^3$ eV).
MeV	Unit of mega electron volt ( $10^6$ eV).
$E$	Kinetic energy. Units of J or MeV.
Energy	The word energy always refers to <i>kinetic</i> energy.
Gy	Unit of Gray $\equiv$ J/kg.
Sv	Unit of Sievert.
$D$	Dose. Units of Gy.
KERMA	Kinetic Energy Released per unit MAAss (or in MAterial). Units of Gy.
$H$	Dose Equivalent. Units of Sv.
$L$	Linear Energy Transfer (LET). Units of keV/ $\mu$ .
$Q(L)$	Quality factor as a function of LET.
RBE	Relative Biological Effectiveness.
SPE	Solar Particle Event.
GCR	Galactic Cosmic Ray.
FLUKA	FLUctuating KAskade.
HETC - HEDS	High Energy Transport Code - Human Exploration and Development of Space.
HETC	In the present paper, the term HETC always means HETC - HEDS.
HZETRN	High charge ( $Z$ ) and Energy TRaNsport.
LEO	Low Earth Orbit.

## Abstract

*The HZETRN deterministic radiation transport code is one of several tools developed to analyze the effects of harmful galactic cosmic rays (GCR) and solar particle events (SPE) on mission planning, astronaut shielding and instrumentation. This paper is a comparison study involving the two Monte Carlo transport codes, HETC - HEDS and FLUKA, and the deterministic transport code, HZETRN. Each code is used to transport ions from the 1977 solar minimum GCR spectrum impinging upon a 20 g/cm<sup>2</sup> Aluminum slab followed by a 30 g/cm<sup>2</sup> water slab. This research is part of a systematic effort of verification and validation to quantify the accuracy of HZETRN and determine areas where it can be improved. Comparisons of dose and dose equivalent values at various depths in the water slab are presented in this report. This is followed by a comparison of the proton fluxes, and the forward, backward and total neutron fluxes at various depths in the water slab. Comparisons of the secondary light ion <sup>2</sup>H, <sup>3</sup>H, <sup>3</sup>He and <sup>4</sup>He fluxes are also examined.*

## 1 Introduction

As part of the NASA strategic plan for the human exploration of space and the desire to provide radiation protection for both astronauts and instrumentation, there is ongoing development, testing, verification and validation of the deterministic radiation transport code HZETRN (High charge (Z) and Energy TRaNsport), which was developed at Langley Research Center over the last twenty - five years by Wilson and co - workers [1]. The present paper, which focuses on galactic cosmic rays (GCR), is an extension of reference [2], which involved a verification of HZETRN for solar particle events (SPE).

HZETRN is a deterministic computer code which has been used for radiation analysis under a variety of shielding conditions in analyzing solar particle events, galactic cosmic rays, and low earth orbit (LEO) trapped proton environments. While the code has endured several rounds of verification and validation in these environments [1, 3, 4], most of the comparisons have focused on integrated quantities, such as dose (D) or dose equivalent (H), and individual ion fluences were not examined in detail. Though dose or dose equivalent were generally viewed as sufficient tests for evaluating code accuracy, recent interest in fluence based approaches to radiation risk assessment demand a higher degree of accuracy [5]. This, along with recent improvements to some of the underlying transport models and numerical procedures within HZETRN [6, 7], provides an opportunity for another round of verification and validation benchmarks.

In this paper, the 1977 solar minimum GCR spectrum is used to compare HZETRN to the Monte Carlo codes HETC - HEDS (High Energy Transport Code - Human Exploration and Development of Space) [8, 9] and FLUKA (FLUctuating KAskade) [10, 11]. Models

of the free space GCR environment developed in the past two decades have provided the most realistic description of the interaction of incoming GCR from outside the heliosphere with solar activity. For the 1977 GCR minimum, the model of reference [12], was used as GCR input into the HZETRN, HETC and FLUKA code systems. This GCR model is based on fitting the existing balloon and satellite measured differential energy spectra from 1954 - 1992 to the stationary Fokker - Planck equation to estimate the appropriate diffusion coefficient. The implementation of this model accurately accounts for the solar modulation of hydrogen through nickel (H - Ni) by propagating the local interplanetary spectrum of each element through the heliosphere. This is accomplished by numerically solving the Fokker - Planck diffusion, convection and energy loss boundary value problem. The model provides a single value of the deceleration parameter,  $\phi(t)$ , describing the level of solar cycle modulation and determines the GCR differential energy spectra for all of the elements at a given radial distance from the sun.

The benchmark problems solved by the three computer codes consist of a 20 g/cm<sup>2</sup> slab of Aluminum shield followed by a 30 g/cm<sup>2</sup> water slab target when exposed to selected ions from the 1977 solar minimum GCR spectrum. The thickness of the Aluminum slab is representative of some spacecraft thicknesses, and the water slab thickness of 30 g/cm<sup>2</sup> was selected because thicknesses between 0 and 30 g/cm<sup>2</sup> can be used, with appropriate interpolation methods, to determine body organ exposures. Due to their prominence in the GCR spectrum, the fluxes associated with Hydrogen, Helium, Oxygen, Carbon, Magnesium, Silicon and Iron were selected as individual boundary conditions to the Aluminum slab.

The computational geometry is illustrated in Figure 1. Figure 2 illustrates the magnitude of the flux boundary terms from the 1977 solar minimum GCR spectrum associated with the various ions of interest. In this study, each code is used to calculate specific radiation quantities at various depths in the water slab. In particular, each code provided the dose rate (cGy/day) and dose equivalent rate (cSv/day) at various depths in the water slab. Here, dose is the mean energy imparted (absorbed) per unit mass, and dose equivalent is a measure of biological effectiveness. This is followed by a comparison of the proton and forward, backward and total neutron fluxes. Comparison graphs for light ion flux calculations associated with <sup>2</sup>H, <sup>3</sup>H, <sup>3</sup>He and <sup>4</sup>He ions are examined. Also included are comparison graphs of selected fluxes associated with heavy ion production.

The benefits of improving HZETRN, when two approaches (HETC, FLUKA) already exist, is that HZETRN is able to run much faster than these other Monte Carlo codes. Therefore, HZETRN is superior in terms of engineering and other trade studies. A description of HZETRN, plus the recent improvements involving neutron and light ion transport, has been fully discussed in reference [2] and will not be repeated here. These recent improvements to HZETRN are used extensively in the present work.

## 2 Monte Carlo codes

The term Monte Carlo, is used to describe a random walk algorithm that simulates an event and then performs a statistical analysis of the results. Monte Carlo techniques are typically constructed whenever there is a high dimensional integral equation that cannot be solved either analytically or numerically with deterministic methods. To reduce the computing time involved in Monte Carlo techniques, variance reduction is often employed. A general description of Monte Carlo methods can be found in reference [13].

In this paper, results from the two Monte Carlo codes, HETC - HEDS [8, 9] and FLUKA [10, 11], are used to compare with the results calculated by the deterministic code HZETRN. The following is a brief description of HETC - HEDS and FLUKA codes used in this comparison study.

### 2.1 HETC - HEDS

The HETC - HEDS computer code is a Monte Carlo based solution method designed specifically for solving space radiation problems [8, 9] associated with secondary particle fields produced by space radiation interacting with shielding and equipment. It is a three dimensional generalized radiation transport code capable of handling and analyzing radiation fields which affect critical body organs of astronauts such as bone marrow and the central nervous system. HETC - HEDS can be applied to a wide range of particle species and energies. It contains a heavy ion collision event generator capable of tracking nuclear interactions and performing statistical analysis of the data. It simulates particle interactions by using a pseudo random number generator, along with the appropriate physics, to follow trajectories of primary particles and all secondary particles involved in the nuclear collision of galactic cosmic rays and solar event particles interacting with shielding material, biological organisms and electronic equipment. The geometry input is simple combinatorial volumes. The cross sections are generated internally, as part of the software. The HETC - HEDS computer code employs all particles of interest for space radiation. In particular, HETC - HEDS considers interactions of protons, neutrons,  $\pi^+$ ,  $\pi^-$ ,  $\mu^+$ ,  $\mu^-$ , light ions and heavy ions. These particles can be arbitrarily assigned position, angle and energy throughout a spatial boundary. This Monte Carlo code follows each particle in a cascade until it undergoes a nuclear collision, absorption, decay or escape from the spatial boundary, or is eliminated by crossing a domain variable cutoff. The nuclear reactions and processes are accounted for by using appropriate physical models to handle such things as energy loss, range straggling, Coulomb scattering, etc. Both elastic and nonelastic collisions are considered using energy and nucleon conservation principles. A user written part of the code generates a source which allows for a simple form of biasing. This Monte Carlo package has no capability to determine when the solution method has converged on the answer sought within some confidence interval. It does provide the means for predicting the interaction product yields, production angles

and energies using nuclear models for transport processes. It has been extensively used for code verification, benchmarking and testing against available laboratory beam data associated with energetic heavy ions.

## 2.2 FLUKA

The FLUKA computer code is a general purpose Monte Carlo computer program used for calculating particle transport and interaction with various materials. It has the ability to transport and interact all elementary hadrons, light and heavy ions, and electrons and photons over an energy range which extends up to  $10^4$  TeV for all particles, and down to thermal energies for neutrons [11]. The code has built-in capabilities for scoring particle fluences, yields, and energy deposition over arbitrary three dimensional meshes, both on an event - by - event basis or averaged over a large number of histories. This code has been extensively benchmarked against available accelerator and cosmic ray experimental data, at beam energies as low as a few MeV and as large as cosmic ray energies.

The code has special add - on modules for the generation of GCR spectra. The spectra are based on a blend of a model originally developed at NASA and extensions and modifications aimed at achieving the best fit of the most recent available experimental data, in particular those of the AMS (Alpha Magnetic Spectrometer) and BESS (Balloon - borne Experiment with a Superconducting Spectrometer) experiments. These spectra can be modulated within FLUKA according to an arbitrary solar activity modulation parameter, or for dates in the past, using the actual solar activity as measured by ground based neutron counters. Three different Earth magnetic field descriptions of increasing complexity can be used. Geomagnetic cut - offs can be input or calculated. Spectra representative of some of the largest solar particle events are also built into the code.

In addition to galactic cosmic rays and solar particle events, this code has a wide range of particle physics application areas where it can be employed. It has been demonstrated that the code can accurately simulate nuclear interactions and events with great accuracy in several fields, including particle physics, dosimetry, accelerator driven nuclear systems, detector characterization, aircraft crew dosimetry, shielding, and hadron therapy. The code can simulate interactions involving over sixty different particle types and can handle complex geometries. The geometry input has two levels: the basic one, consisting of combinatorial volumes, and a second level, the so called "lattice" level, which allows repetition and arbitrary spatial placement of the complex object defined at the first level. It also allows for a voxel (a volume element, representing a value on a regular grid in three dimensional space) input stream which can be combined with a standard combinatorial geometry input, allowing, for example, to embed a detailed voxel description of a human being, such as derived from a computed tomography (CT) scan, within an arbitrary spacecraft shape. The code can account for magnetic fields of arbitrary complexity. The nuclear models and associated cross sections are hard - coded into the software for all particles and energies, with the exception of neutrons below 20 MeV, where a 260

neutron group library obtained from standard international evaluated data files is used. The FLUKA computer code contains many variance reduction algorithms and covers all particles of interest for space radiation research. For most applications, the FLUKA package requires no additional programming. The code provides a large variety of statistical techniques for analyzing nuclear interactions, and it can handle only one source particle type at a time without writing a special subroutine to perform many particle GCR, SPE, and LEO sources. The code can be used in either a biased or unbiased mode. The offline analysis tools provided with the code enable one to perform simple statistical analysis of the results.

The code comes with a powerful Graphical User Interface, FLAIR, which allows an easy setup of the input stream and the geometry. It also provides user friendly tools for running the code and analyzing and plotting the results.

### 3 Analysis of dose and dose equivalent curves

Dose and dose equivalent values for various depths in the water slab are presented in Figures 3 - 9. These curves show some large differences in the dose and dose equivalent calculations generated by the three transport codes. For a quantitative assessment of the dose and dose equivalent curves, we select a root mean square (RMS) analysis of the data. The root mean square between data sets  $\{Y_i\}$  and  $\{y_i\}$  for  $i = 1, \dots, N$  is given by

$$\text{RMS} = \sqrt{\frac{\sum_{i=1}^N (Y_i - y_i)^2}{N}} \quad (1)$$

where  $N$  is the number of ordinates in the data sets with the abscissa values being the same for each set. A RMS comparison between the HZETRN, FLUKA, and HETC - HEDS data sets for dose are presented in Table 1. A similar root mean square difference calculation is performed on the dose equivalent data set, resulting in the values given in Table 2.

One reason for the discrepancies in the values obtained for the dose and dose equivalent curves is due to the different ways that they are calculated by the three codes. Another reason for differences is due to differences in the physics models used for cross section calculations. Another difference is due to different quality factors that are being used in the calculations for dose equivalent. The major differences in the dose and dose equivalent calculations at various depths in the water slab by the three codes can be better understood by an examination of the methods used for calculation of the dose and dose equivalent values. Note that the following description of dose and dose equivalent calculations, employed by the three computer codes also applies to the previous comparison study [2].

Table 1: Dose rate (Gy/day) RMS differences between codes.

Element	HZETRN, HETC	HZETRN, FLUKA	HETC, FLUKA
H (Figure 3)	0.0115	0.0119	0.0026
He (Figure 4)	0.0003	0.0088	0.0089
C (Figure 5)	0.0003	0.0002	0.0002
O (Figure 6)	0.0003	0.0002	0.0003
Mg (Figure 7)	0.0001	0.0022	0.0020
Si (Figure 8)	0.0001	0.0002	0.0001
Fe (Figure 9)	0.0001	0.0004	0.0003

Table 2: Dose Equivalent rate (Sv/day) RMS differences between codes.

Element	HZETRN, HETC	HZETRN, FLUKA	HETC, FLUKA
H (Figure 3)	0.0112	0.0124	0.0212
He (Figure 4)	0.0049	0.0155	0.0112
C (Figure 5)	0.0010	0.0009	0.0019
O (Figure 6)	0.0011	0.0020	0.0030
Mg (Figure 7)	0.0003	0.0121	0.0119
Si (Figure 8)	0.0001	0.0009	0.0010
Fe (Figure 9)	0.0005	0.0037	0.0043

### 3.1 FLUKA calculation of dose and dose equivalent

FLUKA calculates the dose by scoring energy deposition events by all transported particles in a given volume and dividing by the mass. The dose equivalent is not a physical quantity, and consequently its calculation can be done in several ways. The FLUKA code does not compute dose equivalent directly. The three ways that dose equivalent related quantities are estimated by FLUKA are now described. The FLUKA dose and dose equivalent calculations in this paper were calculated using method 3 below.

#### 3.1.1 Method 1

FLUKA calculates ambient dose equivalent by folding particle fluences (in volumes or on a surface) with appropriate fluence - to - dose conversion coefficients [14, 15]. When fluences on a surface are used, they must be properly computed by counting the particles crossing the surface weighted by unity divided by the cosine of the incident angle.

### 3.1.2 Method 2

This method involves the use of KERMA factors as defined by NCRP [16]. KERMA is a acronym for Kinetic Energy Released per unit MAAss or Kinetic Energy Released in MAterial. Therefore KERMA is similar to Dose and has the same units of Gray (Gy). A KERMA factor represents the ratio of the summation of the initial kinetic energies of all the charged particles which are liberated by uncharged particles, per unit mass of specified material. KERMA can be calculated for any specified material, at a point in free space, or at a point in an absorbing medium. Calculation of dose equivalent involves the weighting of each energy deposition event by a proper quality factor, defined by  $Q(L)$ , given by the ICRP60 curve [17]. FLUKA has technical issues implementing this weighting with neutrons below 20 MeV where average KERMA, rather than recoiled spectra, is usually employed. A special treatment for this type of calculation has been devised and is suitable, but it is limited to dose equivalent calculations as defined by ICRP 60 [17] and must be implemented in a user routine.

### 3.1.3 Method 3

This method uses the weighting of charged particle fluences, in a volume or on a surface, by the quality factor corresponding to their linear energy transfer (LET). This approach again gives the ICRP 60 kind of dose equivalent [17], because the code has estimators for the LET spectra. However, this method implicitly neglects the neutron and partial photon contributions, since neutron recoils below 20 MeV are not explicitly generated (apart from recoil protons on H). Note also that recoils are often so low in energy as to be either below transport cut off or, given the short range, are hard to sample in a statistically meaningful way. Again, it is mandatory for a correct fluence estimation at surfaces to use inverse cosine weighted scoring. The FLUKA dose and dose equivalent calculations in this paper were calculated using this method.

## 3.2 HETC - HEDS calculation of dose and dose equivalent

The computer code HETC - HEDS employs other codes such as MORSE [18], EGS [19] and MCNP [20]. The histories generated by HETC - HEDS are stored in output files. Transport of neutrons below 20 MeV and electrons is not carried out by HETC - HEDS. Instead, the output file of neutrons having energies of 20 MeV and below is fed as input into MORSE or MCNP to be transported by those codes. Electrons and photons from the HETC - HEDS output file are fed into EGS for transport. All primary and secondary charged particles, except electrons, are transported by HETC - HEDS and have their histories contained in the HETC - HEDS output file. The energy depositions from HETC - HEDS and EGS are straightforward. They are calculated by examining the energy of the particle at one position and then at another, usually defined by boundary

crossings, collisions, or end of range. The energy deposited is then the difference in the energies at the two sites. This is a standard Monte Carlo approach. Since the particle type and energy are known, the LET quality factor  $Q$ , [17], can be applied to convert from Gray to Sievert. For the low energy ( $< 20$  MeV) neutrons, the flux is calculated as follows. The flux - to - energy deposited KERMA factors are integrated with the flux to obtain Gray. The neutron energy dependent quality factors are used with the KERMA factors to convert the Gray to Sievert. The KERMA factors used by HETC are those for water. For the proton source data, where the neutron dose is important, the outdated neutron energy dependent quality factors were used instead of the most recent ones, which is another source of error for the differences in dose equivalent. For the heavy ion data, the low energy neutron doses are of less importance. It should be noted that new Sievert data, using the more recent quality factors, was provided for the solar flare results [2], and the revised data compared favorably with other calculations.

### 3.3 HZETRN calculation of dose and dose equivalent

In HZETRN, absorbed dose  $D$ , due to energy deposition at a given location  $x$  by all particles, is calculated according to

$$D(x) = \sum_j \int_0^\infty S_j(E) \phi_j(x, E) dE \quad (2)$$

where  $\phi_j(x, E)$  is the fluence or flux of type  $j$  ion at depth  $x$  with kinetic energy  $E$ , and  $S_j(E)$  is the stopping power of type  $j$  ion with energy  $E$ .

For human tissue exposure estimation, HZETRN calculates the dose equivalent  $H$  in terms of the product of dose  $D$  and quality factor  $Q$ , where the ICRP 60 quality factors [17] are based upon cancer risks. These factors relate the biological damage incurred from any ionizing radiation to the damage produced by the reference soft X - ray exposure. By definition,  $Q$  is a function of LET of the radiation field, which depends on both the ion type and its energy. The exact functional form of  $Q$  is prescribed in the process of setting radiation guidelines as defined by the ICRP publication 60 [17], and expressed below; hence,  $Q$  is a legislated quantity rather than the result of a particular measurement. However, the dependence of  $Q(L)$  on the value  $L \equiv \text{LET}$ , is intended to reflect a judgment related to the dependence of relative biological effectiveness (RBE) on LET at the anticipated level of exposure. In calculation of the dose equivalent, the HZETRN code uses the linear energy transfer quality factor  $Q(L)$ , as defined in reference [17]

$$Q(L) = \begin{cases} 1, & L < 10 \text{ keV}/\mu\text{m} \\ 0.32L - 2.2, & 10 \leq L \leq 100 \text{ keV}/\mu\text{m} \\ 300/\sqrt{L}, & L > 100 \text{ keV}/\mu\text{m} \end{cases} \quad (3)$$

The graph of  $Q(L)$ , is illustrated in Figure 10. Note the difference in the quality factors for the ICRP 60 [17] and ICRP 26 [21] in the region  $10 \leq L \leq 1000 \text{ keV}/\mu\text{m}$ , where the ICRP 26 values are given by [21]

$$Q(L) = \begin{cases} 1, & L \leq 1 \text{ keV}/\mu\text{m} \\ 13.7 \log(1 + L/466), & 1 < L < 20 \text{ keV}/\mu\text{m} \\ 20, & L \geq 20 \text{ keV}/\mu\text{m} \end{cases} \quad (4)$$

The value of dose equivalent is computed at a given location  $x$  from all particles present according to the relation

$$H(x) = \sum_j \int_0^\infty Q_j(E) S_j(E) \phi_j(x, E) dE \quad (5)$$

## 4 Comments on dose and dose equivalent

The HZETRN, FLUKA and HETC - HEDS transport codes use different ICRP standards for calculating dose and dose equivalent as illustrated in Figure 10 [13, 16, 22]. HZETRN does not transport certain particles such as pions, muons, positrons, electrons or photons. These particles are used in calculating dose and dose equivalent by both HETC - HEDS and FLUKA. The contribution of these particles to dose and dose equivalent values can be significant. For low energy neutrons, the HETC - HEDS code uses the NCRP 132 and 142 [16, 22], conversion factors in combination with the DABL69 KERMA factors [23]. The HZETRN code does not use KERMA factors in the calculation of dose and dose equivalent. HZETRN transports light target fragments explicitly, so all of the neutron dose and dose equivalent is coming from target fragmentations and recoils with charge greater than 2. HZETRN uses a parameterization to do this. (No documentation exists for this parameterization. Future work must correct this.) Also, note that the FLUKA code neglects the contribution from low energy ( $< 20 \text{ MeV}$ ) neutrons altogether. The number and type of particles used and the algorithms employed by the three codes for calculating the dose and dose equivalent values are the probable causes for the differences in the dose and dose equivalent curves [13, 16, 22, 23].

## 5 Flux calculations

A quantitative measure of “goodness of fit” for each of the flux comparison curves found in Figures 11 - 65 is constructed for comparison purposes. At any fixed energy value where the flux values from HZETRN, HETC - HEDS, and FLUKA are well defined, one can calculate the absolute value of the percent errors between HZETRN and HETC - HEDS, as well as the absolute percent error between HZETRN and FLUKA. These two

percent error absolute values are then added to get a sum of the percent errors at the selected energy value. We define this as the percent error norm at the selected energy value  $E$ , and use the notation  $\| E \|_{\%}$  to denote this sum of errors at energy  $E$ . Each of Figures 11 - 61 is examined and for each set of curves, three energy values are selected. The first energy value  $E_1$  is selected in the range  $1 \leq E_1 \leq 10$  MeV, the second energy value  $E_2$  is selected in the range  $10 < E_2 \leq 100$  MeV, and the third energy value  $E_3$  is selected in the range  $E_3 > 100$  MeV. The values  $\{E_1, E_2, E_3\}$  are selected to maximize

$$F = \text{Int} \left[ \frac{1}{6} (\| E_1 \|_{\%} + \| E_2 \|_{\%} + \| E_3 \|_{\%}) \right] \quad (6)$$

where the integer calculated for  $F$  can be interpreted as a weighted average worst case percent error value assigned to a set of graphs. These  $F$  value error calculations are summarized in Tables 3 - 4. The blank portions in Tables 3 - 4 indicate that flux calculations were not provided for comparisons by either HETC - HEDS or FLUKA.

Compare the  $F$  values in Tables 3 - 4 with an examination of the set of curves in the corresponding figure number and note that for  $F$  values less than 100 the agreement between the curves is quite good. For  $F$  values satisfying  $100 < F < 1000$ , there are regions within the graphs where the three curves differ and for  $F$  values greater than 1000, there are major differences in the three sets of curves. The major differences are possibly the result of using inaccurate cross sections in performing the calculations. This hypothesis can be investigated and tested at a later date.

Table 5 gives the average  $F$  values for the sets of flux graphs corresponding to the forward neutrons, backward neutrons, total neutrons, protons,  $^2\text{H}$ ,  $^3\text{H}$ ,  $^3\text{He}$  and  $^4\text{He}$ .

## 6 Additional graphs

The light ion contribution is one of the major contributors to the dose and dose equivalent calculations. It is also known that there are some charge removal processes resulting from the collision of heavy ions which can also contribute to the dose and dose equivalent calculations. Figures 66 - 69 represent nuclear fragmentation effects in transport processes using the spectra of GCR Carbon, Oxygen, Magnesium and Iron. For example, Figure 66 illustrates transmitted Carbon, Boron and Beryllium flux versus energy at the Aluminum - water interface from GCR Carbon ions incident upon the  $20 \text{ g/cm}^2$  Aluminum slab. Similar graphs are given in the Figures 67 - 69. The  $F$  - norm for these set of curves are given in Table 6. Clearly, Beryllium production from Carbon needs the most improvement.

## 7 Conclusions

The HZETRN space radiation code has been developed to analyze the effects of galactic cosmic rays and solar particle events on mission planning and shielding for astronauts and instrumentation. We have provided a comparison study involving two Monte Carlo transport codes, HETC - HEDS and FLUKA and the deterministic code, HZETRN. Each code is used to transport an ion from the 1977 solar minimum GCR spectrum impinging upon a 20 g/cm<sup>2</sup> aluminum slab followed by a 30 g/cm<sup>2</sup> water slab. We have compared dose, dose equivalent and fluence of a variety of particles at various depths in water.

A parameter  $F$  has been calculated that can be interpreted as a weighted average worst case percent error value, and this value is assigned to a set of graphs depicting the transport code results. The large  $F$  value associated with a set of flux graphs indicates that there is significant difference between the HZETRN results and the HETC - HEDS and FLUKA results. A large  $F$  value will always occur whenever there is a significant spread between the curves HETC - HEDS and FLUKA. There are many instances where the curves for HETC - HEDS and FLUKA do not agree. This is possibly due to the cross sections used within these codes. Whenever HETC - HEDS and FLUKA disagree, further investigation and verification of results needs to be performed. The significantly high  $F$  values in Table 5 indicate that HETC - HEDS and FLUKA have large differences with HZETRN. Cross section calculations are a cause of error that need to be examined by updating cross sections models in all three computer codes. Another source of error is possibly due to how the light ion flux calculations are performed within HZETRN. These calculation methods need to be investigated in more detail.

Figures 64 - 65 are magnified views of selected data sets illustrating that there are still major differences in the flux calculations as performed by HZETRN, HETC - HEDS and FLUKA, which in turn lead to large  $F$  values. These differences are perhaps due to the cross section values used during calculations. The magnified views are presented over the energy regions  $1 \leq E \leq 500$  MeV, because it is in this region that the quality factors have their greatest rate of change. These differences in values are another possible reason why the dose and dose equivalent calculations are not in agreement.

Future research into a comparison of the results from the HZETRN, HETC-HEDS and FLUKA transport codes for the same shield/target configuration, will aid in trying to isolate causes for the differences between the codes found herein. Results from this study and future comparison studies can provide insight into the HZETRN code operation and bring the code to a high standard of performance so that design engineers can have increased confidence in its abilities to analyze particle transport associated with a variety of radiation environments.

Table 3:  $F$  values and quantitative comparison of flux graphs. Abbreviations are as follows: forward neutron (f - n), backward neutron (b - n), total neutron (t - n), proton (p). The decimal number after the figure number refers to the value of the water depth in g/cm<sup>2</sup>. For example, 11.0 refers to Figure 11 at a water depth of 0 g/cm<sup>2</sup>, which is the upper left panel of Figure 11.

	Hydrogen				Helium				Carbon				Oxygen				
f-n	43	51	51	50	135	65	66	72	91	87	77	75	101	67	52	47	
Fig.	11.0	11.10	11.20	11.30	16.0	16.10	16.20	16.30	22.0	22.10	22.20	22.30	30.0	30.10	30.20	30.30	
b-n	83	143	323		99	113	191		146	199	422		376	305	386		
Fig.	12.0	12.10	12.20		17.0	17.10	17.20		23.0	23.10	23.20		31.0	31.10	31.20		
t-n	44	49	46	59	86	76	78	101	47	47	37	64	84	66	53	46	
Fig.	13.0	13.10	13.20	13.30	18.0	18.10	18.20	18.30	24.0	24.10	24.20	24.30	32.0	32.10	32.20	32.30	
p	30	34	29	31	55	48	51	66	8	8	6	11	41	29	15	32	
Fig.	14.0	14.10	14.20	14.30	19.0	19.10	19.20	19.30	25.0	25.10	25.20	25.30	33.0	33.10	33.20	33.30	
<sup>2</sup> H				2085	1555	1227	1087	471	372	291	311	832	504	406	325		
Fig.	15.0	15.10	15.20	15.30	20.0	20.10	20.20	20.30	26.0	26.10	26.20	26.30	34.0	34.10	34.20	34.30	
<sup>3</sup> H									16582	5922	2938	2623	8755	2704	1126	915	
Fig.									27.0	27.10	27.20	27.30	35.0	35.10	35.20	35.30	
<sup>3</sup> He									14382	3892	2679	1698	5719	2243	1745	1560	
Fig.									28.0	28.10	28.20	28.30	36.0	36.10	36.20	36.30	
<sup>4</sup> He					544	929	464	542	1500	539	316	242	387	126	112	105	
Fig.					21.0	21.10	21.20	21.30	29.0	29.10	29.20	29.30	37.0	37.10	37.20	37.30	

Table 4: Table 3 continued.

		Magnesium				Silicon				Iron			
f-n	95	54	45	39	100	72	57	47	48	39	34	29	
Fig.	38.0	38.10	38.20	38.30	46.0	46.10	46.20	46.30	54.0	54.10	54.20	54.30	
b-n	1829	1394	1311		1413	1203	1240		1003	825	953		
Fig.	39.0	39.10	39.20		47.0	47.10	47.20		55.0	55.10	55.20		
t-n	77	55	46	43	57	50	45	47	47	42	40	43	
Fig.	40.0	40.10	40.20	40.30	48.0	48.10	48.20	48.30	56.0	56.10	56.20	56.30	
p	29	22	24	28	23	22	15	26	16	16	10	15	
Fig.	41.0	41.10	41.20	41.30	49.0	49.10	49.20	49.30	57.0	57.10	57.20	57.30	
<sup>2</sup> H	510	461	373	339	502	529	427	391	657	556	480	421	
Fig.	42.0	42.10	42.20	42.30	50.0	50.10	50.20	50.30	58.0	58.10	58.20	58.30	
<sup>3</sup> H	5117	1885	1306	821	3973	1671	1110	1044	2843	1072	798	646	
Fig.	43.0	43.10	43.20	43.30	51.0	51.10	51.20	51.30	59.0	59.10	59.20	59.30	
<sup>3</sup> He	2743	2518	1962	1871	2681	2076	1442	1532	4570	2019	1586	1096	
Fig.	44.0	44.10	44.20	44.30	52.0	52.10	52.20	52.30	60.0	60.10	60.20	60.30	
<sup>4</sup> He	203	127	97	98	180	130	108	103	165	144	144	128	
Fig.	45.0	45.10	45.20	45.30	53.0	53.10	53.20	53.30	61.0	61.10	61.20	61.30	

Table 5: Average  $F$  values.

Forward Neutrons	64
Backward Neutrons	753
Total Neutrons	56
Protons	26
$^2\text{H}$	630
$^3\text{H}$	3193
$^3\text{He}$	3001
$^4\text{He}$	310

Table 6:  $F$  values heavy ions

Figure 66, Incident ion is Carbon	
Carbon	59
Boron	66
Beryllium	5850
Figure 67, Incident ion is Oxygen	
Oxygen	74
Nitrogen	106
Carbon	53
Figure 68, Incident ion is Magnesium	
Magnesium	78
Sodium	162
Neon	103
Figure 69, Incident ion is Iron	
Iron	215
Magnesium	241
Chromium	136

## References

- [1] Wilson, J.W., Townsend, L.W., Schimmerling, W., Khandelwal, G.S., Khan, F., Nealy, J.E., Cucinotta, F.A., Simonsen, L.C., Shinn, J.L., and Norbury, J.W., Transport Methods and Interactions for Space Radiations, NASA Research Publication 1257, 1991.
- [2] Heinbockel, J.H., Slaba, T.C., Blattnig, S.R., Tripathi, R.K., Townsend, L.W., Handler, T., Gabriel, T.A., Pinsky, L.S., Redell, B., Cloudsley, M.S., Singleterry, R.C., Norbury, J.W., Badavi, F.F., and Aghara, S.K., Comparison of Radiation Transport Codes, HZETRN, HETC and FLUKA, using the 1956 Webber SPE Spectrum, NASA Technical Paper 215560, 2009.
- [3] Nealy, J.E., Cucinotta, F.A., Wilson, J.W., Badavi, F.F., Dachev, Ts.P., Tomov, B.T., Walker, S.A., De Angelis G., Blattnig S.R., and Atwell, W., Pre - engineering Spaceflight Validation of Environmental Models and the 2005 HZETRN Simulation Code, Advances in Space Research 40, 1593 - 1610, 2007.
- [4] Wilson, J.W., Tripathi, R.K., Mertens, C.J., Blattnig, S.R., Cloudsley, M.S., Cucinotta, F.A., Tweed, J., Heinbockel, J.H., Walker S.A., and Nealy, J.E., Verification and Validation: High Charge and Energy (HZE) Transport Codes and Future Development, NASA Technical Paper 213784, 2005.
- [5] Cucinotta, F.A., Wilson, J.W., Saganti, P., Hu, X., Kim, M.Y., Cleghorn, T., Zeitlin, C., and Tripathi, R.K., Isotopic Dependence of GCR Fluence Behind Shielding, Radiation Measurements 41, 1235 - 1249, 2006.
- [6] Slaba, T.C., Blattnig, S.R., Walker, S.A., Wilson, J.W., and Badavi, F.F., An Improved Neutron Transport Algorithm for HZETRN, Advances in Space Research, submitted, 2009.
- [7] Wilson, J.W., Badavi, F.F., Cucinotta, F.A., Shinn, J.L., Badhwar, G.D., Silberberg, R., Tsao, C.H., Townsend L.W., and Tripathi, R.K., HZETRN: Description of a Free - Space Ion and Nucleon Transport and Shielding Computer Program, NASA Technical Paper 3495, 1995.
- [8] Gabriel, T.A., Bishop, B.L., Alsmiller, F.S., Alsmiller, R.G., and Johnson, J.O., CALOR95: A Monte Carlo Program Package for the Design and Analysis of Calorimeter Systems, Oak Ridge National Laboratory Technical Memorandum 11185, 1995.
- [9] Townsend, L.W., Miller, T.M., and Gabriel, T.A., HETC Radiation Transport Code Development for Cosmic Ray Shielding Applications in Space, Radiation Protection Dosimetry 115, 135 - 139, 2005.

- [10] Fasso, A., Ferrari, A., Ranft, J., and Sala, P.R., FLUKA: a multi-particle transport code, CERN-2005-10, INFN/TC 05/11, SLAC-R-773, 2005.
- [11] Battistoni, G., Muraro, S., Sala, P.R., Cerutti, F., Ferrari, A., Roesler, S., Fasso, A., and Ranft, J., The FLUKA code: Description and Benchmarking, Proceedings of the Hadronic Shower Simulation Workshop 2006, Fermilab 6 - 8 September 2006, Albrow, M., and Raja R., eds., American Institute of Physics Conference Proceeding 896, 31 - 49, 2007.
- [12] Badhwar, J.D., O'Neill, P. M., An Improved Model of GCR for Space Exploration Mission, Nucl. Tracks, Radiation Measurements, 20, 403 - 410, 1992.
- [13] National Council on Radiation Protection and Measurements (NCRP), Conceptual Basis for Calculations of Absorbed Dose Distributions, NCRP Report 108, 1995.
- [14] International Commission on Radiological Protection (ICRP), Conversion Coefficients for use in Radiological Protection against External Radiation, ICRP Publication 74, Elsevier, New York, 1997.
- [15] Pelliccioni, M., Overview of Fluence to Effective Dose and Fluence to Ambient Dose Equivalent Conversion Coefficients for High Energy Radiation Calculated using the FLUKA Code, Radiation Protection Dosimetry 88, 279 - 297, 2000.
- [16] National Council on Radiation Protection and Measurements (NCRP), Operational Radiation Safety Program for Astronauts in Low - Earth Orbit: A Basic Framework, NCRP Report 142, 2002.
- [17] International Commission on Radiological Protection (ICRP), The 1990 Recommendations of the International Commission on Radiological Protection, ICRP Publication 60, Elsevier, New York, 1993.
- [18] Emmett, M.B., MORSE-CGA, A Monte Carlo Radiation Transport Code with Array Geometry Capability, Oak Ridge National Laboratory Report 6174, 1985.
- [19] Bielajew, A.F., Hirayama, H., Nelson, W.R., and Rogers, D.W.O., History, Overview and Recent Improvements of EGS4, Stanford Linear Accelerator Center (SLAC) Publication 6499, 1994.
- [20] Hendricks, J.S., McKinney, G.W., Fensin, M.L., James, M.R., Johns, R.C., Durdee, J.W., Finch, J.P., Pelowitz, D.B., Waters, L.S., and Johnson, M.W., MCNPX 26F Extensions, Los Alamos National Laboratory Report LA-UR-08-1808, 2008. Available at <http://mcnpx.lanl.gov/opendocs/versions/v26f/v26f.pdf>.

- [21] International Commission on Radiological Protection (ICRP), Recommendations of the International Commission on Radiological Protection, ICRP Publication 26, Pergamon, New York, 1977.
- [22] National Council on Radiation Protection and Measurements (NCRP), Radiation Protection Guidance for Activities in Low - Earth Orbit, NCRP Report 132, 2000.
- [23] Ingersoll, D.T., Roussin, R.W., Fu, C.Y., and White, J.E., DABL69: A Broad Group Neutron / Photon Cross Section Library for Defense Nuclear Applications, Oak Ridge National Laboratory Technical Memorandum 10568, 1988.

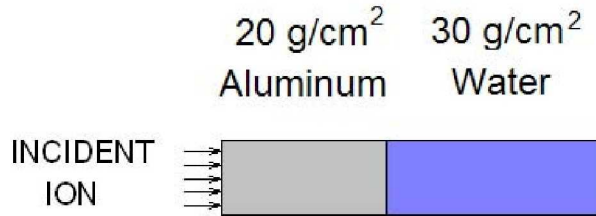


Figure 1: Computational Geometry. The prominent GCR incident ions are H, He, C, O, Mg, Si and Fe.

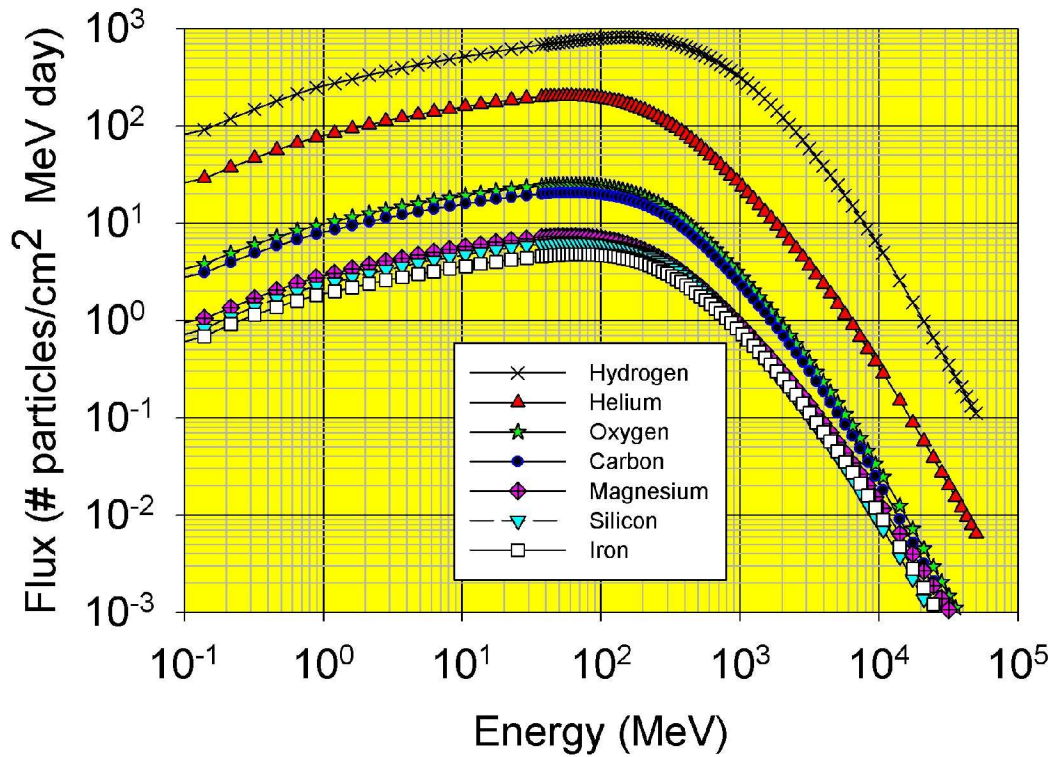


Figure 2: Boundary Conditions for Aluminum shield.

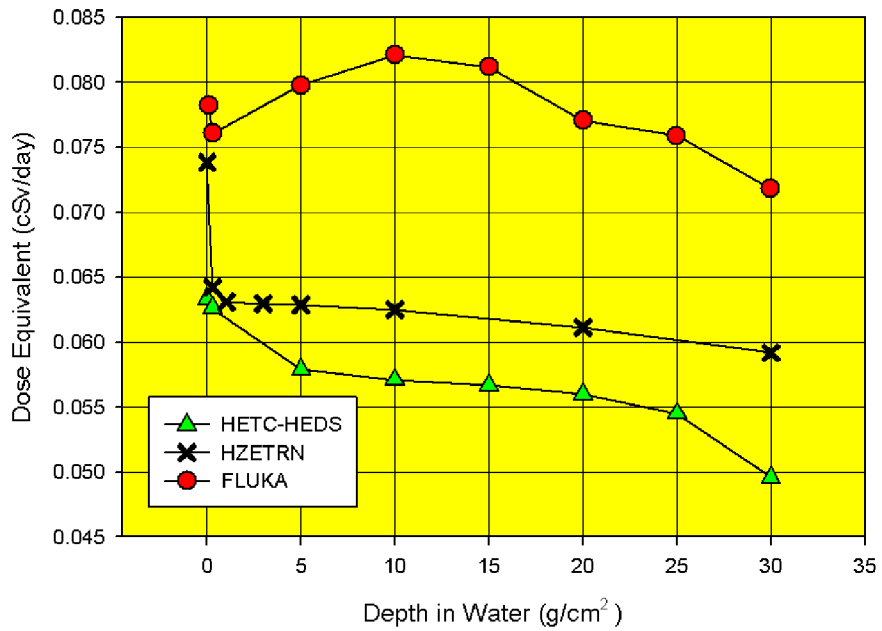
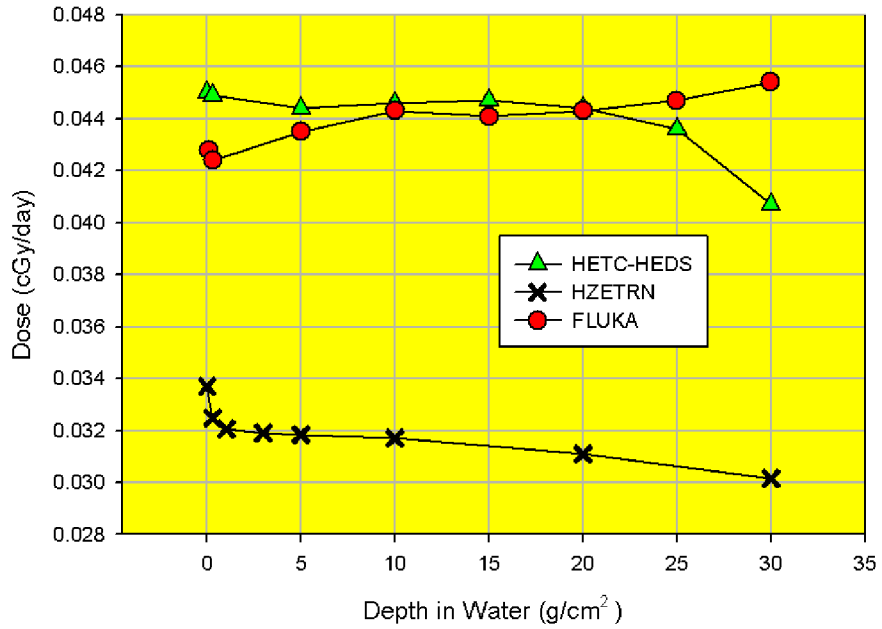


Figure 3: Dose (upper panel) and Dose Equivalent (lower panel) versus Depth in Water for Hydrogen on Aluminum shield.

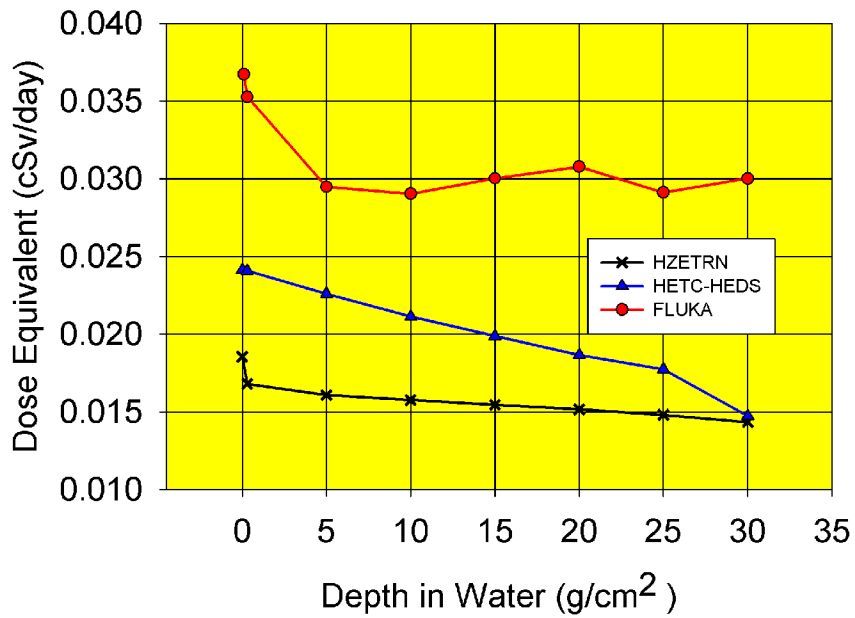
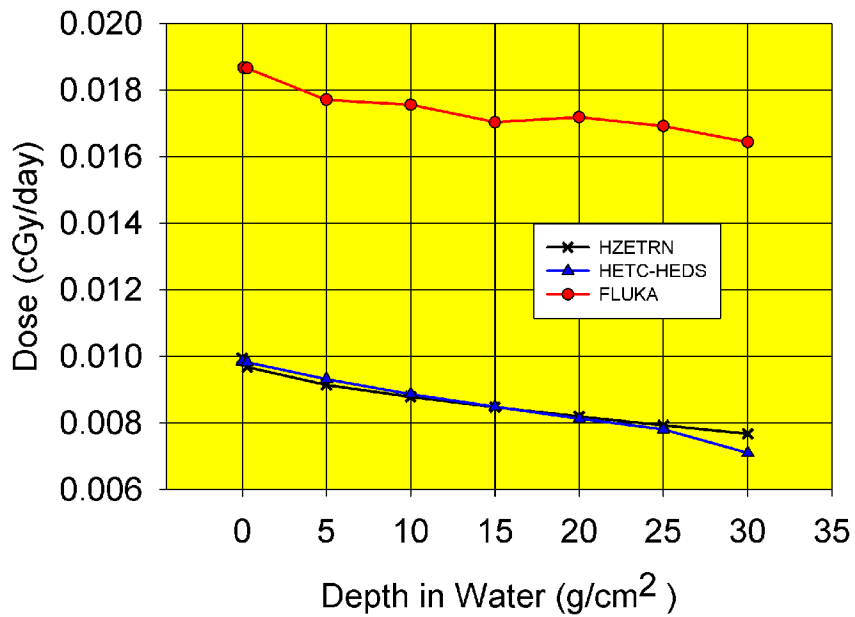


Figure 4: Same as Figure 3, except for Helium.

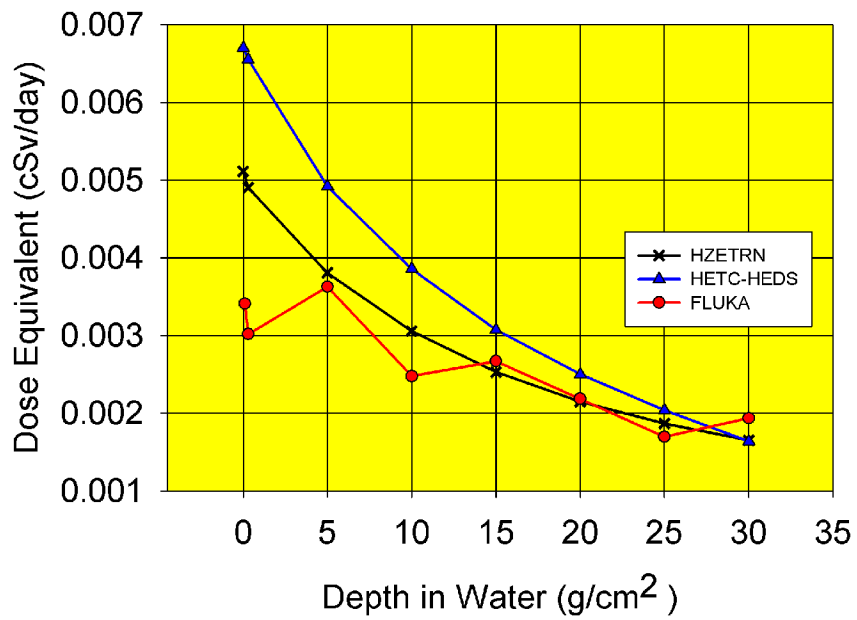
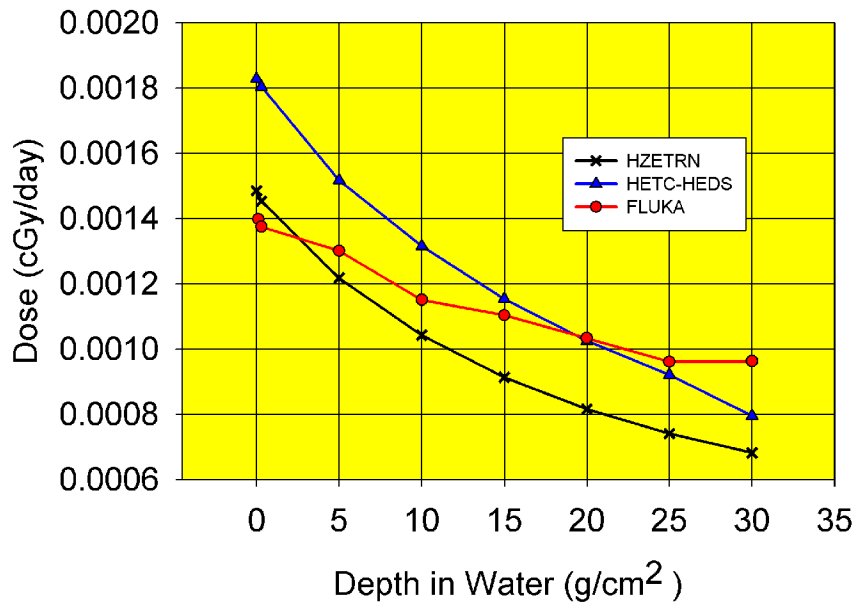


Figure 5: Same as Figure 3, except for Carbon.

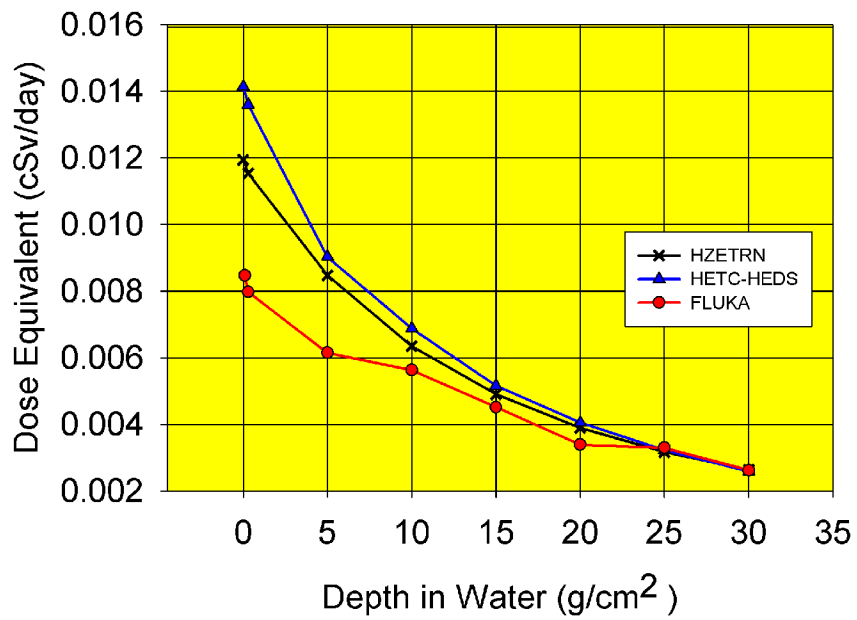
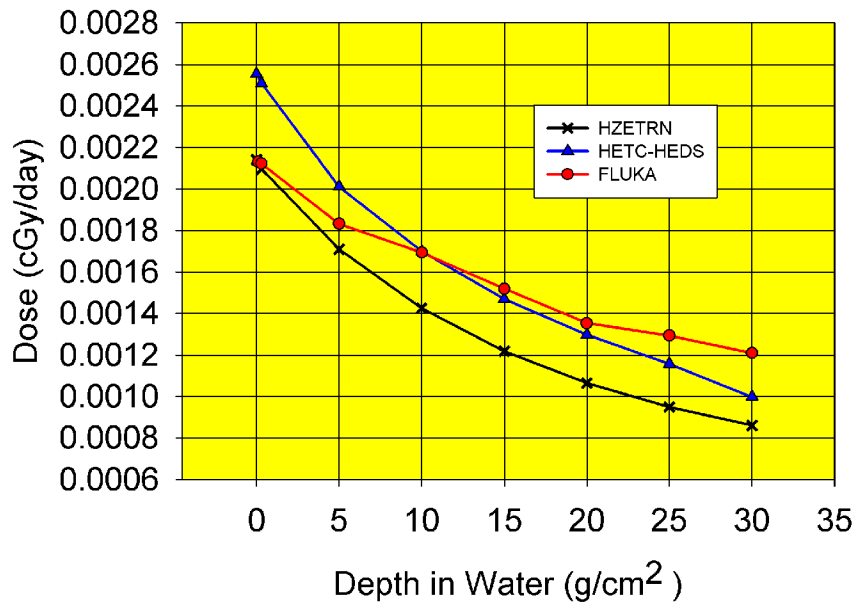


Figure 6: Same as Figure 3, except for Oxygen.

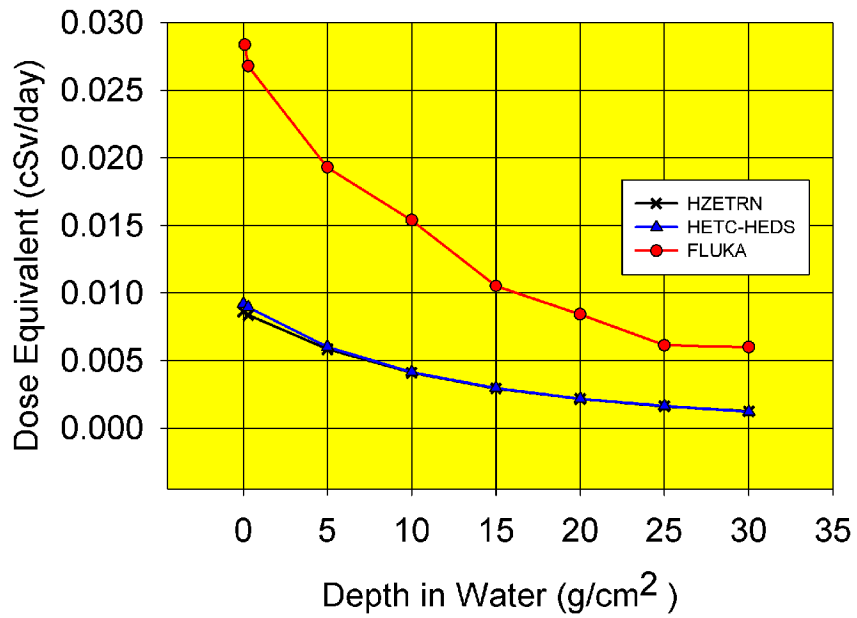
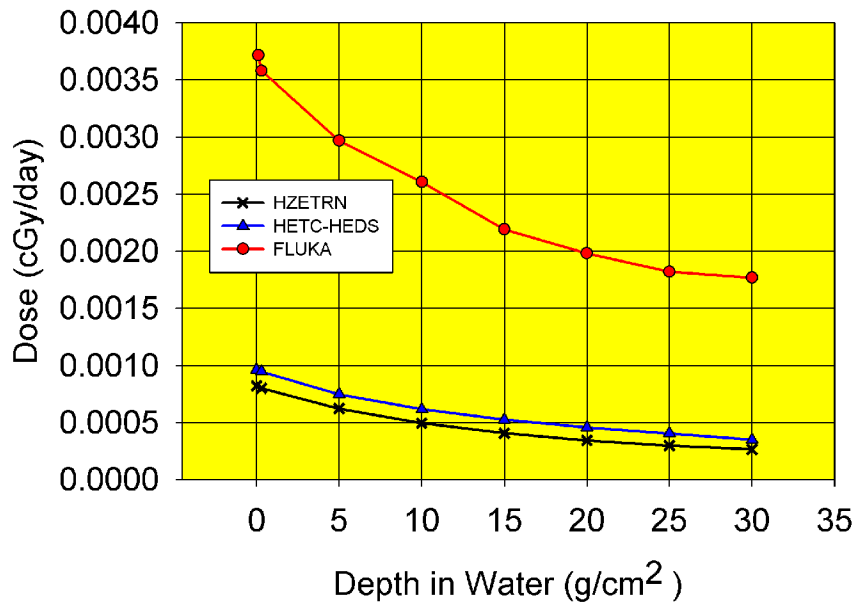


Figure 7: Same as Figure 3, except for Magnesium.

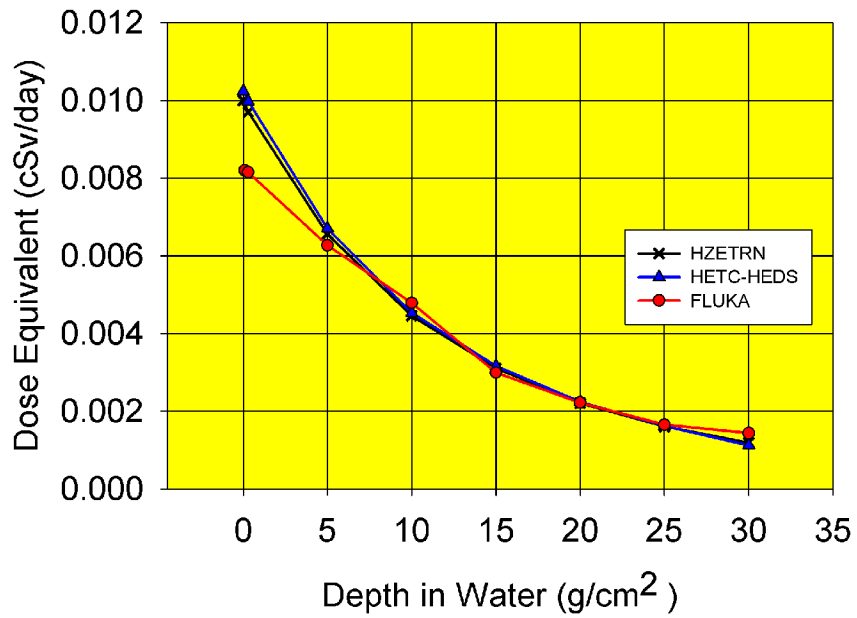
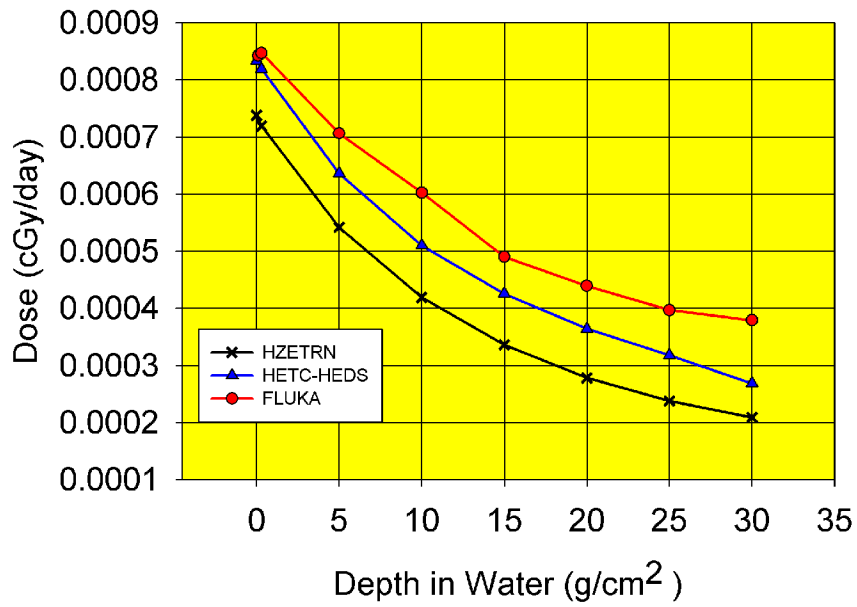


Figure 8: Same as Figure 3, except for Silicon.

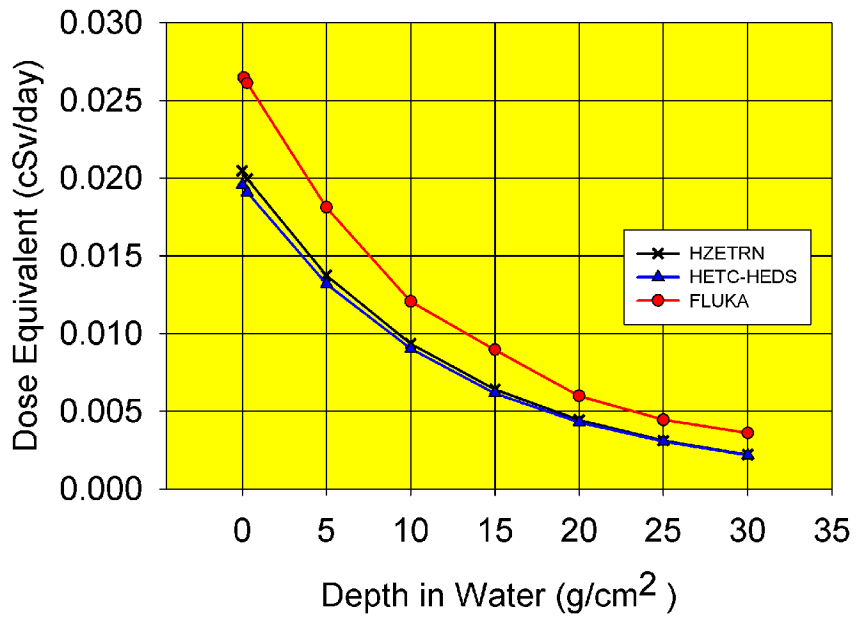
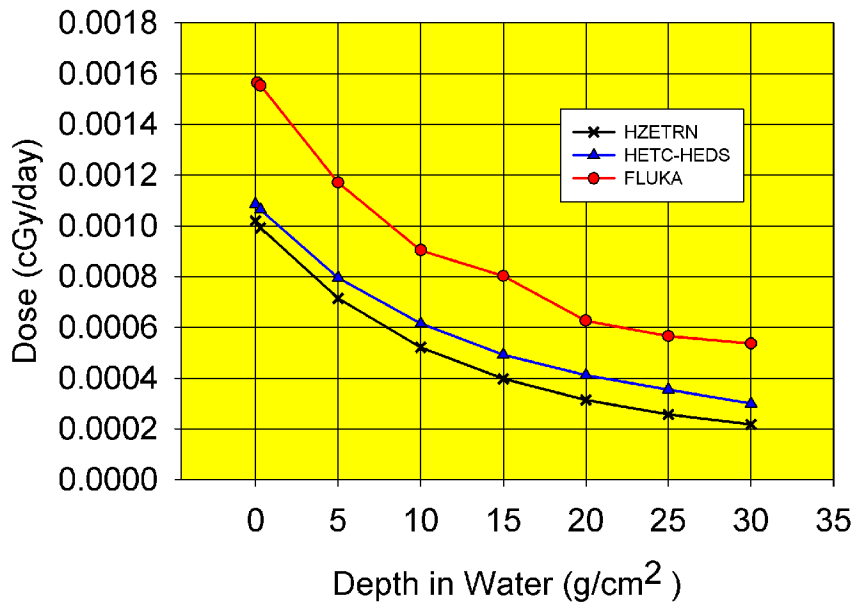


Figure 9: Same as Figure 3, except for Iron.

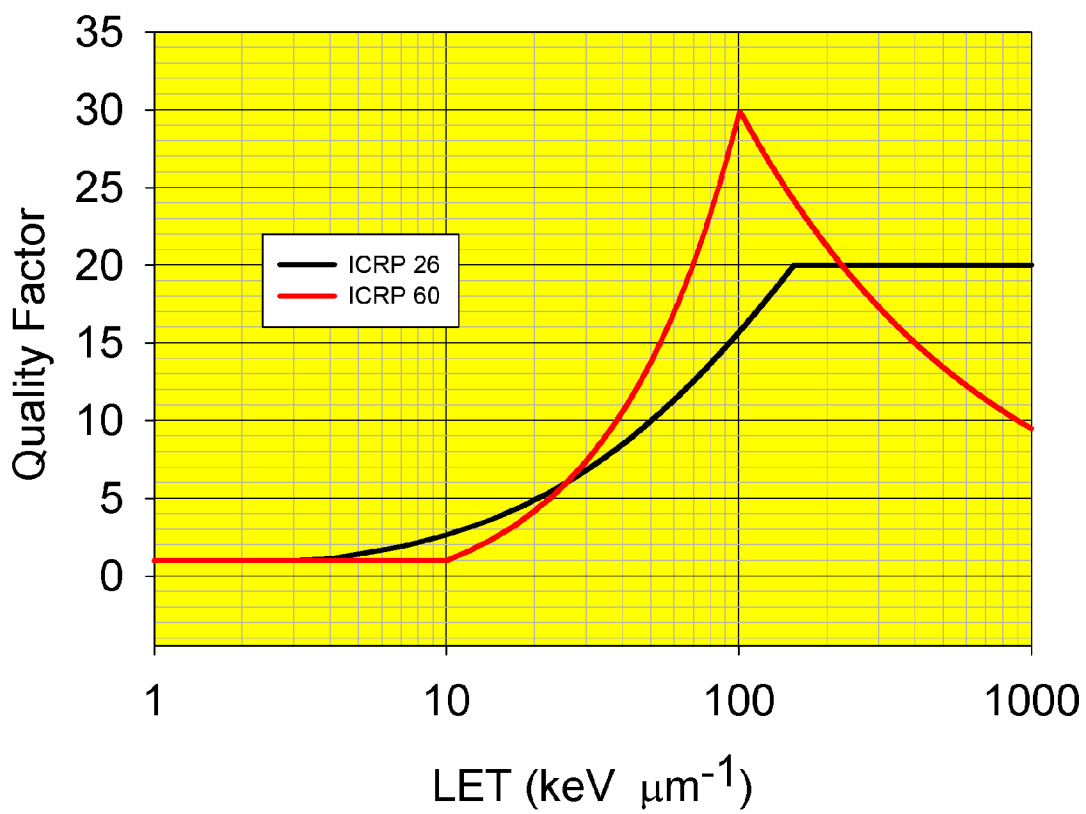


Figure 10: Quality factor versus LET.

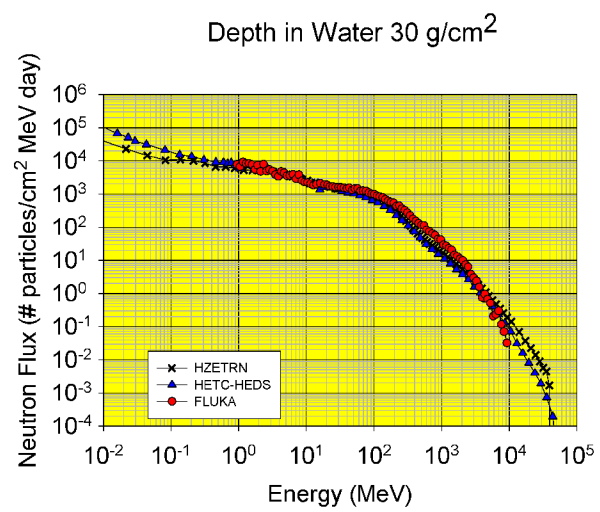
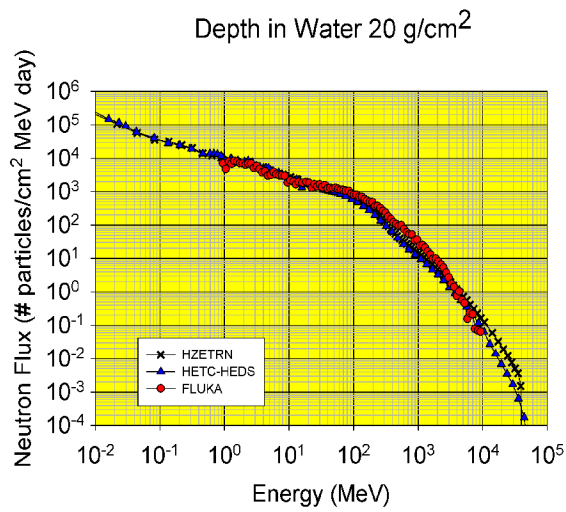
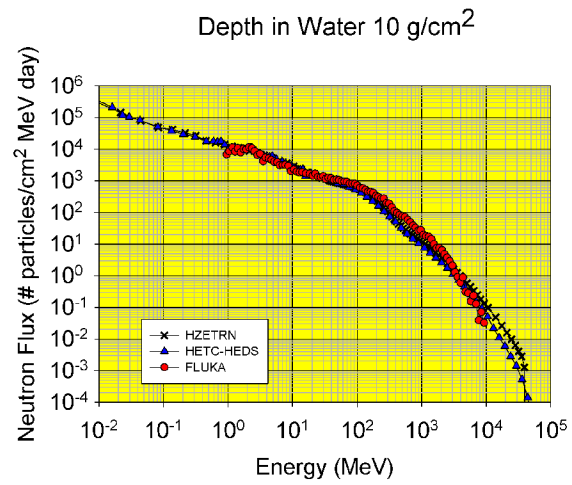
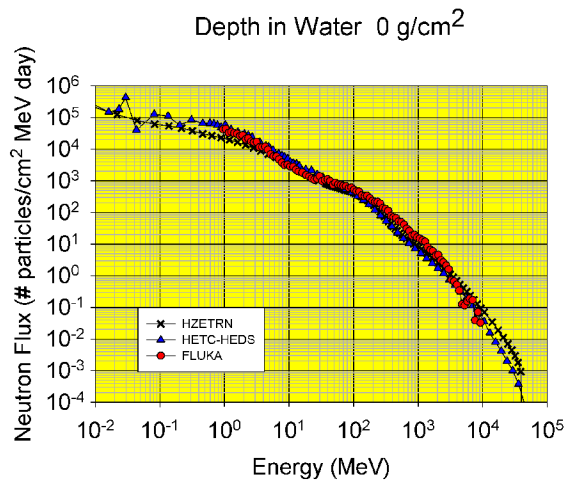


Figure 11: Forward Neutron flux for Hydrogen on Aluminum shield.

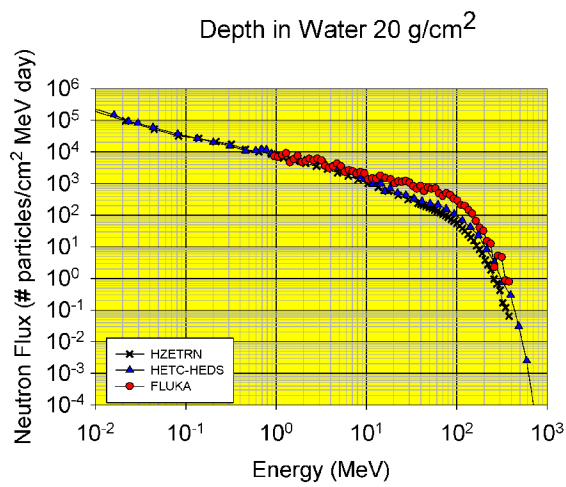
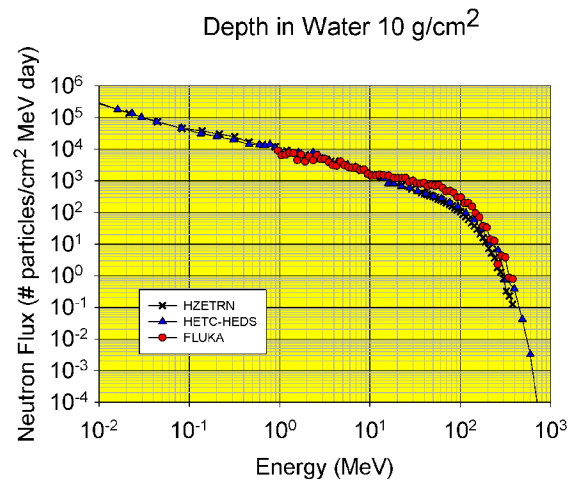
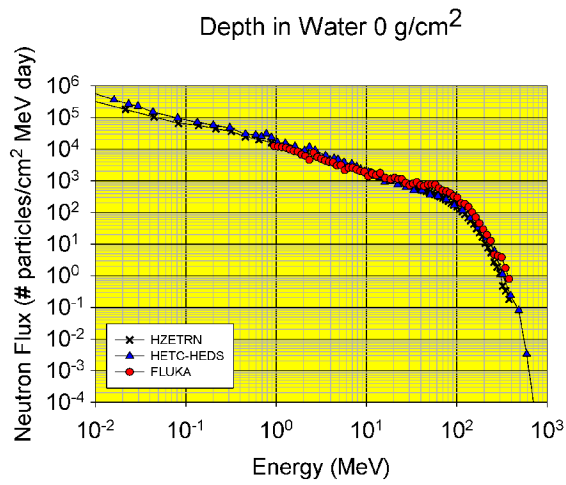


Figure 12: Backward Neutron flux for Hydrogen on Aluminum shield.

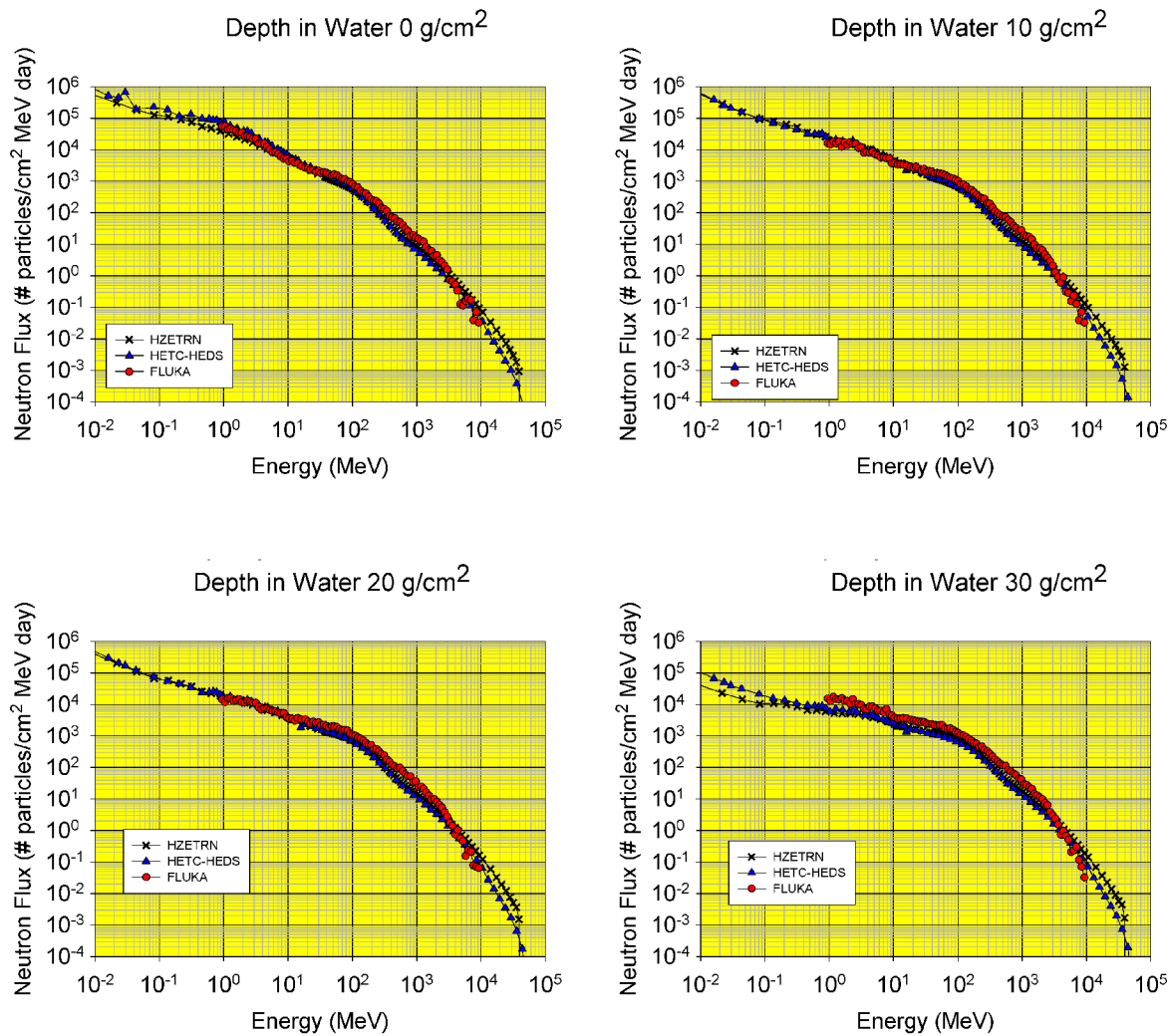


Figure 13: Total Neutron flux for Hydrogen on Aluminum shield.

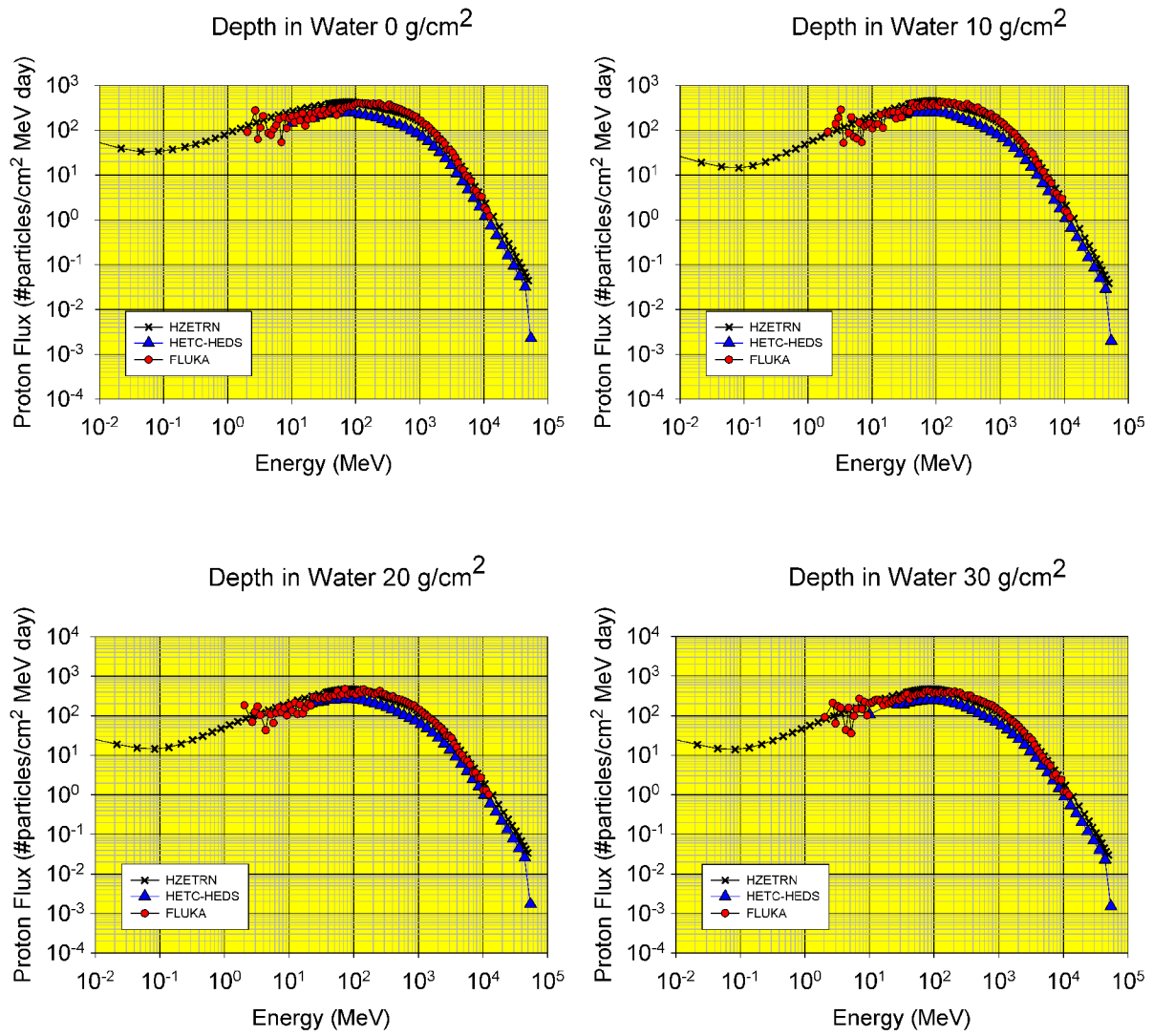


Figure 14: Proton flux for Hydrogen on Aluminum shield.

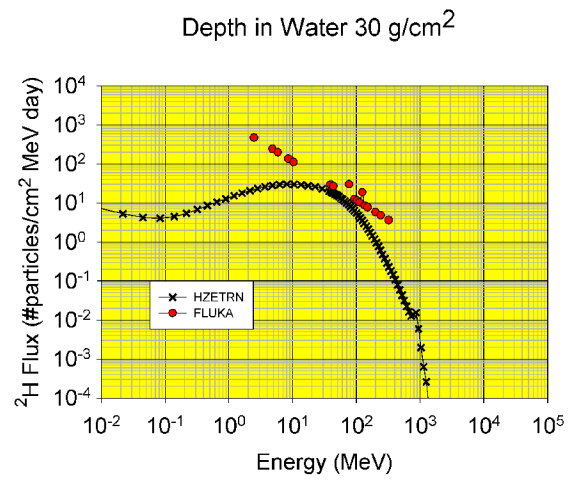
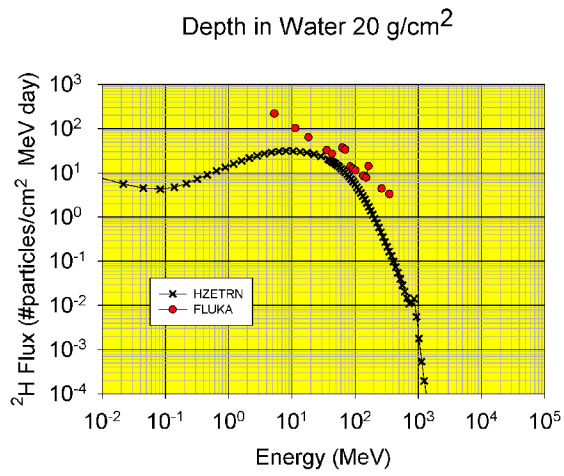
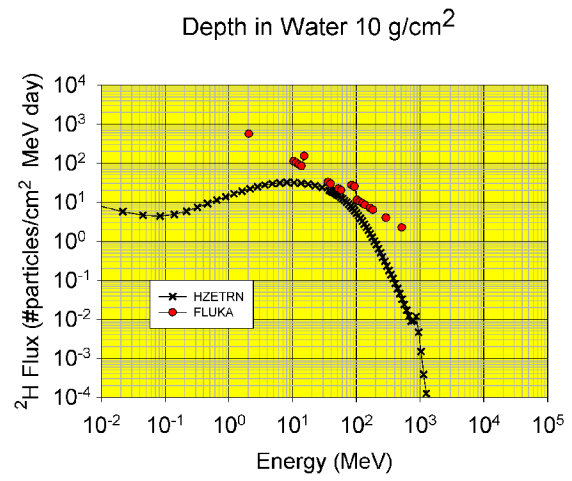
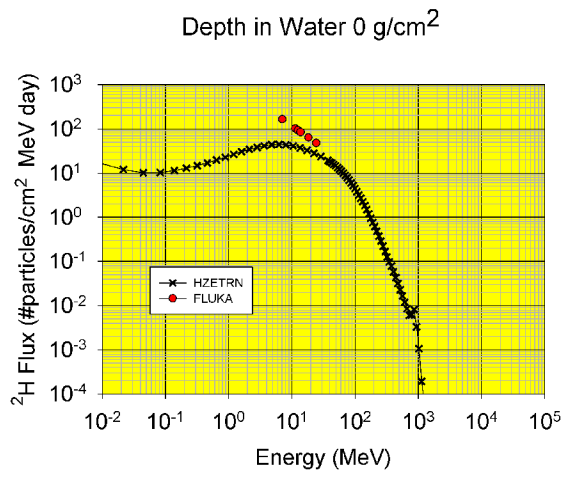


Figure 15: <sup>2</sup>H flux for Hydrogen on Aluminum shield.

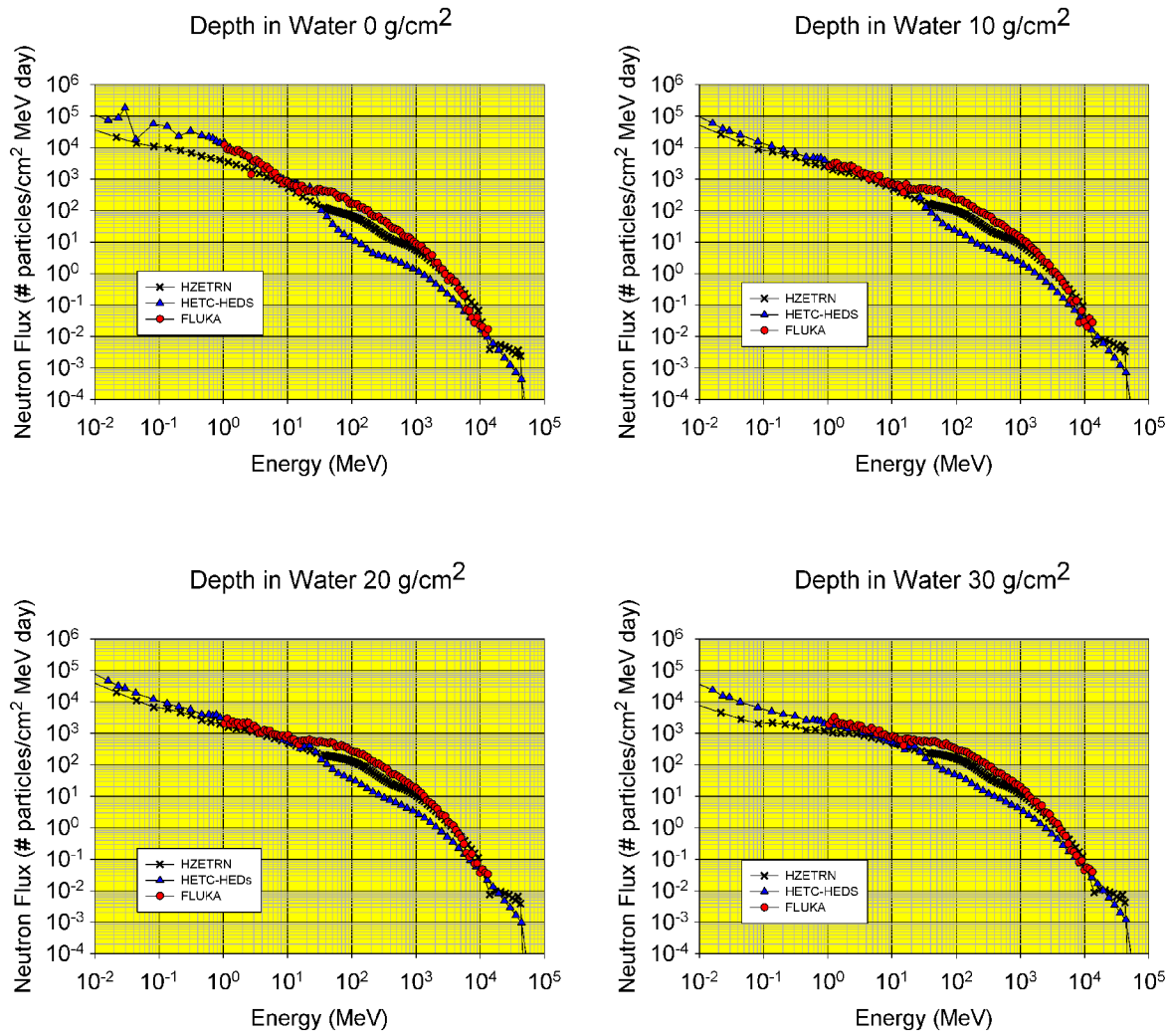


Figure 16: Forward Neutron flux for Helium on Aluminum shield.

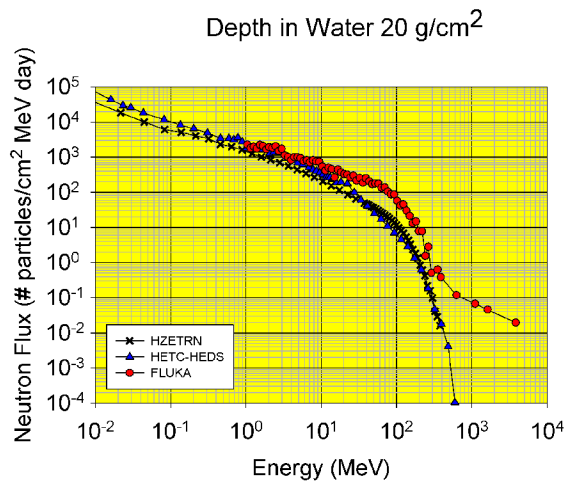
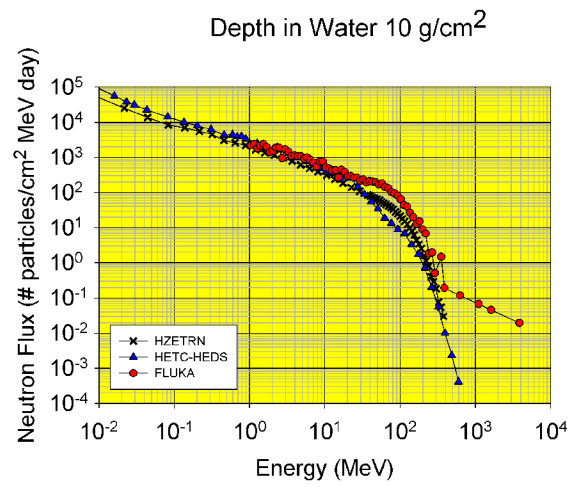
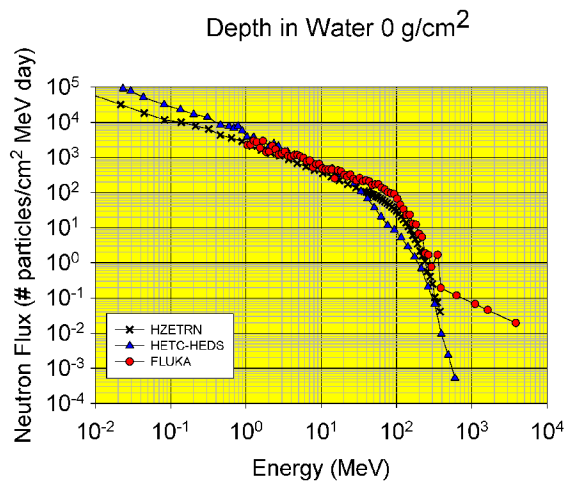


Figure 17: Backward Neutron flux for Helium on Aluminum shield.

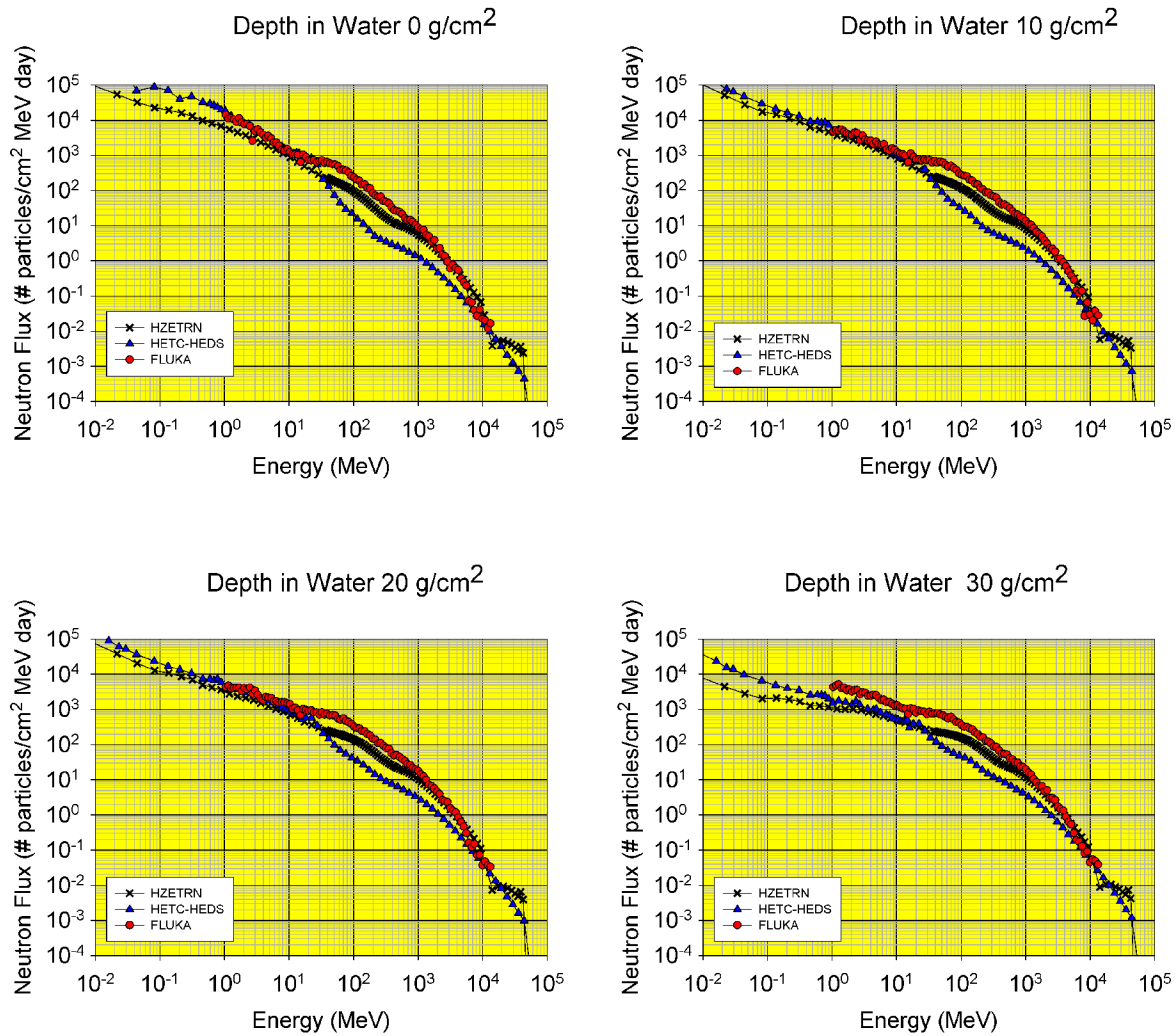


Figure 18: Total Neutron flux for Helium on Aluminum shield.

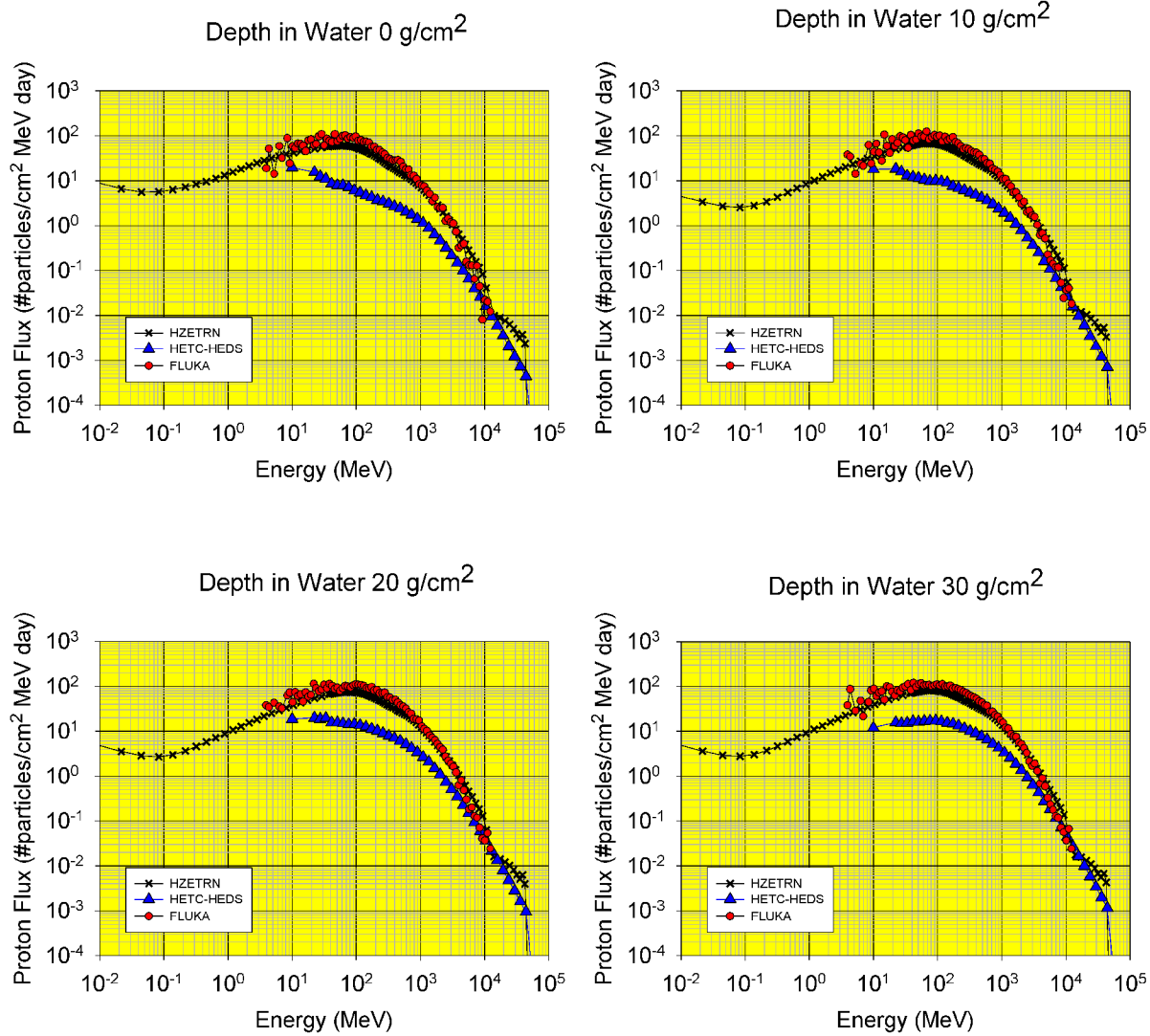


Figure 19: Proton flux for Helium on Aluminum shield.

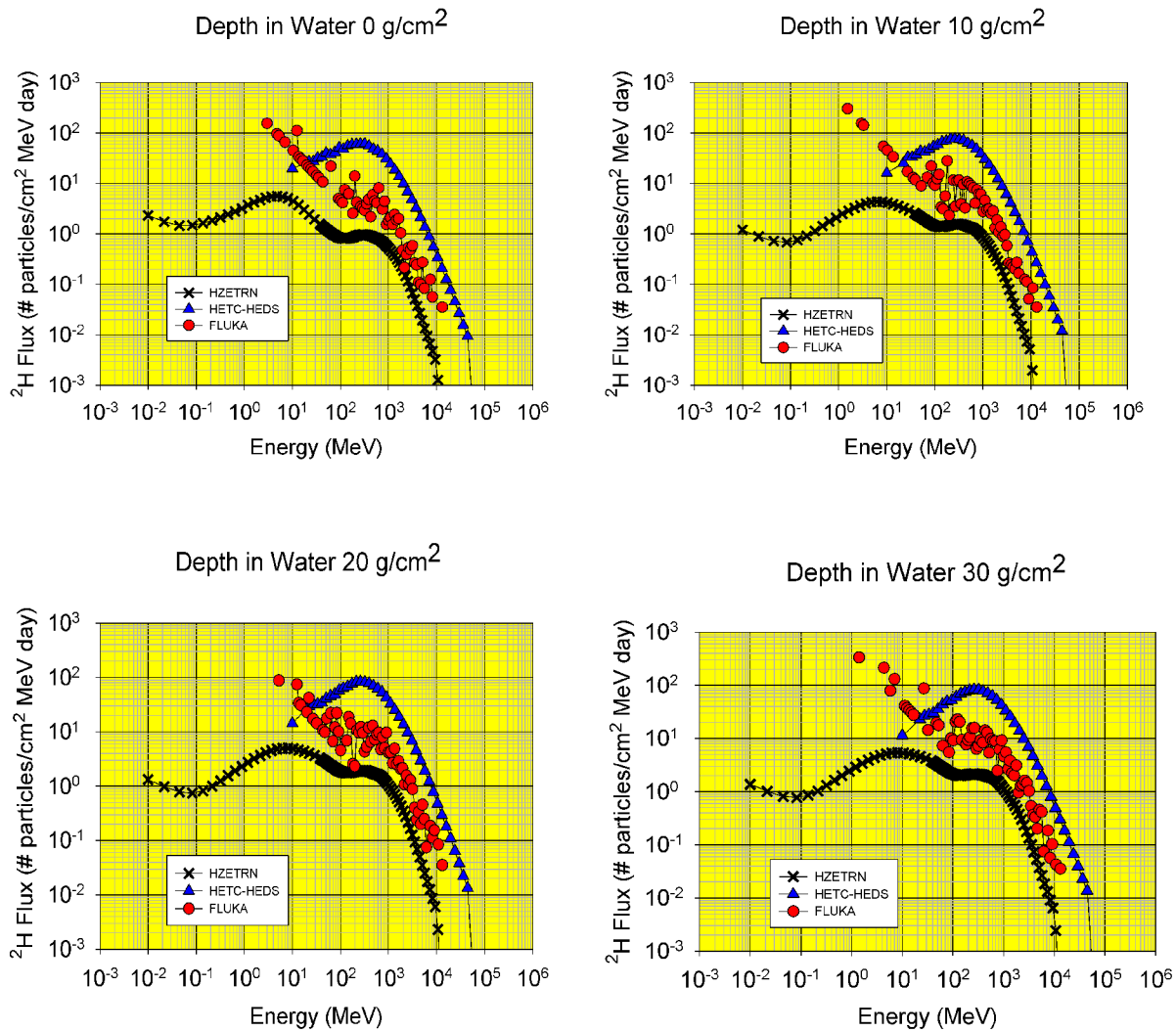


Figure 20:  $^2\text{H}$  flux for Helium on Aluminum shield.

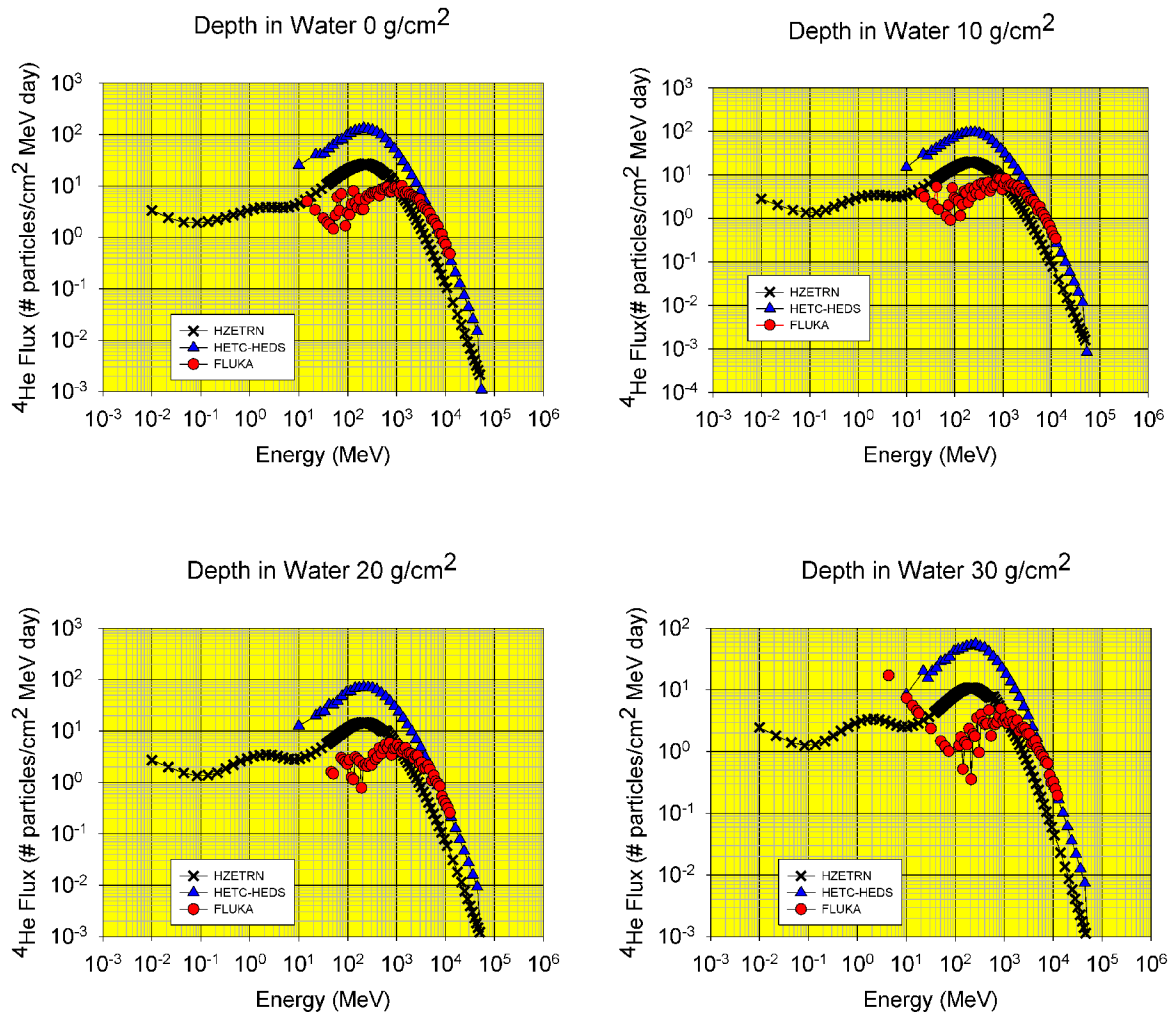


Figure 21:  $^4\text{He}$  flux for Helium on Aluminum shield.

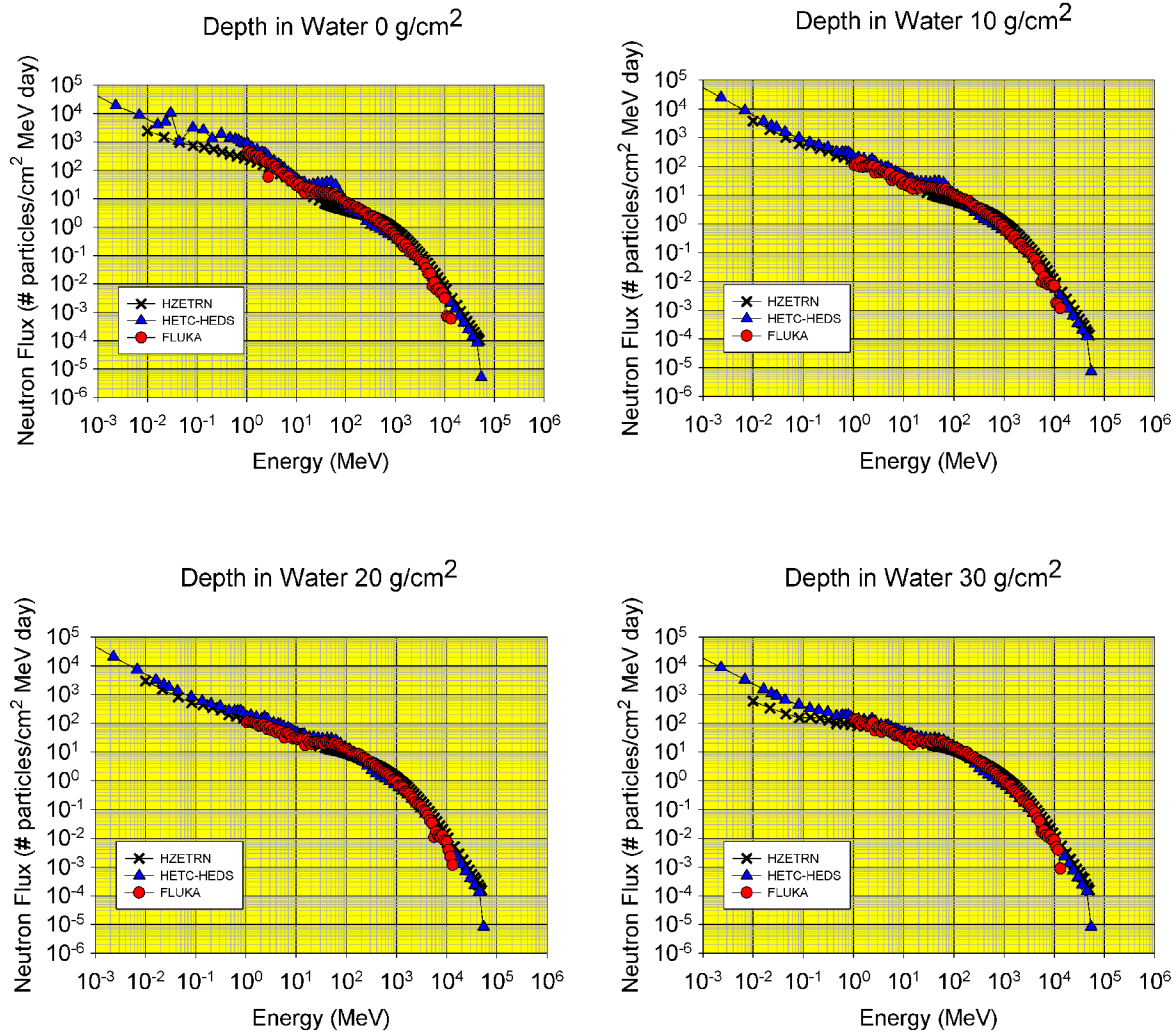


Figure 22: Forward Neutron flux for Carbon on Aluminum shield.

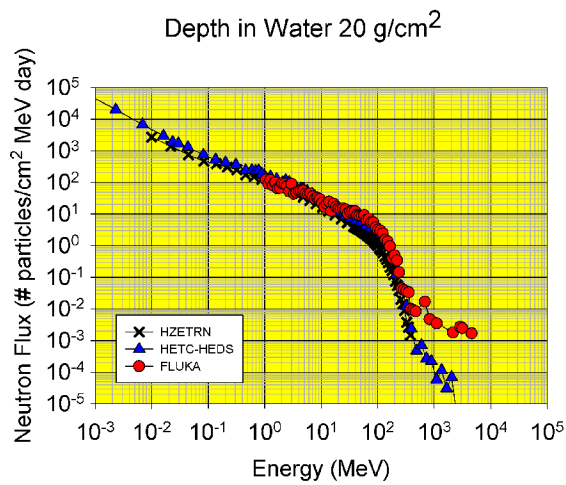
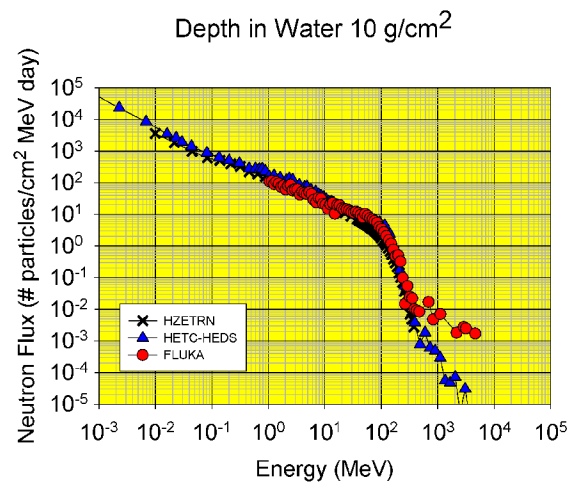
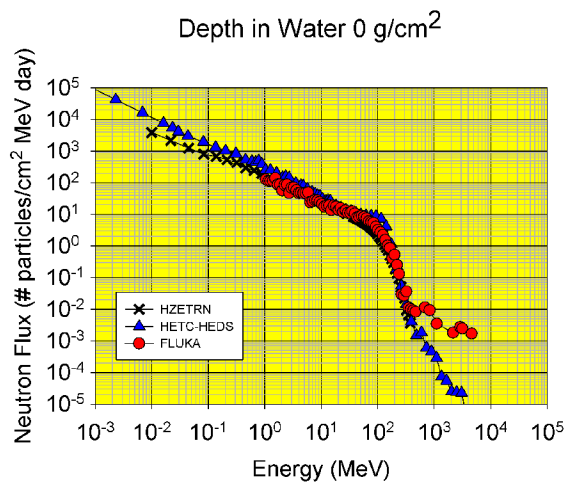


Figure 23: Backward Neutron flux for Carbon on Aluminum shield.

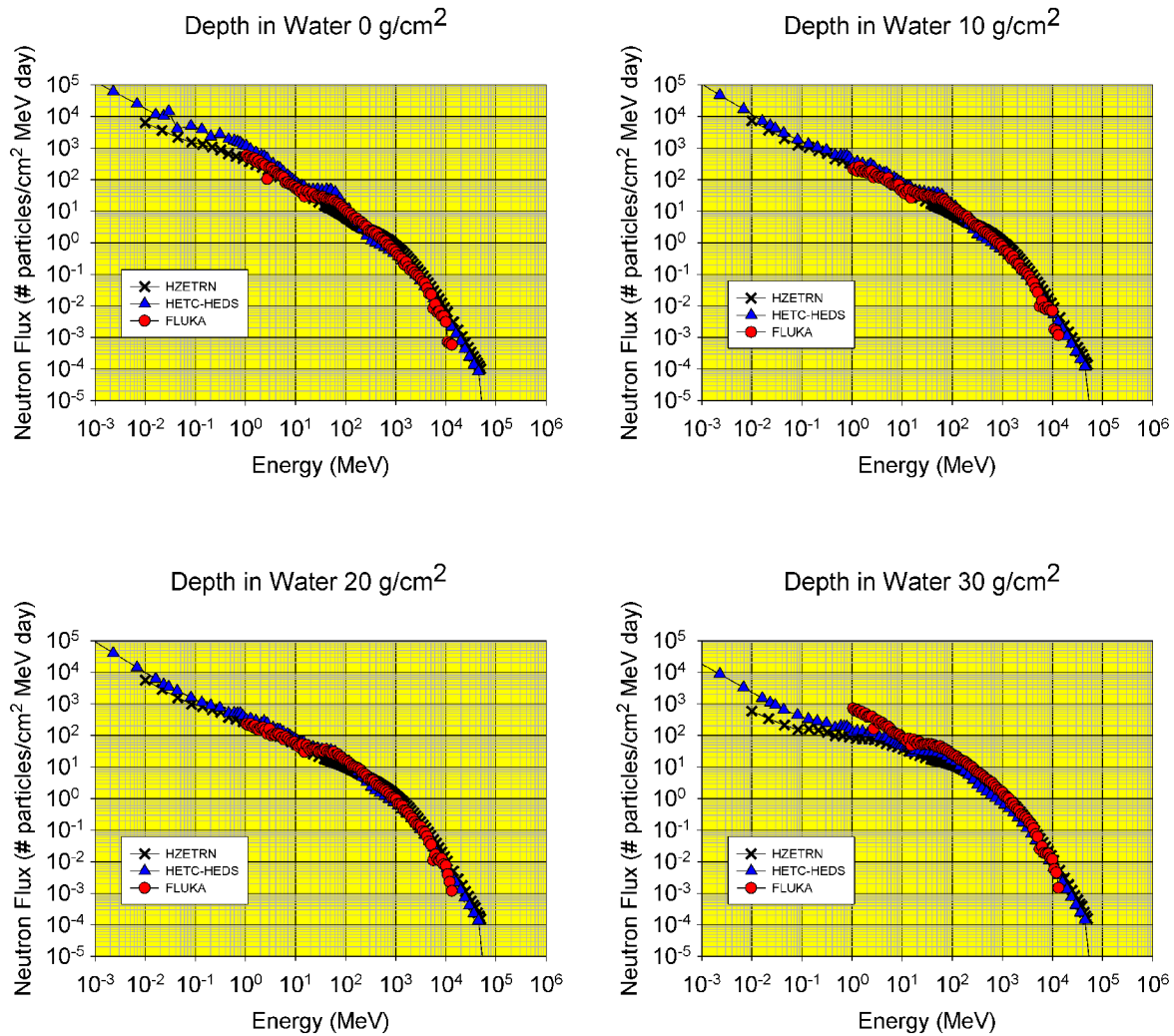


Figure 24: Total Neutron flux for Carbon on Aluminum shield.

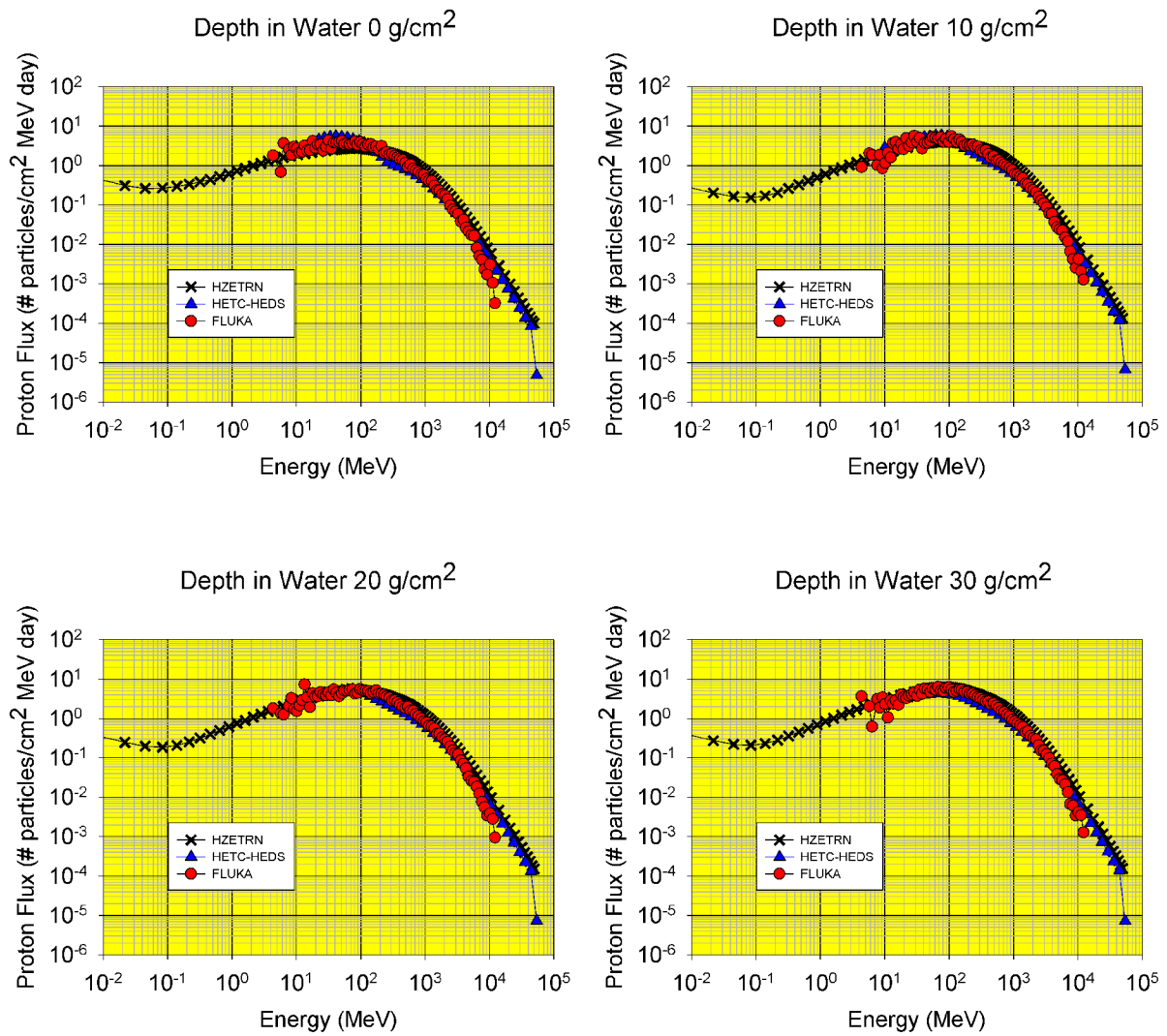


Figure 25: Proton flux for Carbon on Aluminum shield.

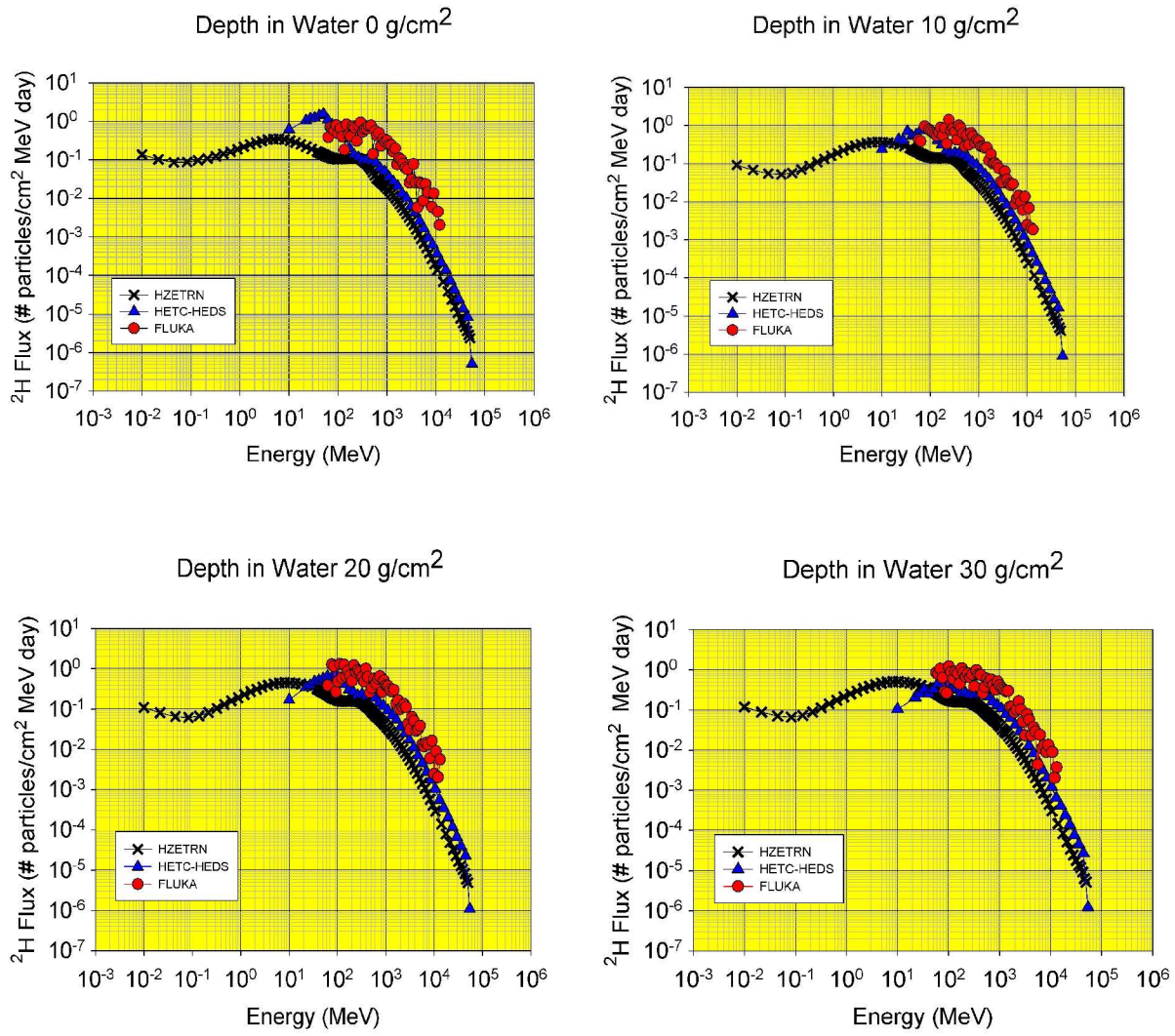


Figure 26:  $^2\text{H}$  flux for Carbon on Aluminum shield.

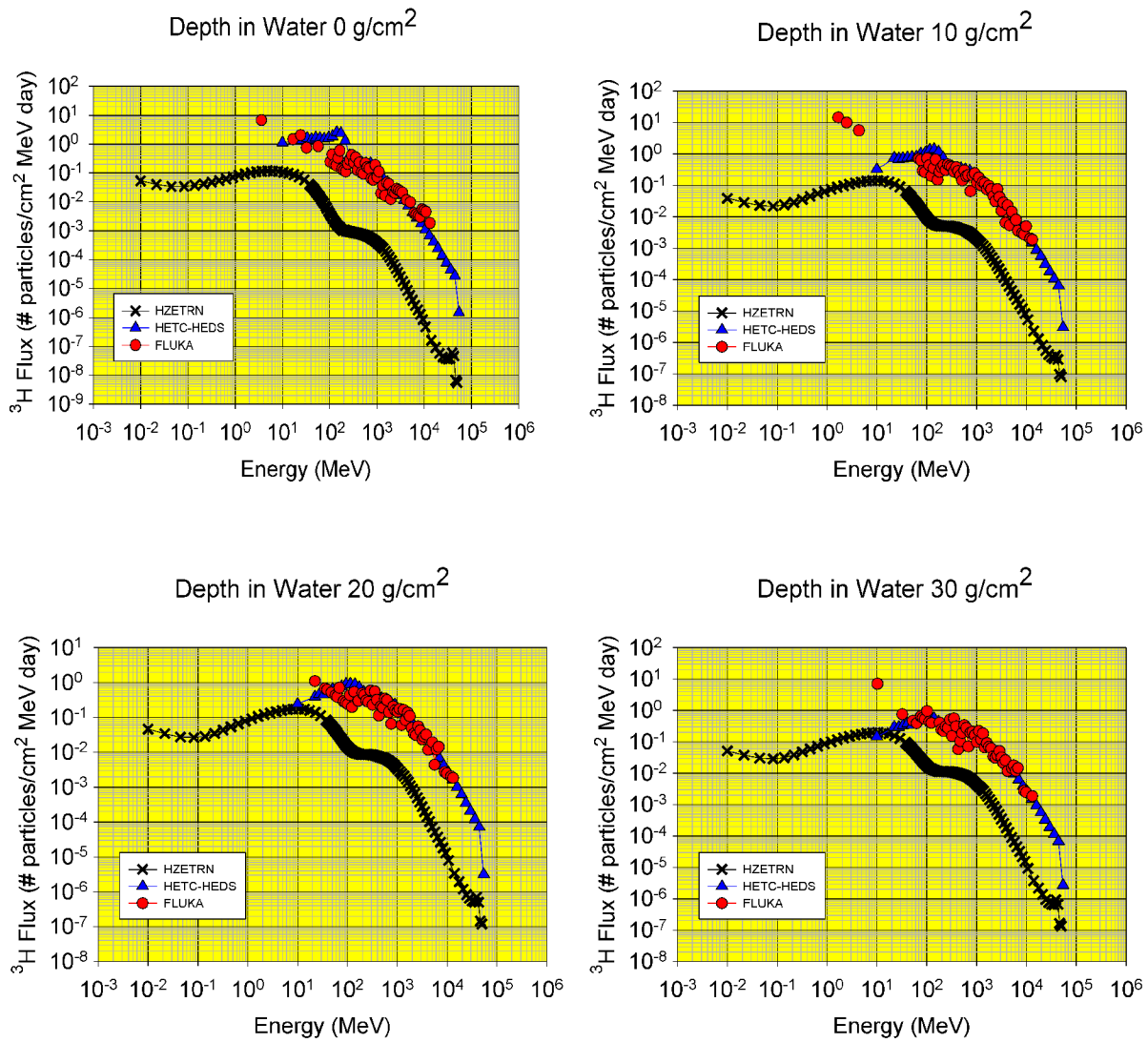


Figure 27: <sup>3</sup>H flux for Carbon on Aluminum shield.

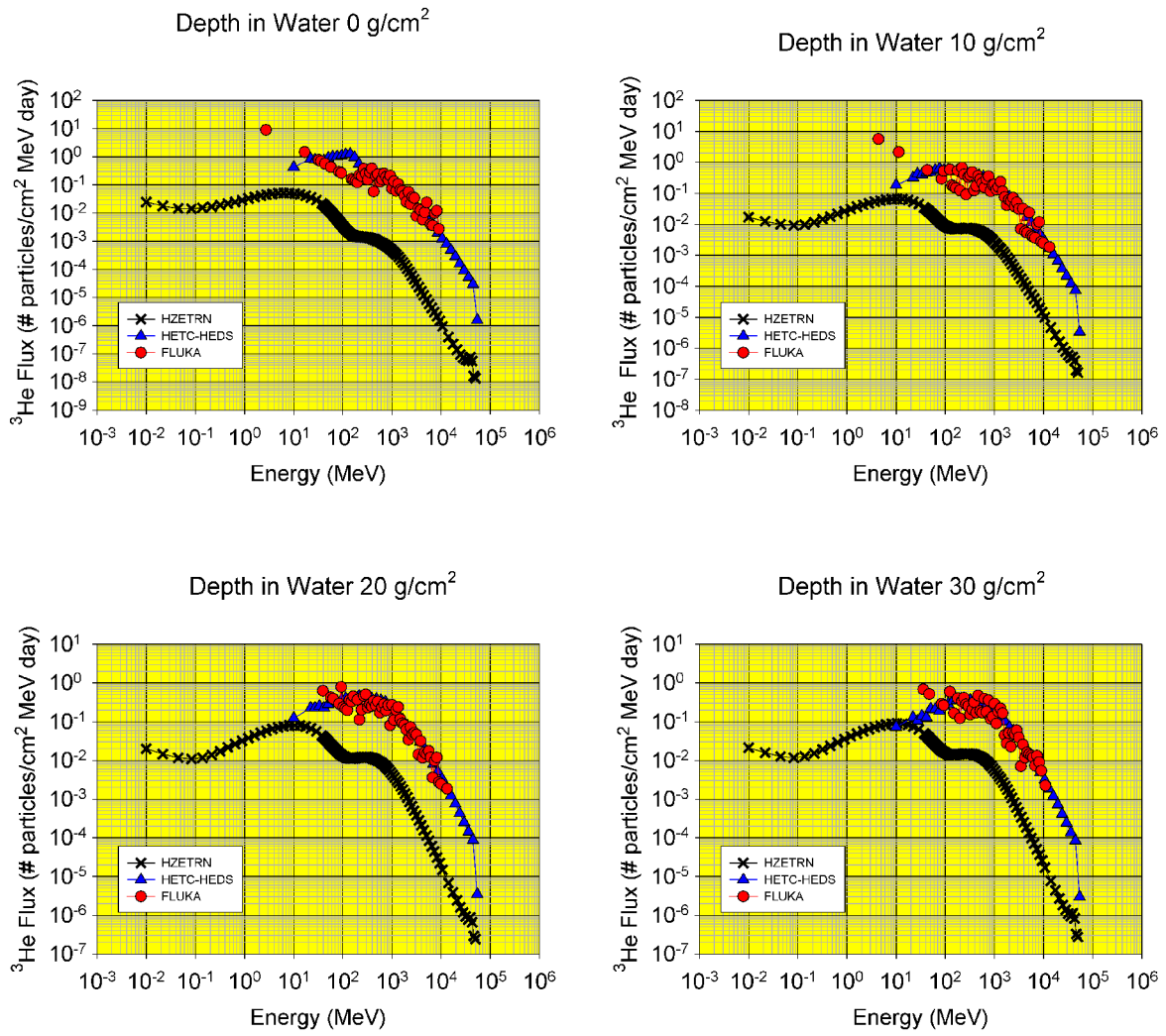


Figure 28:  $^3\text{He}$  flux for Carbon on Aluminum shield.

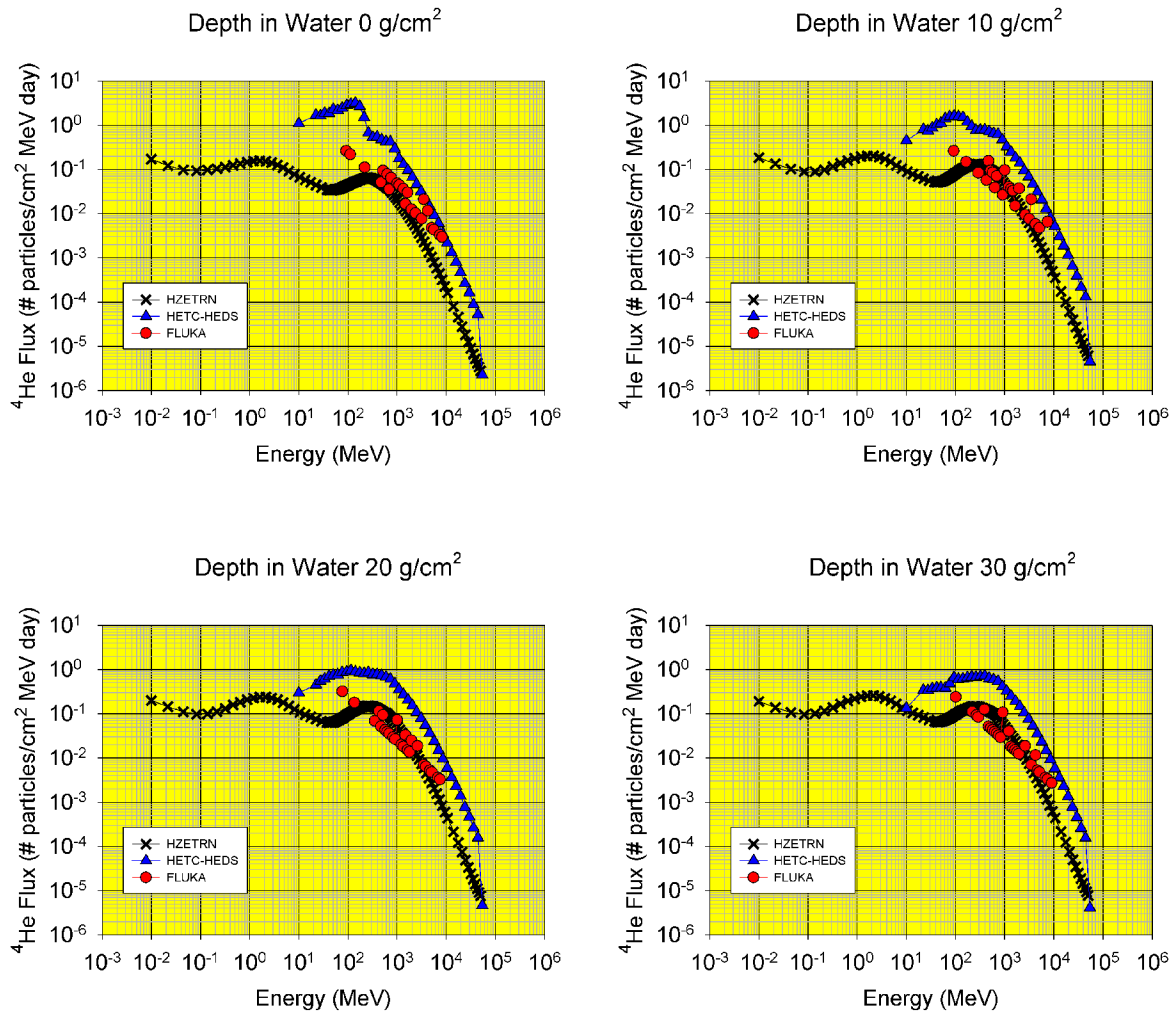


Figure 29:  $^4\text{He}$  flux for Carbon on Aluminum shield.

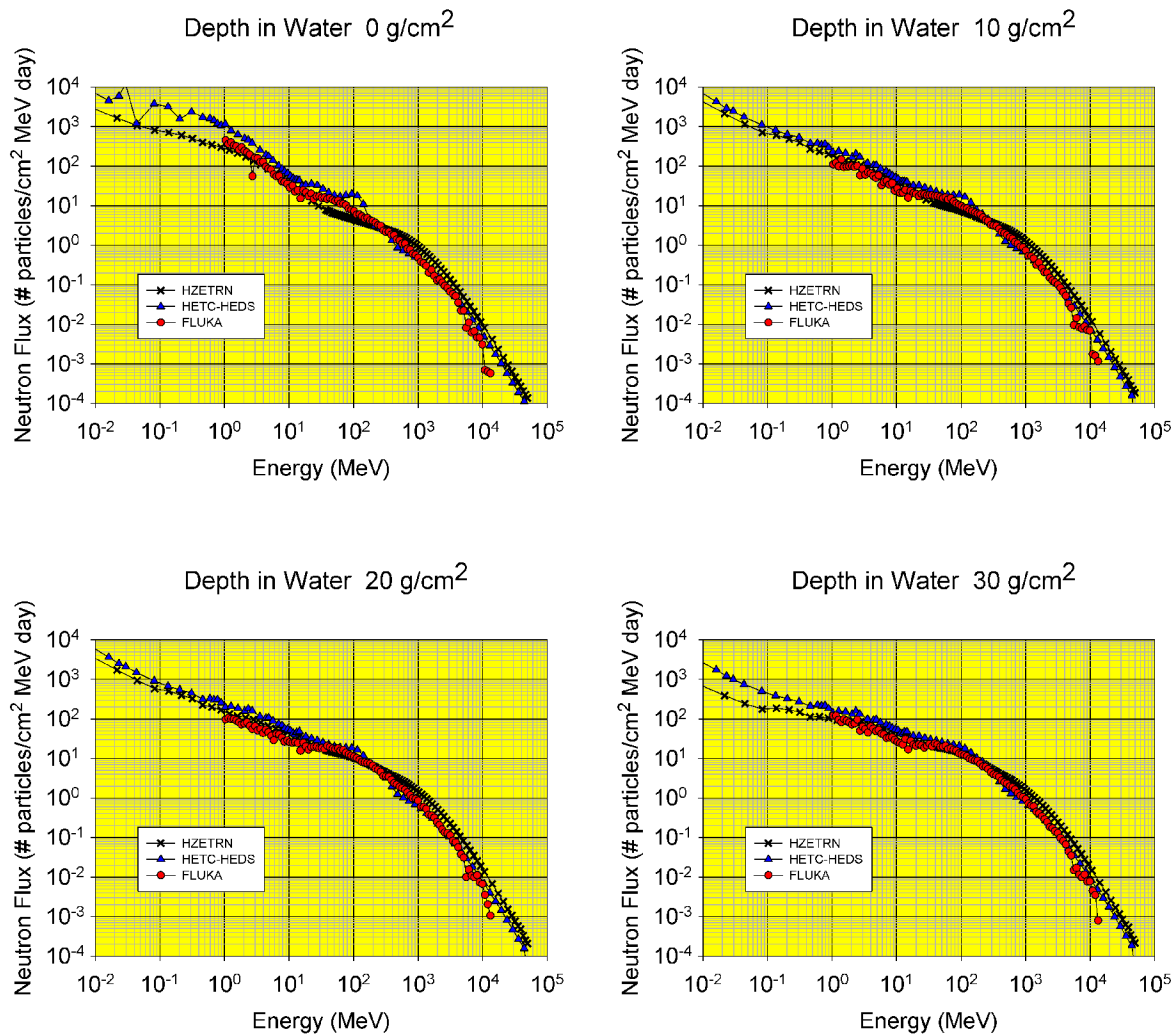


Figure 30: Forward Neutron flux for Oxygen on Aluminum shield.

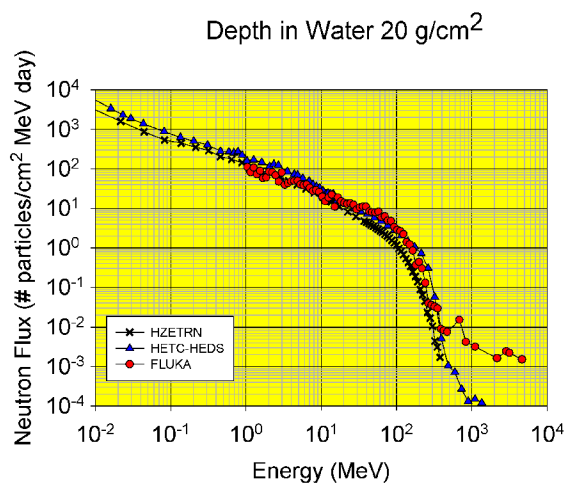
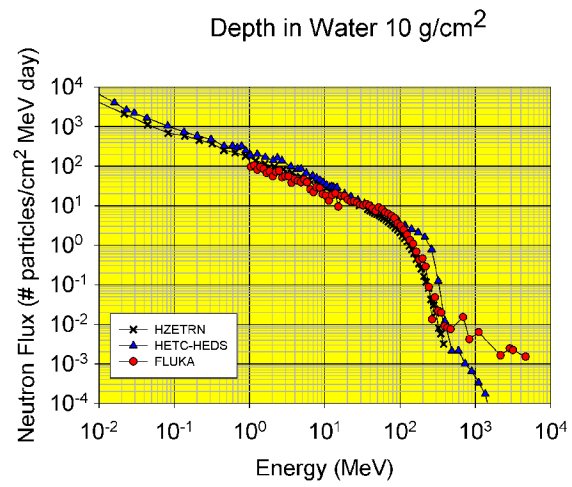
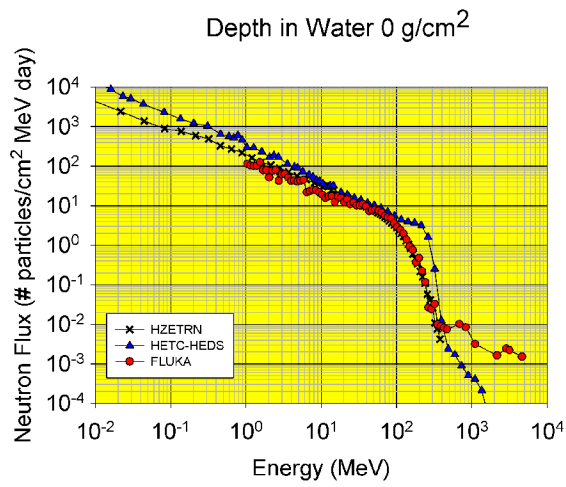


Figure 31: Backward Neutron flux for Oxygen on Aluminum shield.

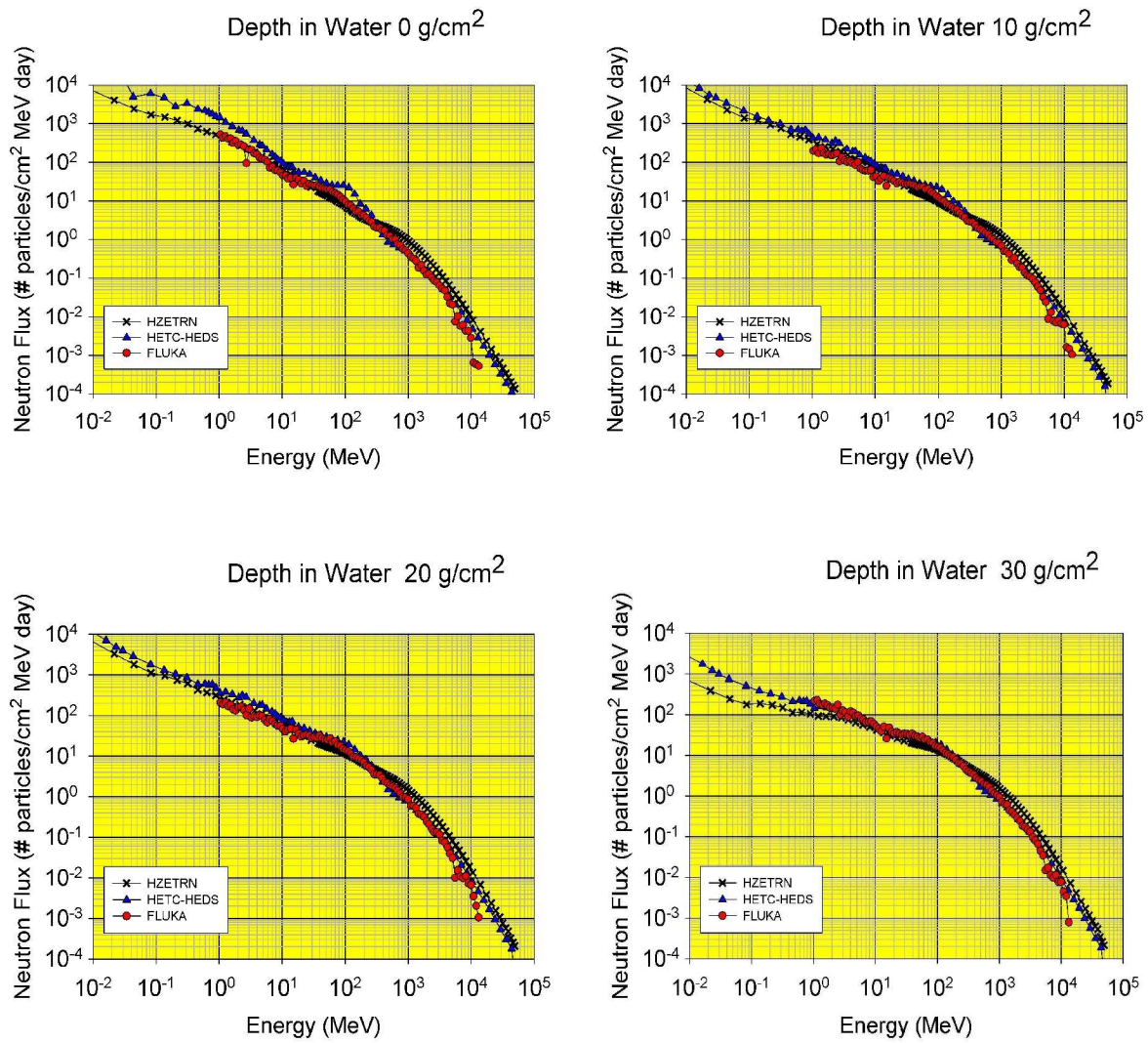


Figure 32: Total Neutron flux for Oxygen on Aluminum shield.

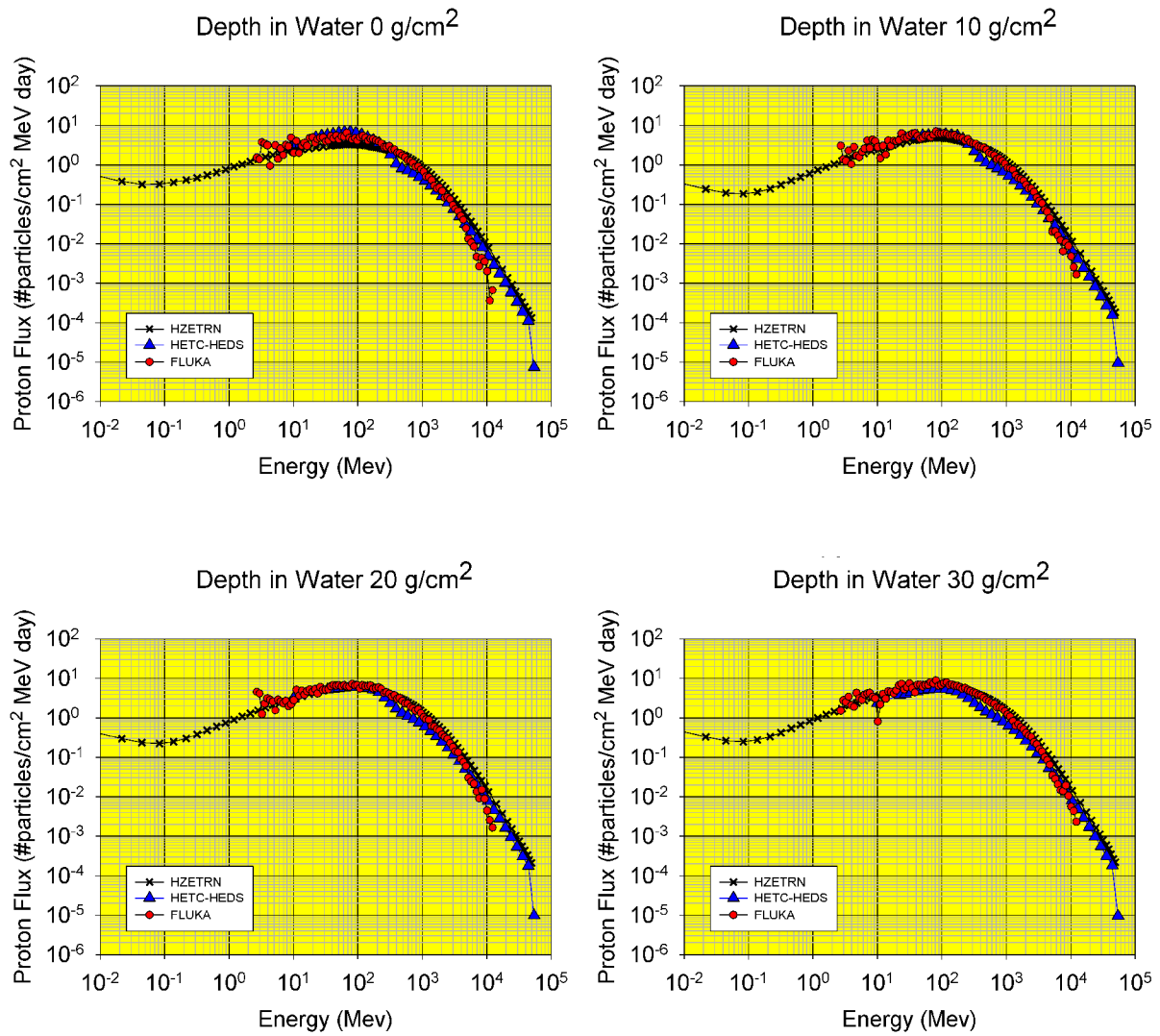


Figure 33: Proton flux for Oxygen on Aluminum shield.

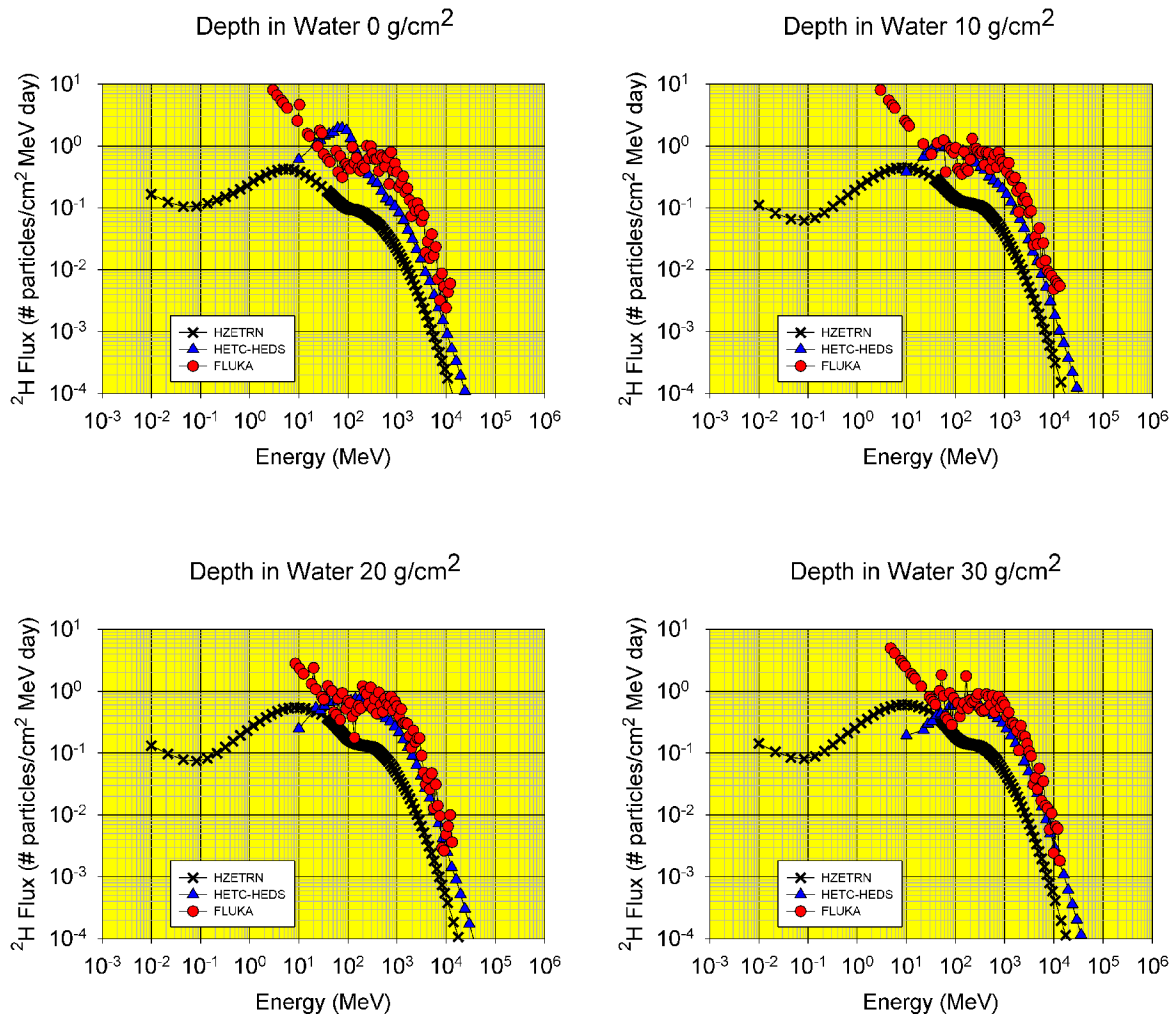


Figure 34:  $^2\text{H}$  flux for Oxygen on Aluminum shield.

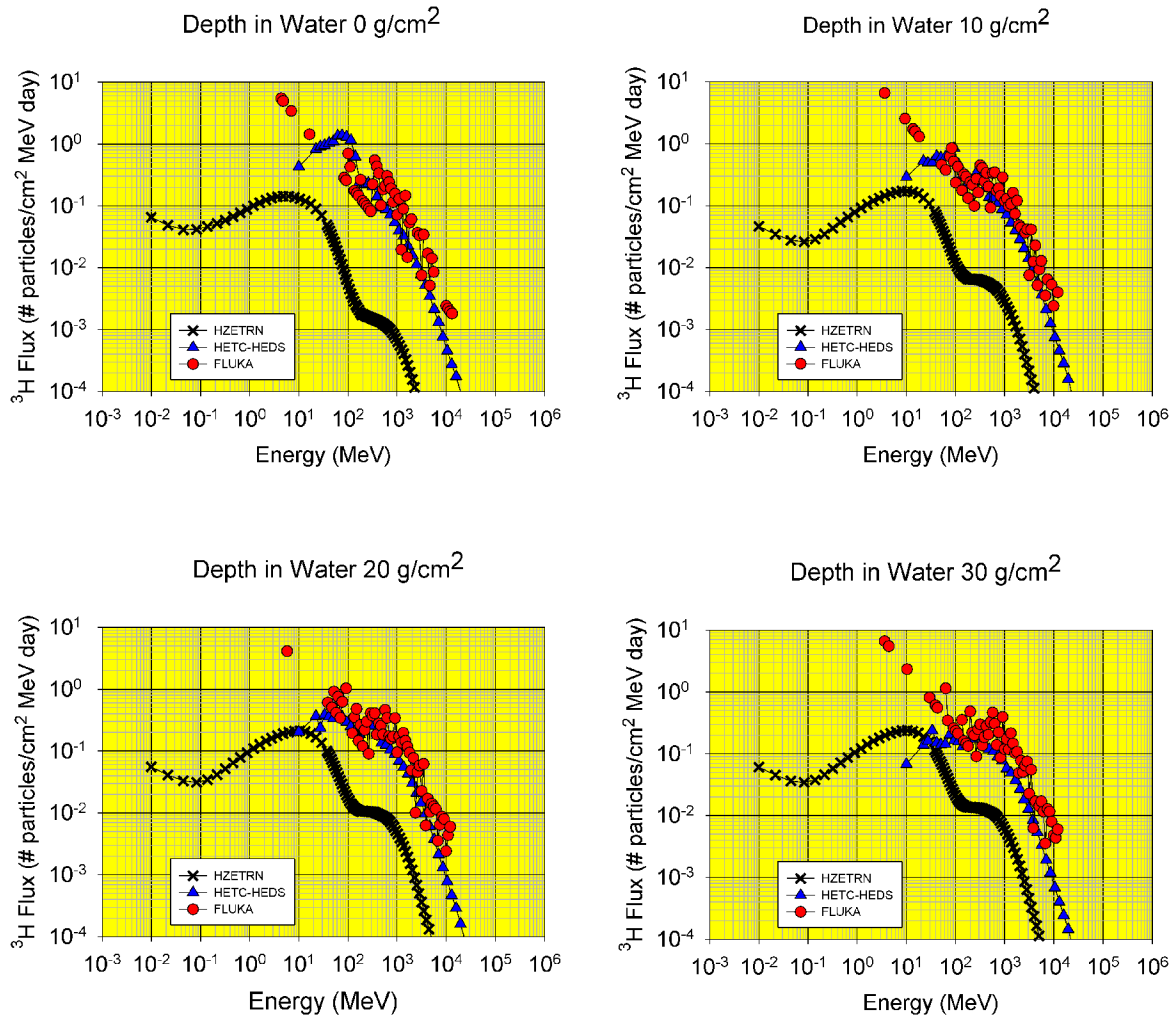


Figure 35:  $^3\text{H}$  flux for Oxygen on Aluminum shield.

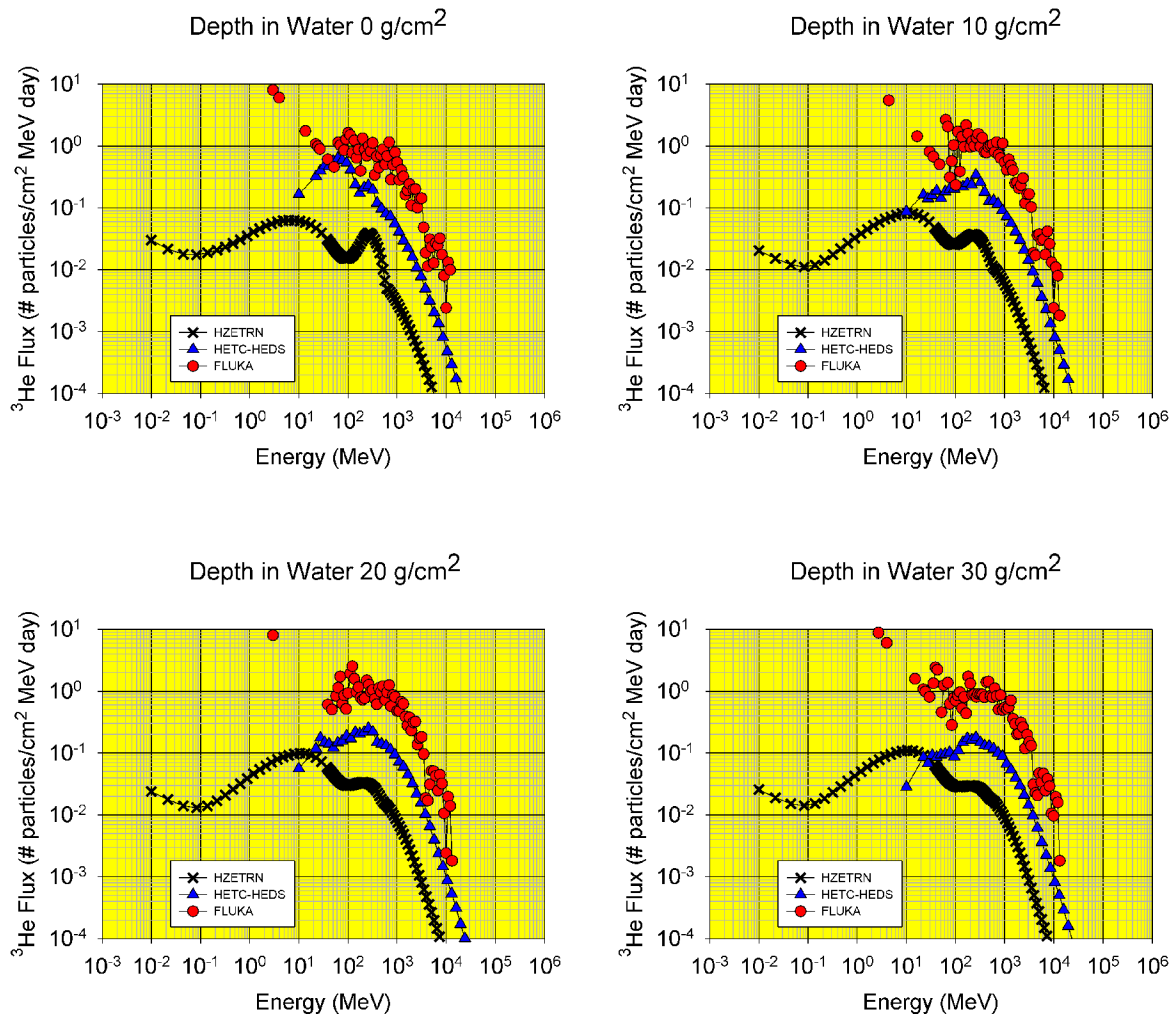


Figure 36:  $^3\text{He}$  flux for Oxygen on Aluminum shield.

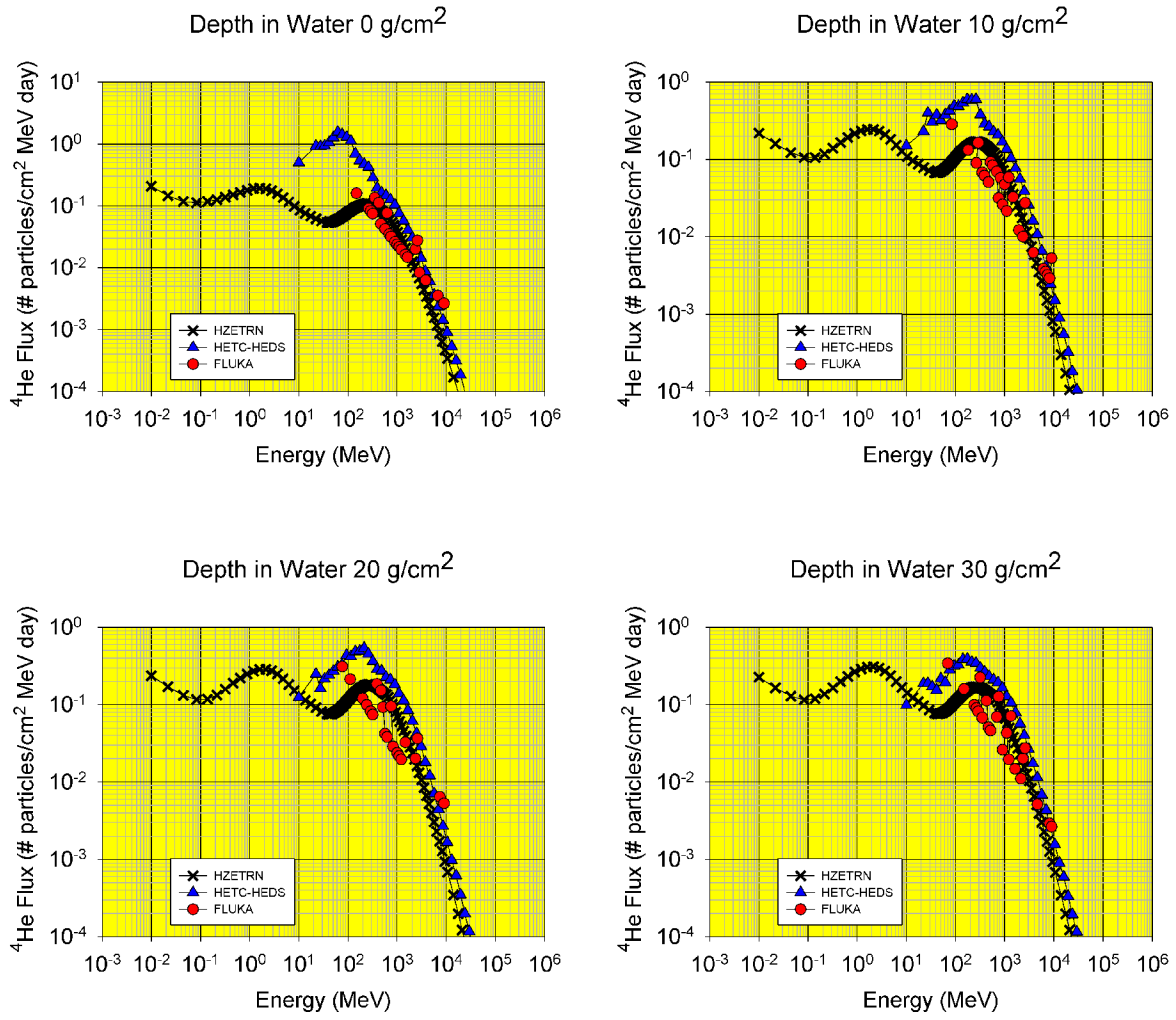


Figure 37:  $^4\text{He}$  flux for Oxygen on Aluminum shield.

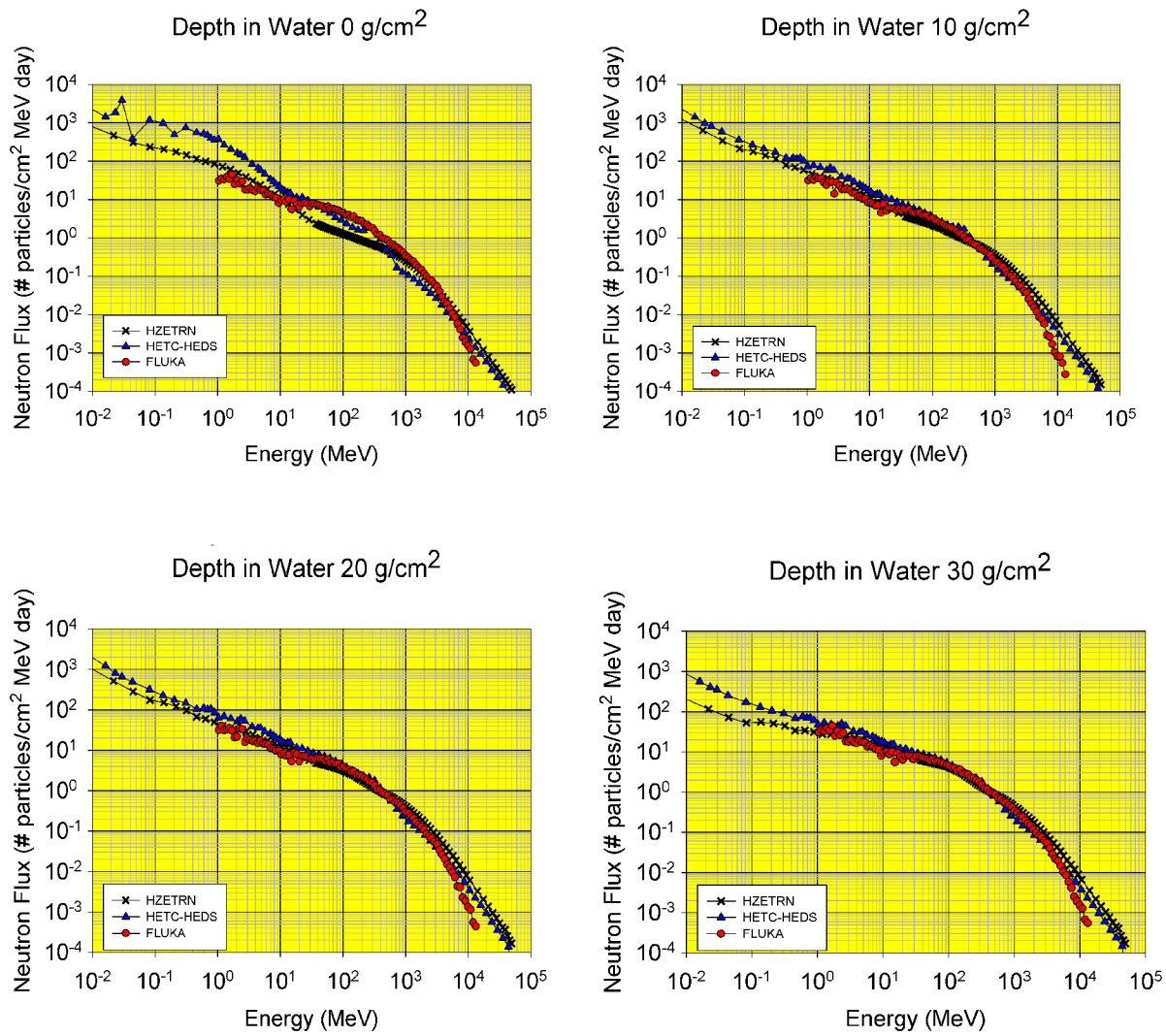


Figure 38: Forward Neutron flux for Magnesium on Aluminum shield.

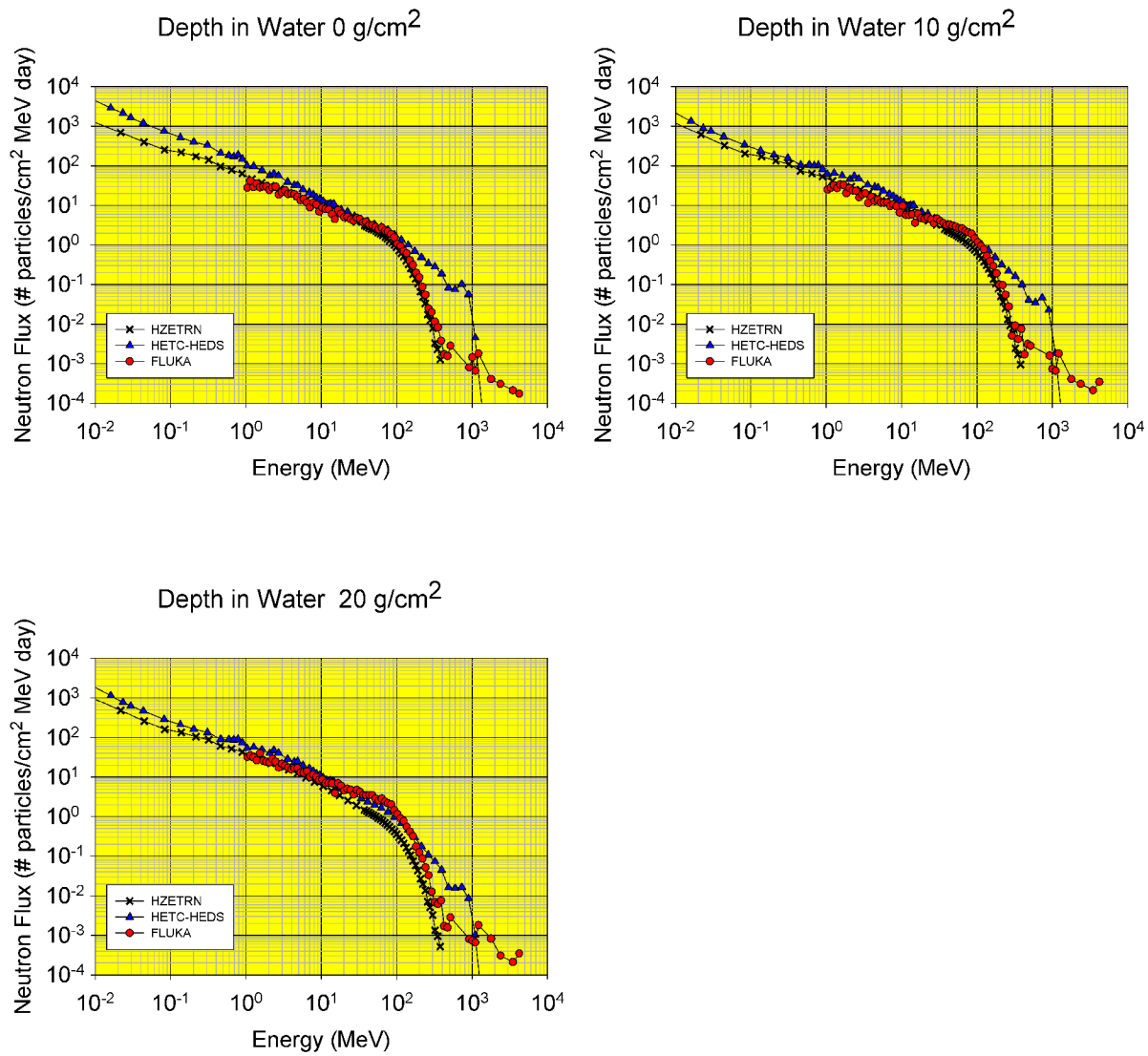


Figure 39: Backward Neutron flux for Magnesium on Aluminum shield.

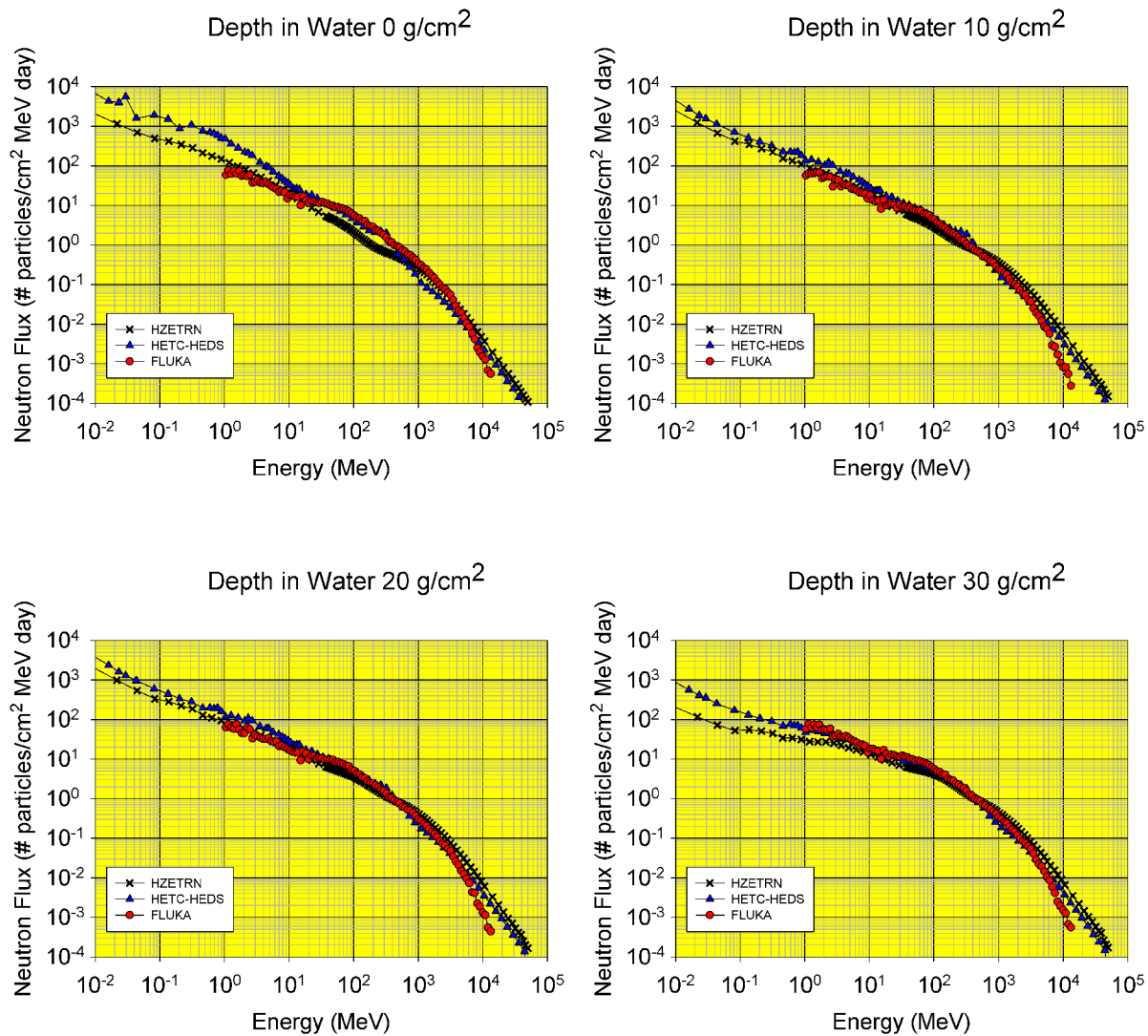


Figure 40: Total Neutron flux for Magnesium on Aluminum shield.

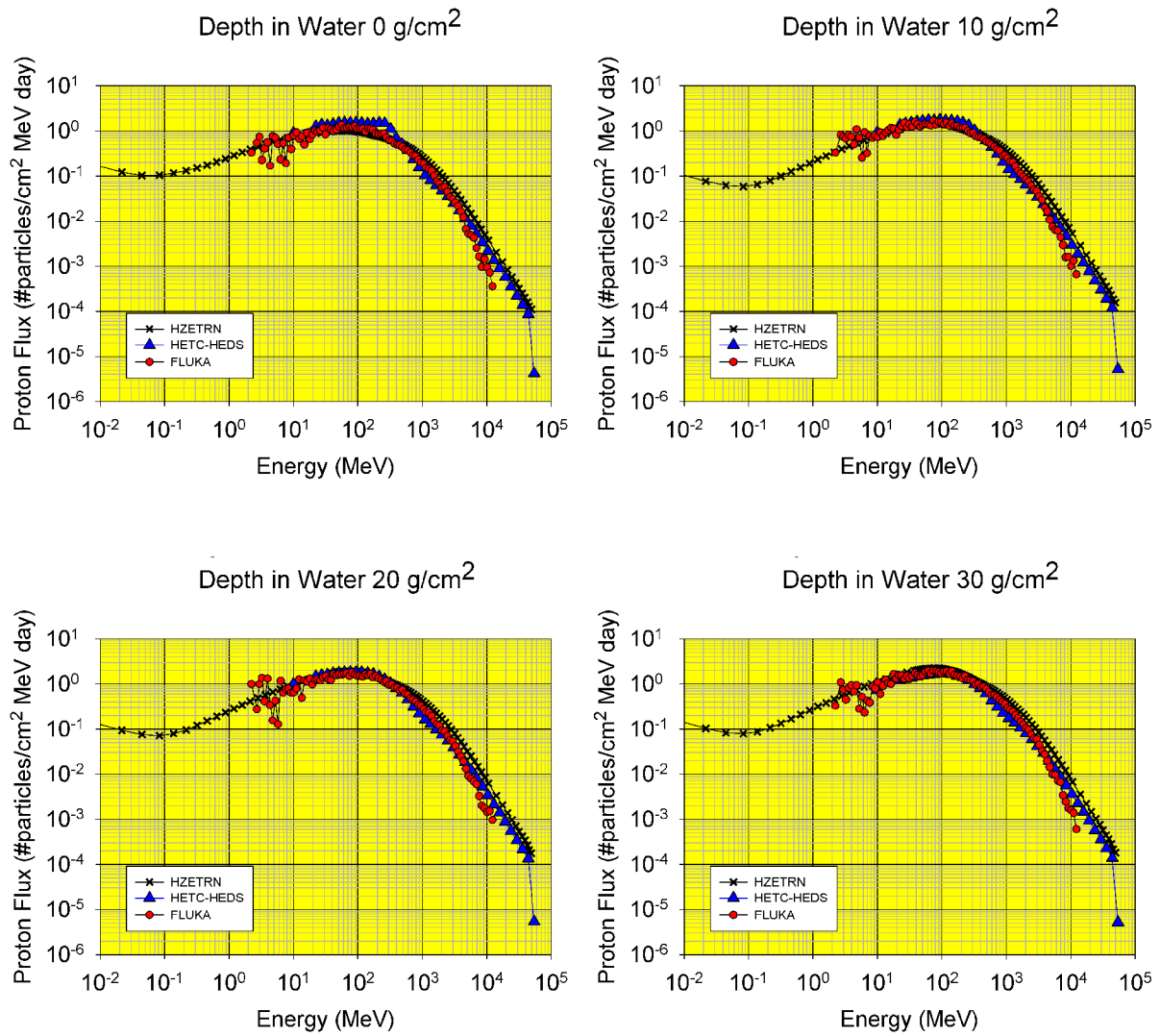


Figure 41: Proton flux for Magnesium on Aluminum shield.

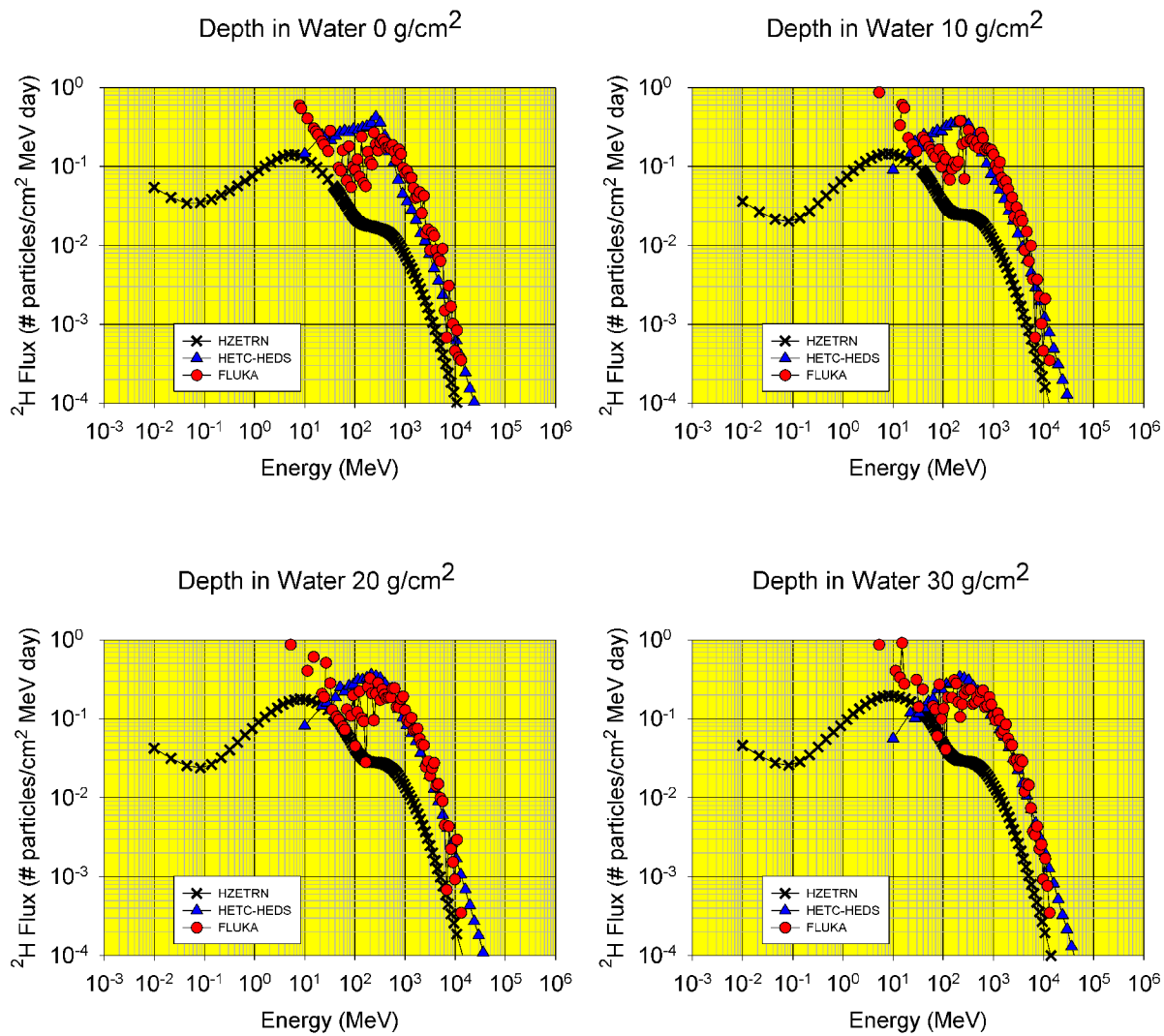


Figure 42:  $^2\text{H}$  flux for Magnesium on Aluminum shield.

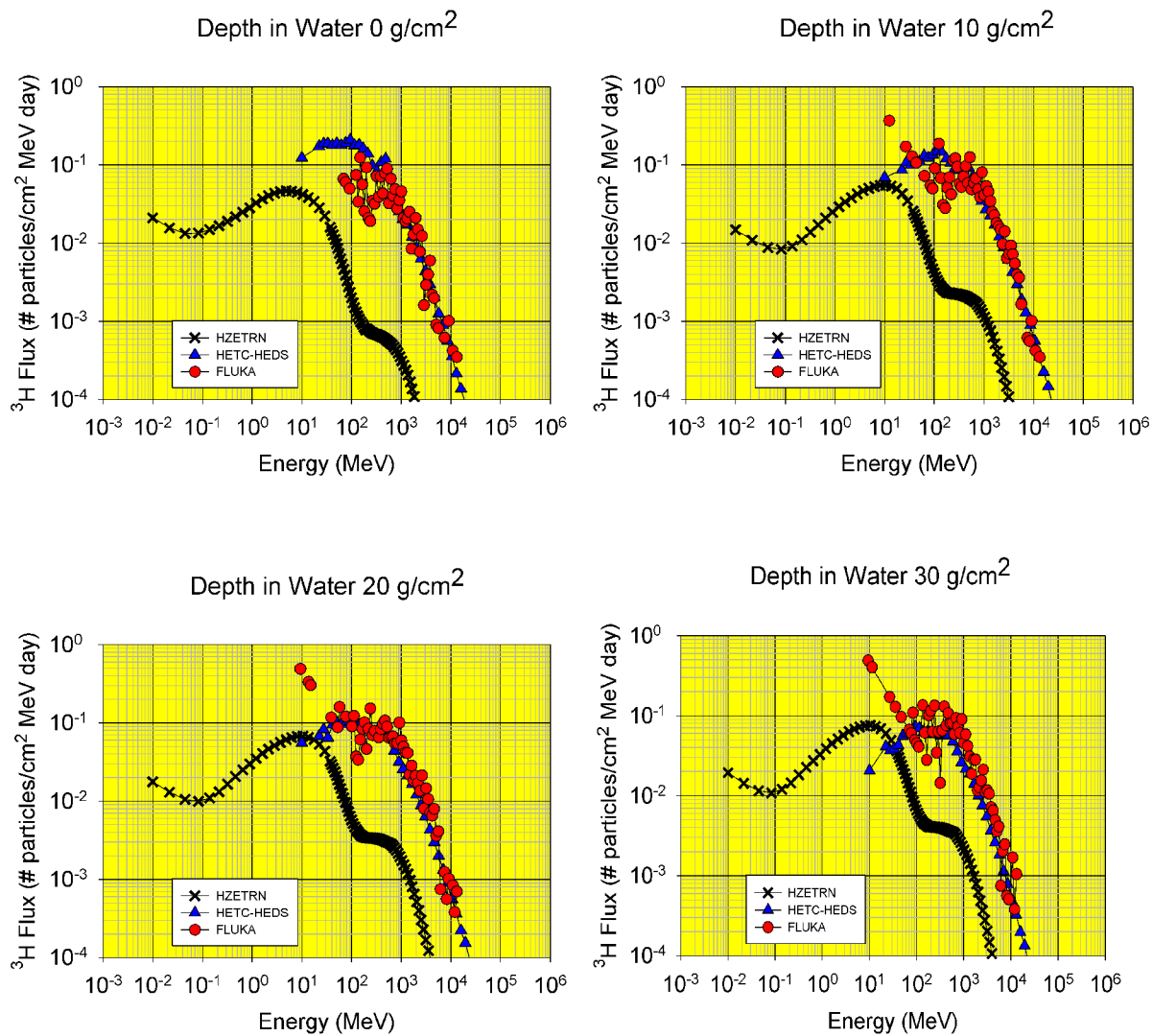


Figure 43:  $^3\text{H}$  flux for Magnesium on Aluminum shield.

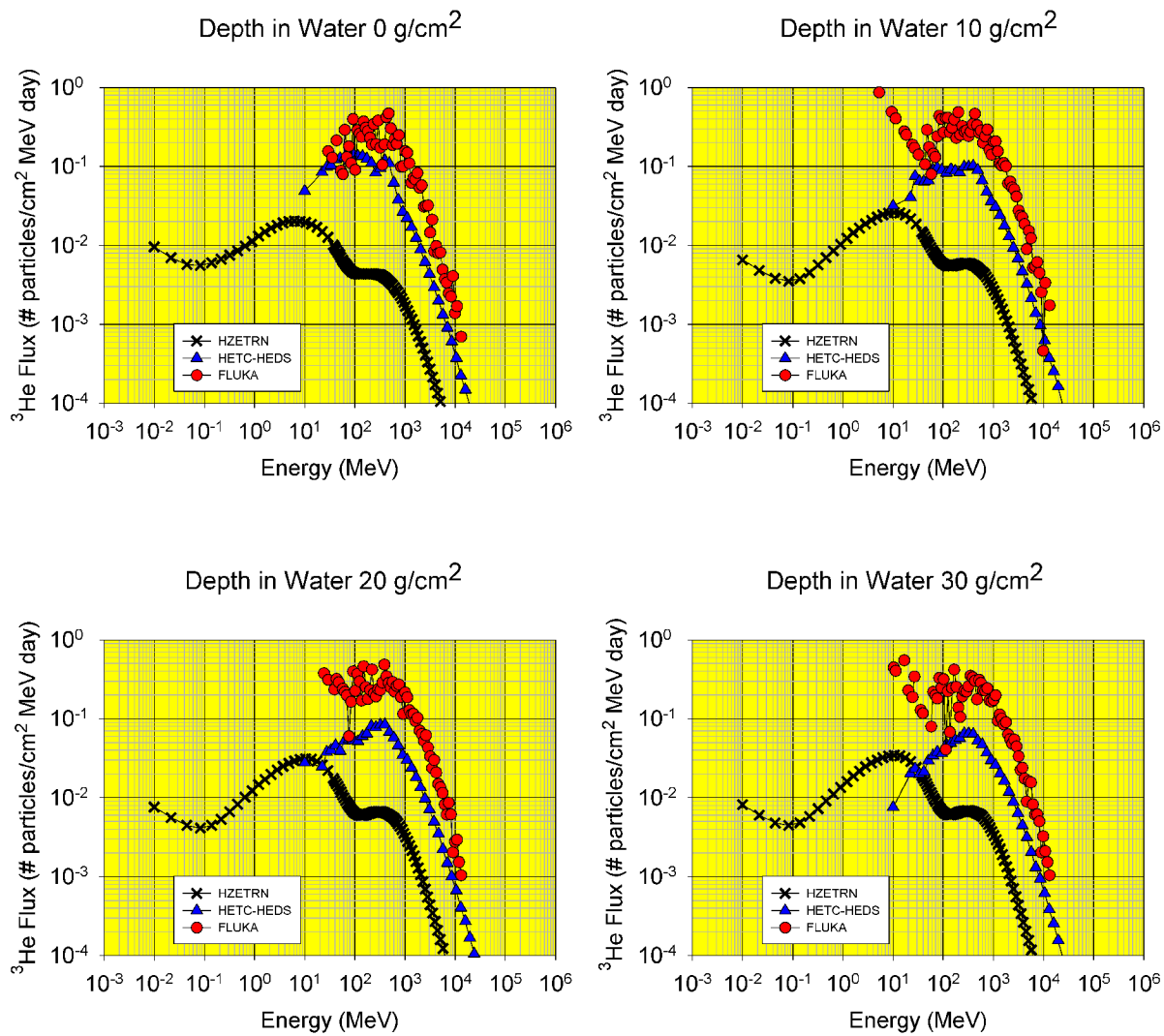


Figure 44:  $^3\text{He}$  flux for Magnesium on Aluminum shield.

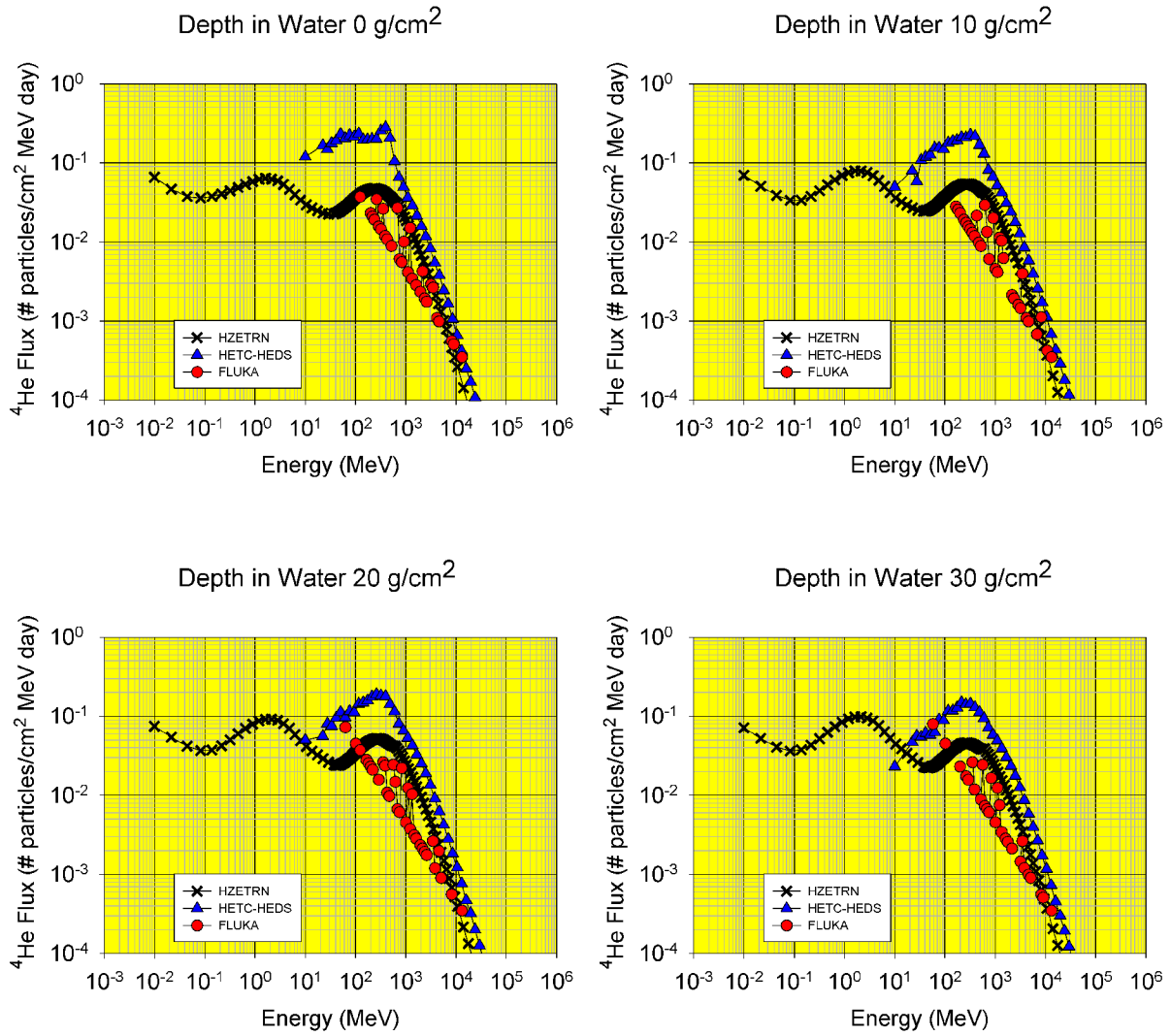


Figure 45:  $^4\text{He}$  flux for Magnesium on Aluminum shield.

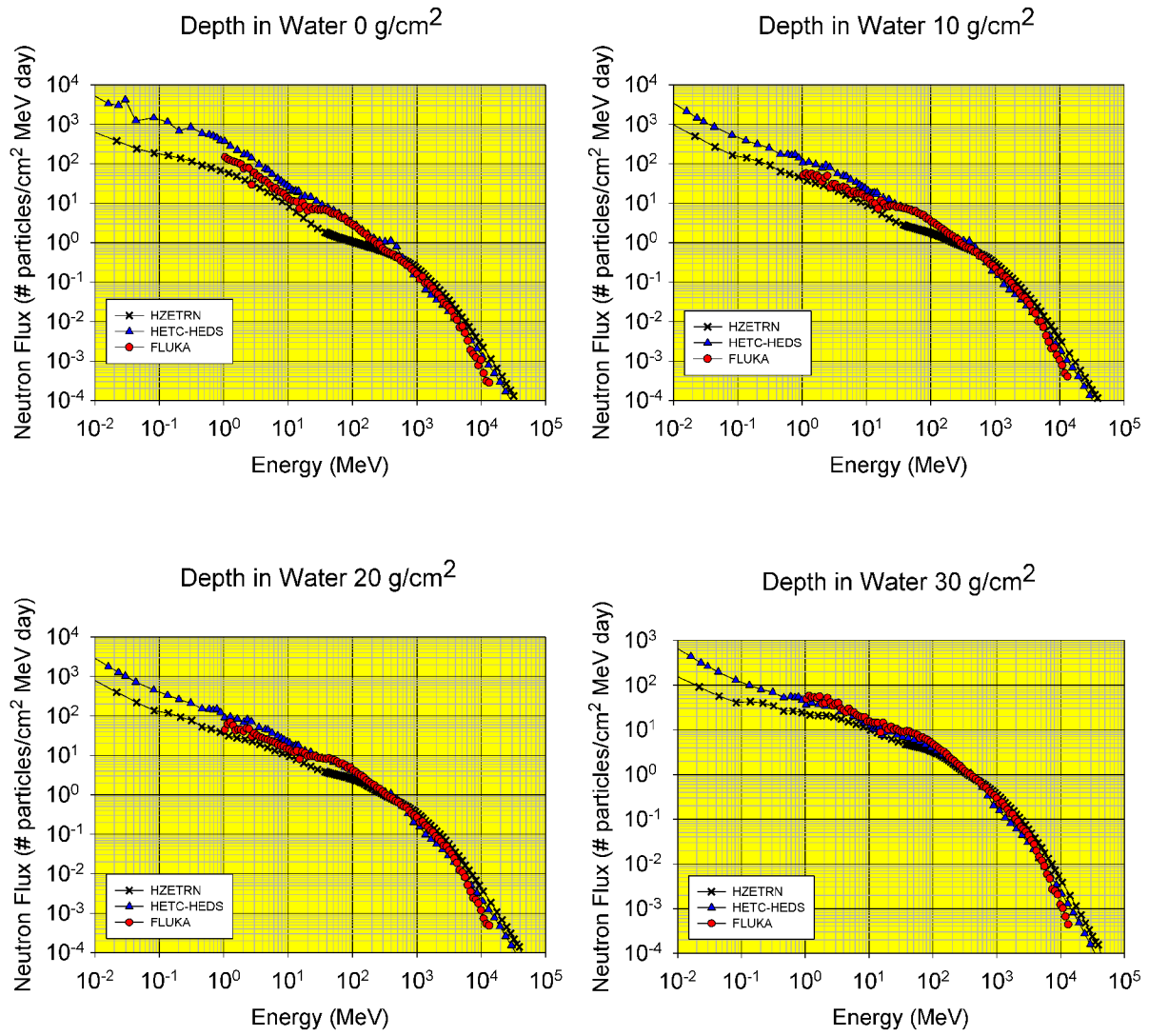


Figure 46: Forward Neutron flux for Silicon on Aluminum shield.

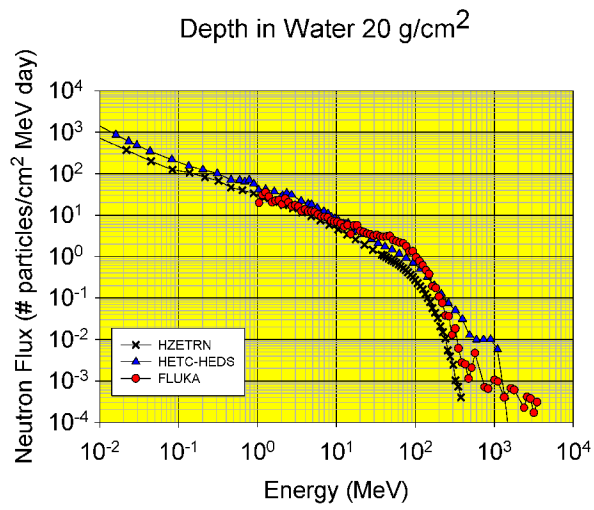
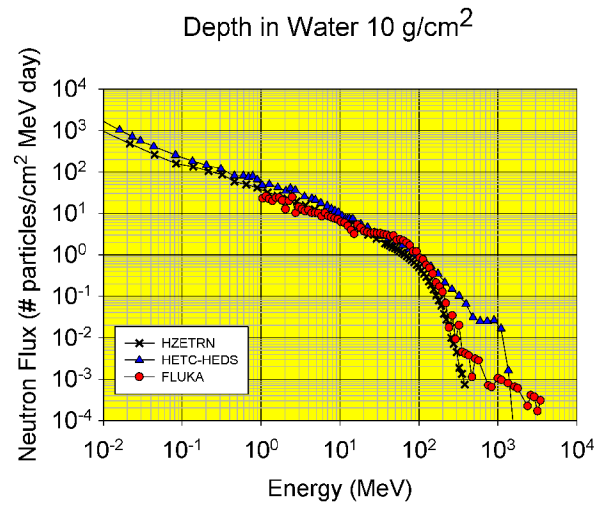
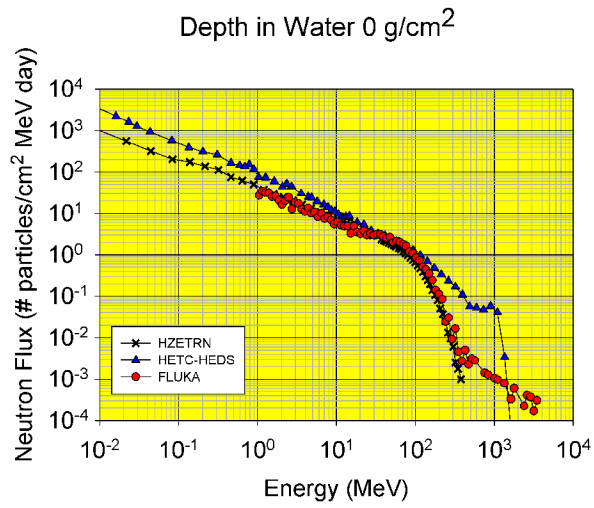


Figure 47: Backward Neutron flux for Silicon on Aluminum shield.

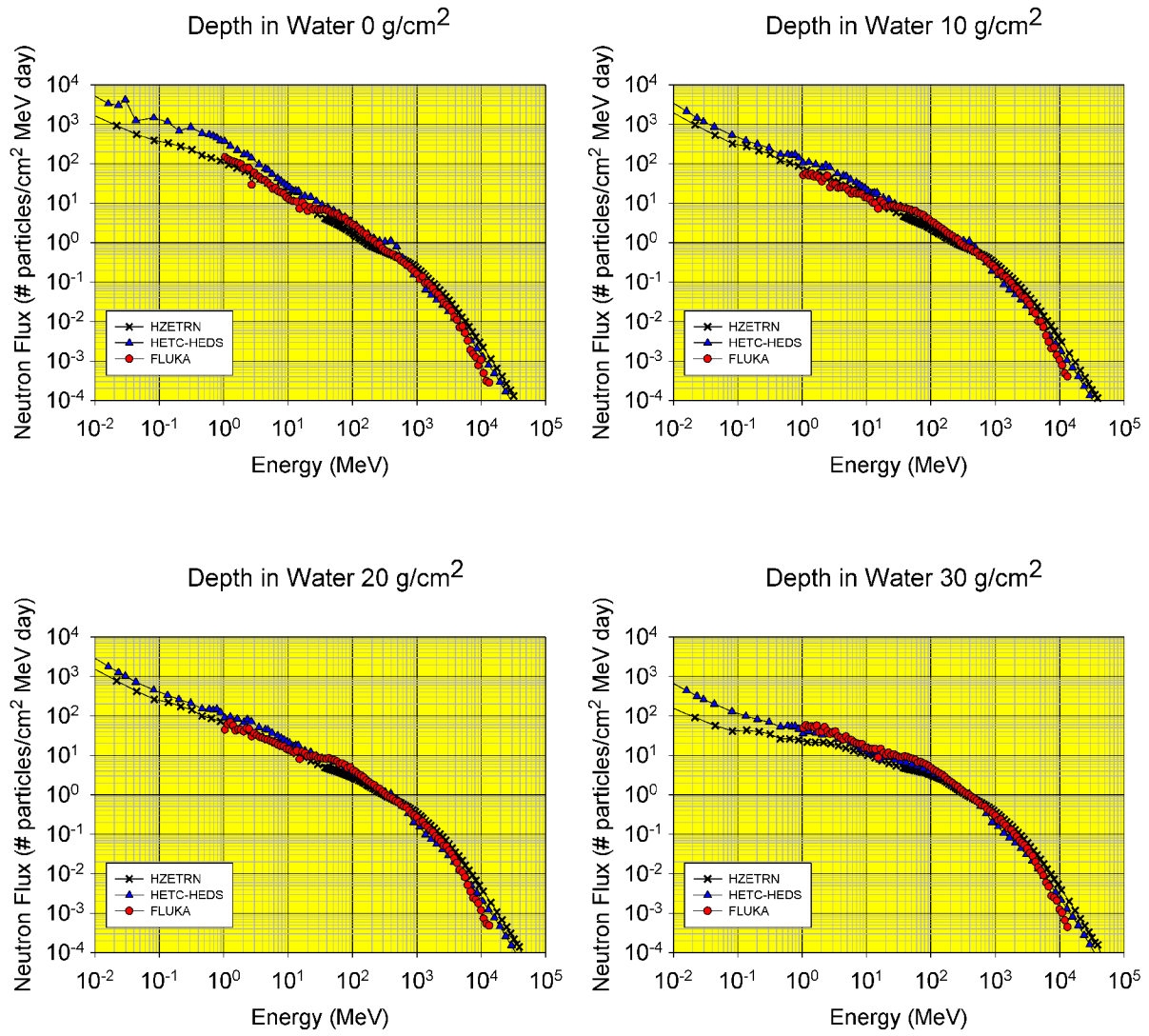


Figure 48: Total Neutron flux for Silicon on Aluminum shield.

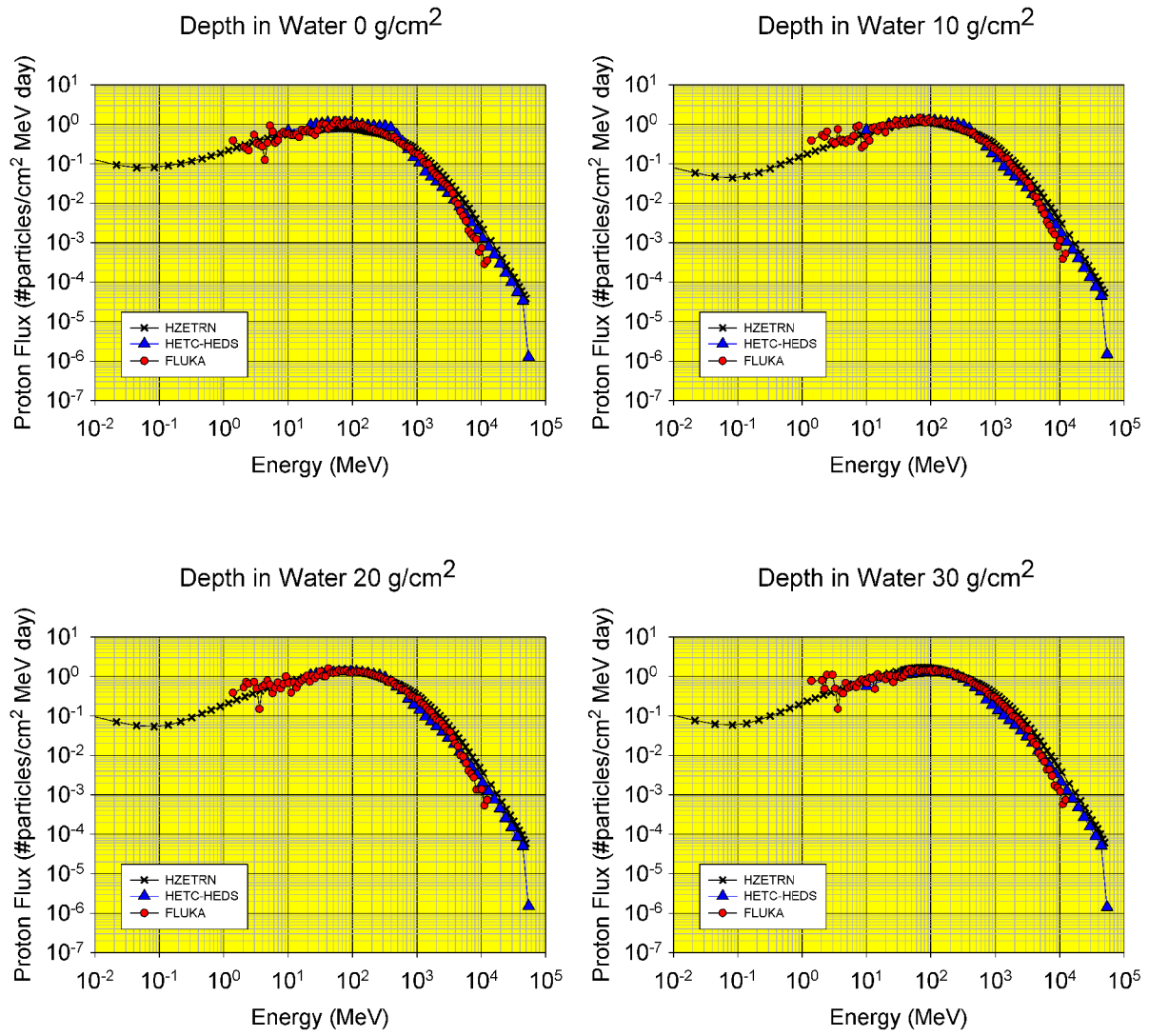


Figure 49: Proton flux for Silicon on Aluminum shield.

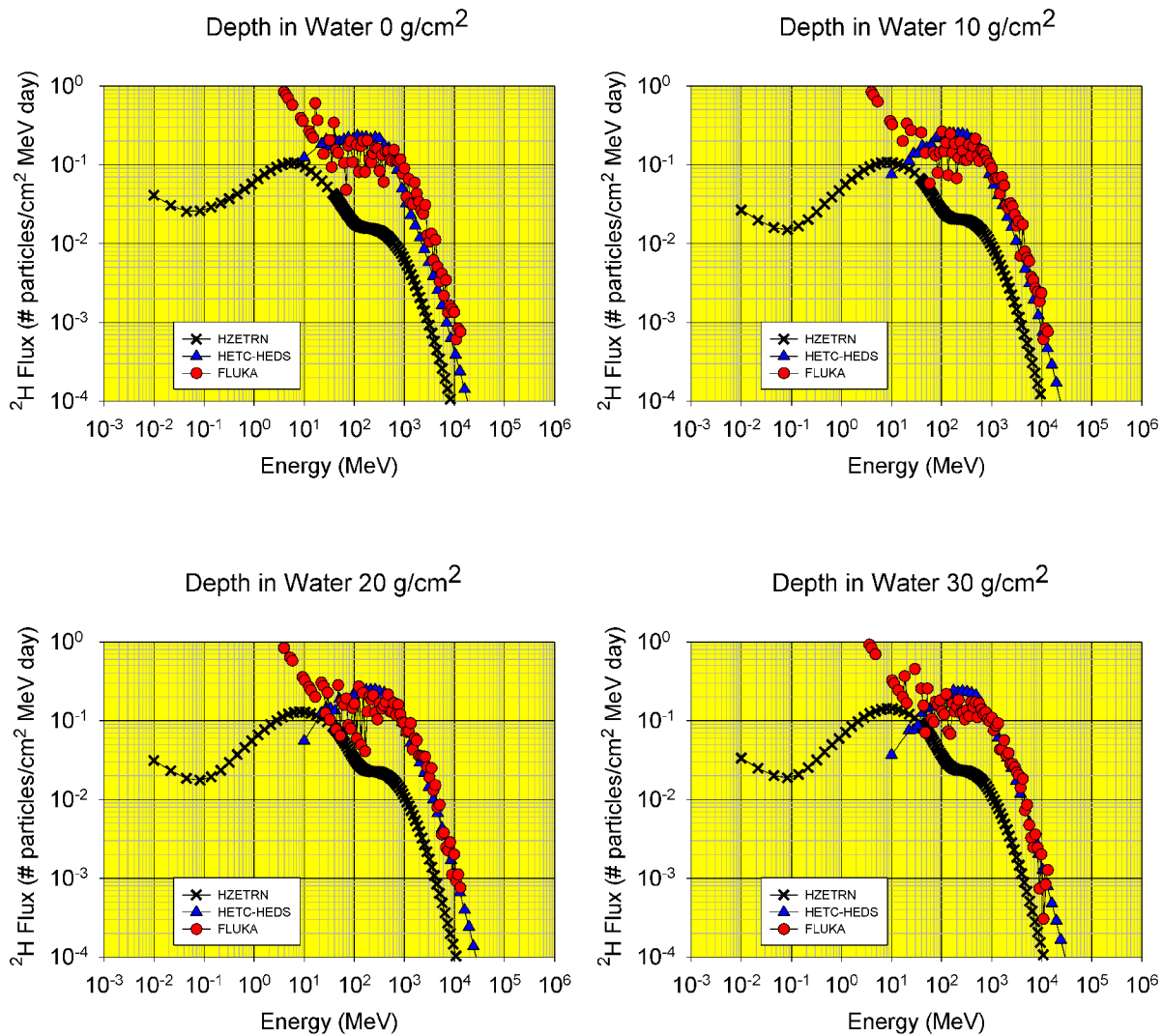


Figure 50:  $^2\text{H}$  flux for Silicon on Aluminum shield.

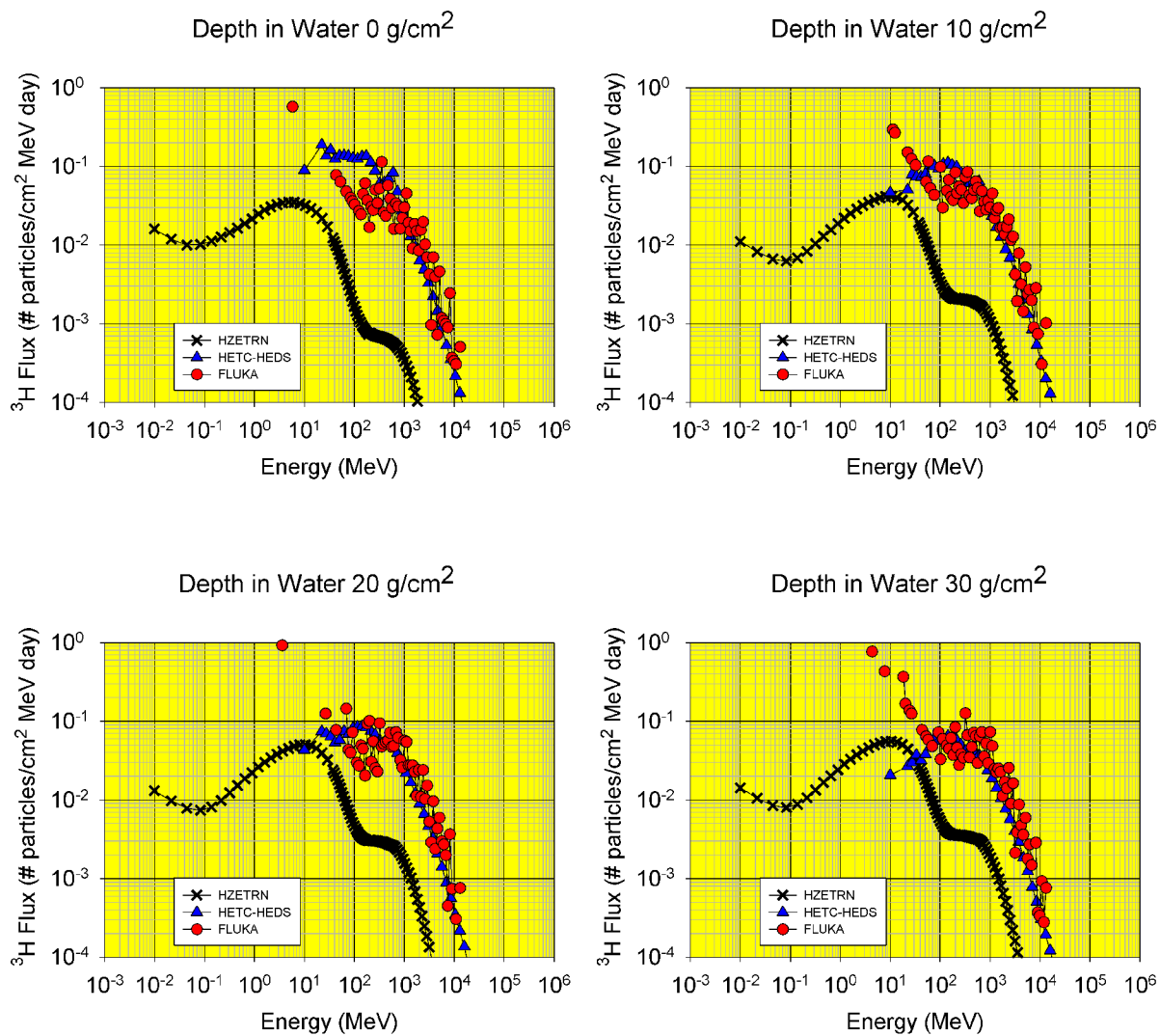


Figure 51:  $^3\text{H}$  flux for Silicon on Aluminum shield.

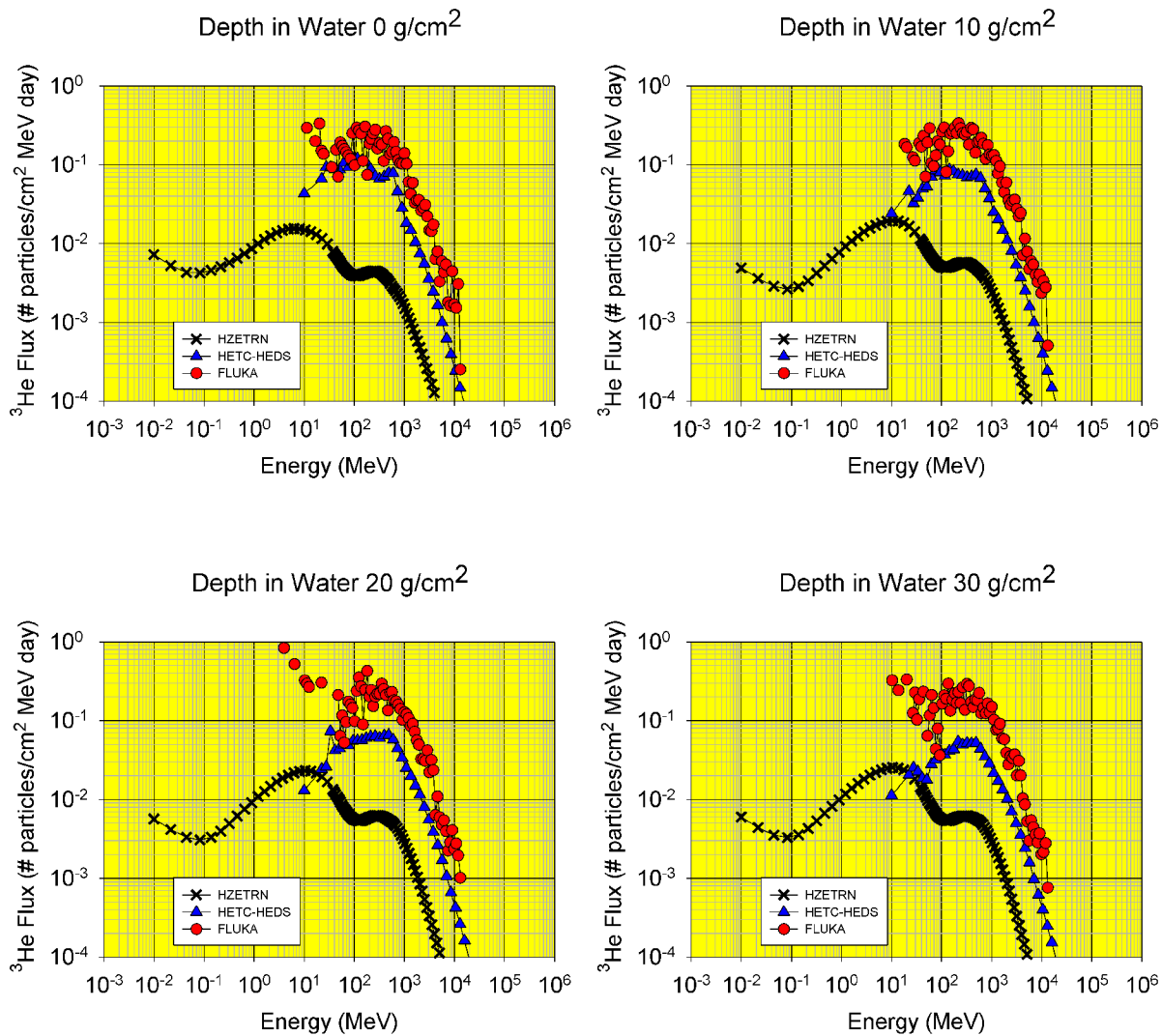


Figure 52:  $^3\text{He}$  flux for Silicon on Aluminum shield.

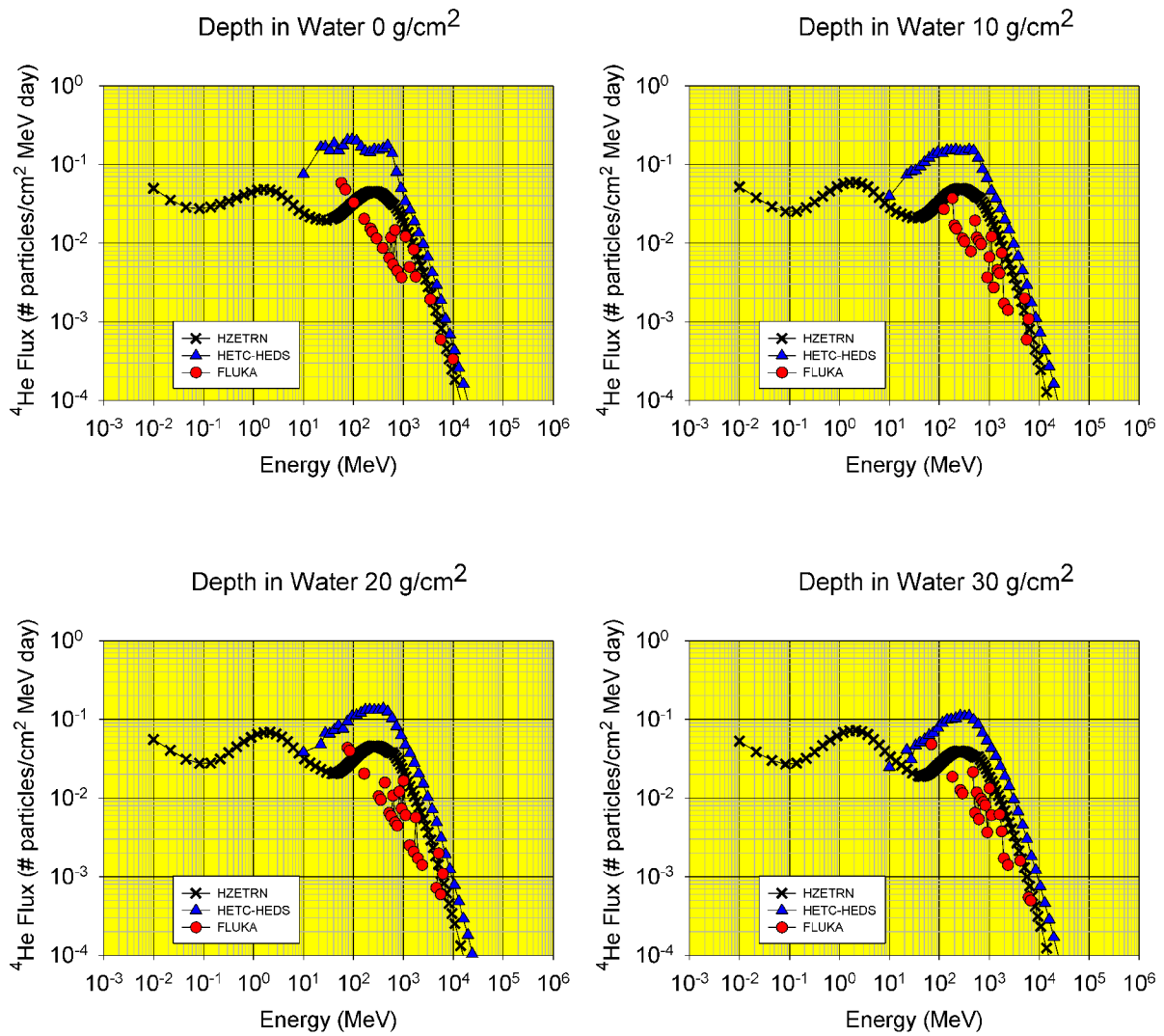


Figure 53:  $^4\text{He}$  flux for Silicon on Aluminum shield.

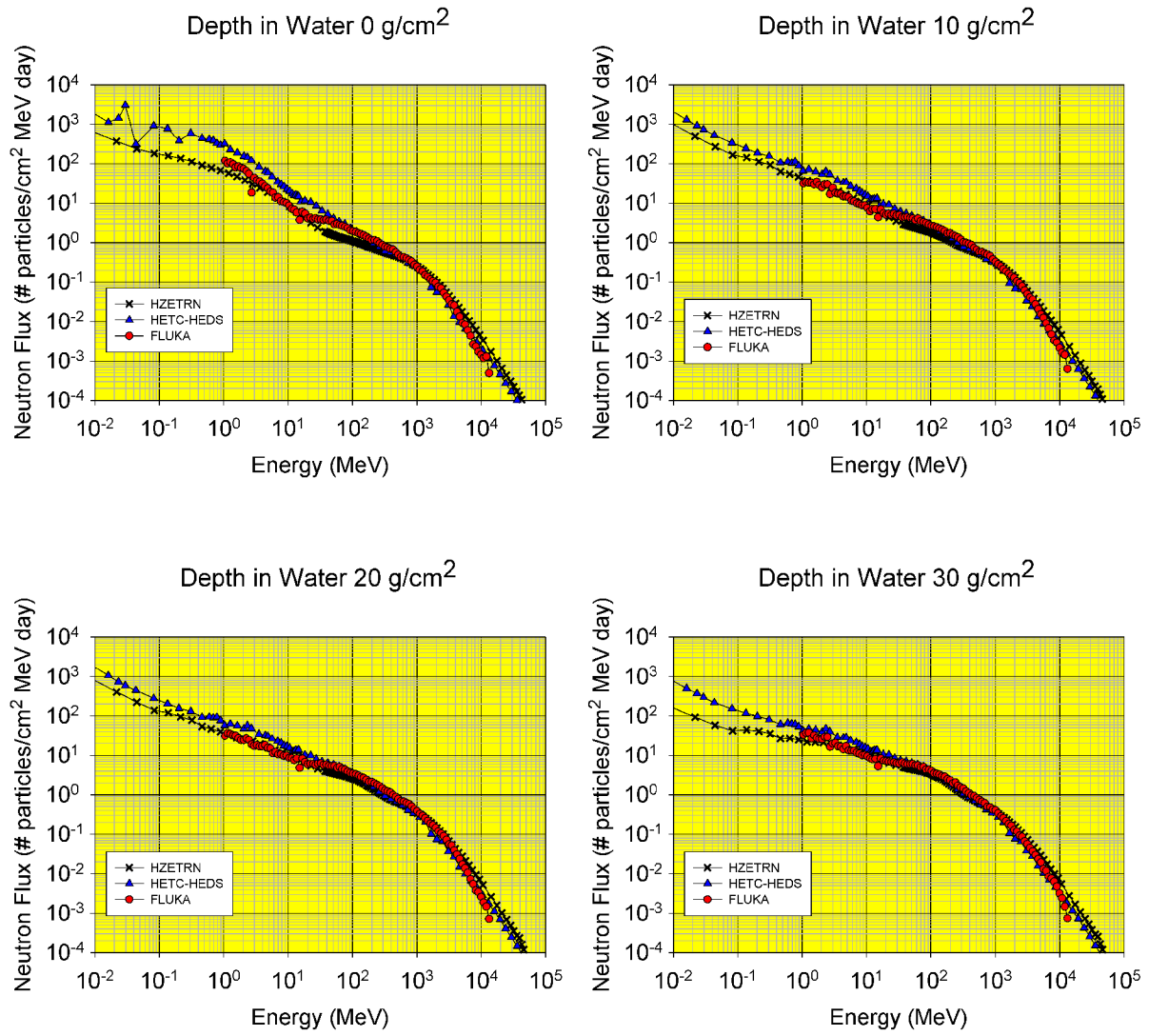


Figure 54: Forward Neutron flux for Iron on Aluminum shield.

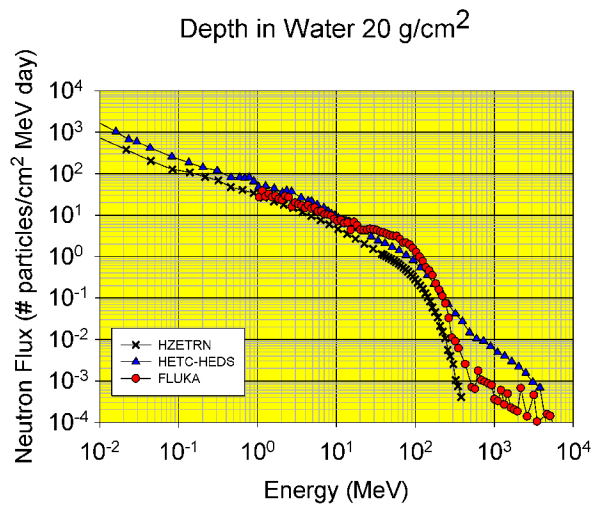
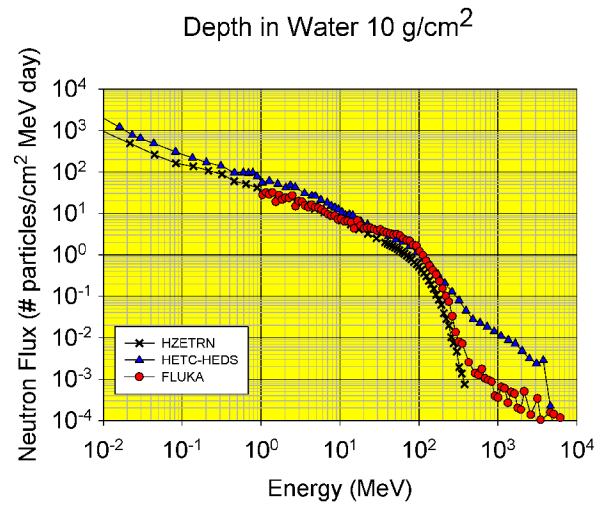
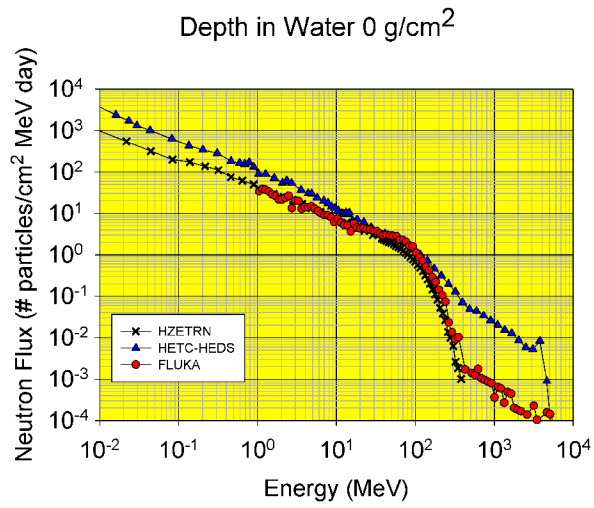


Figure 55: Backward Neutron flux for Iron on Aluminum shield.

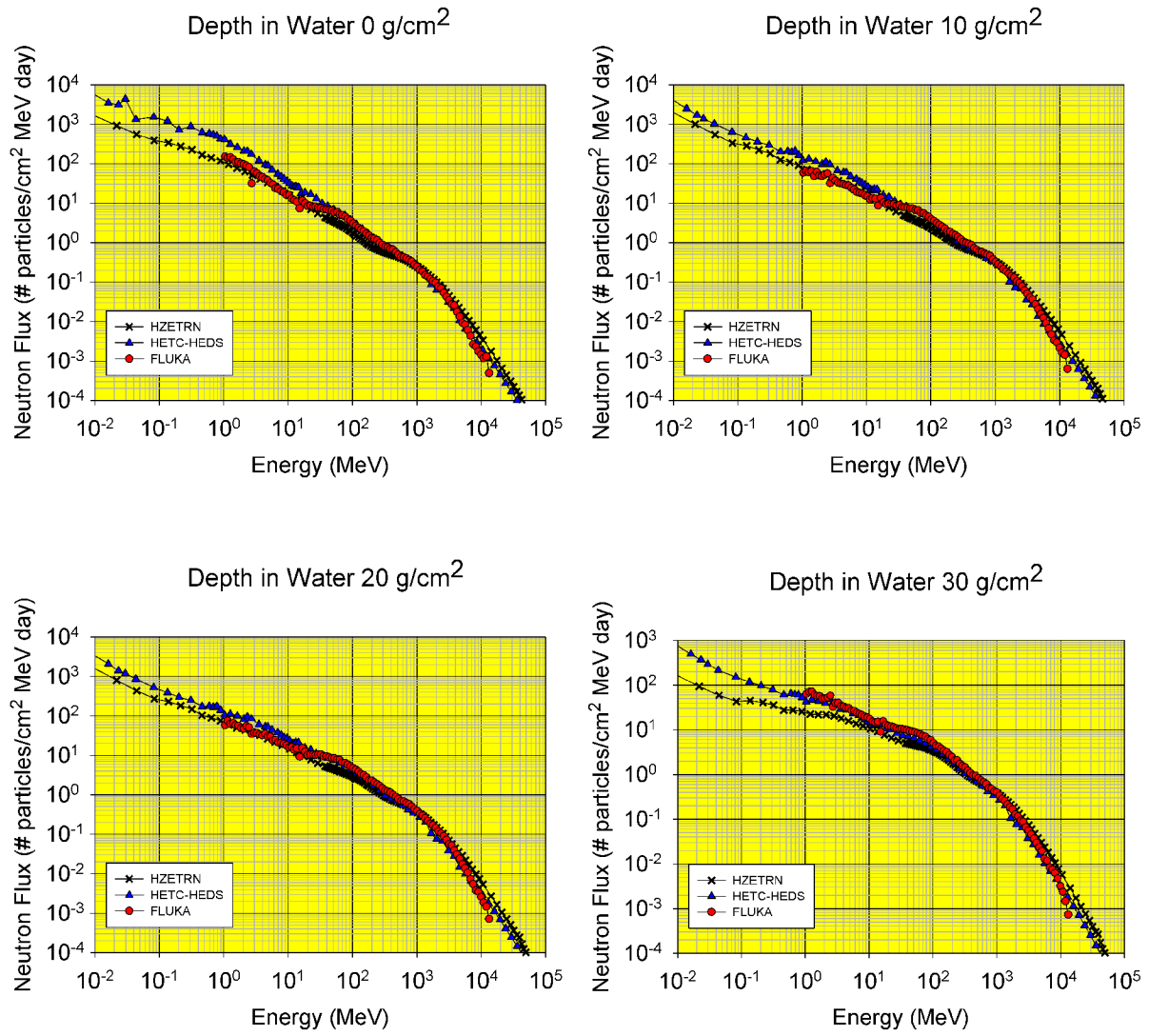


Figure 56: Total Neutron flux for Iron on Aluminum shield.

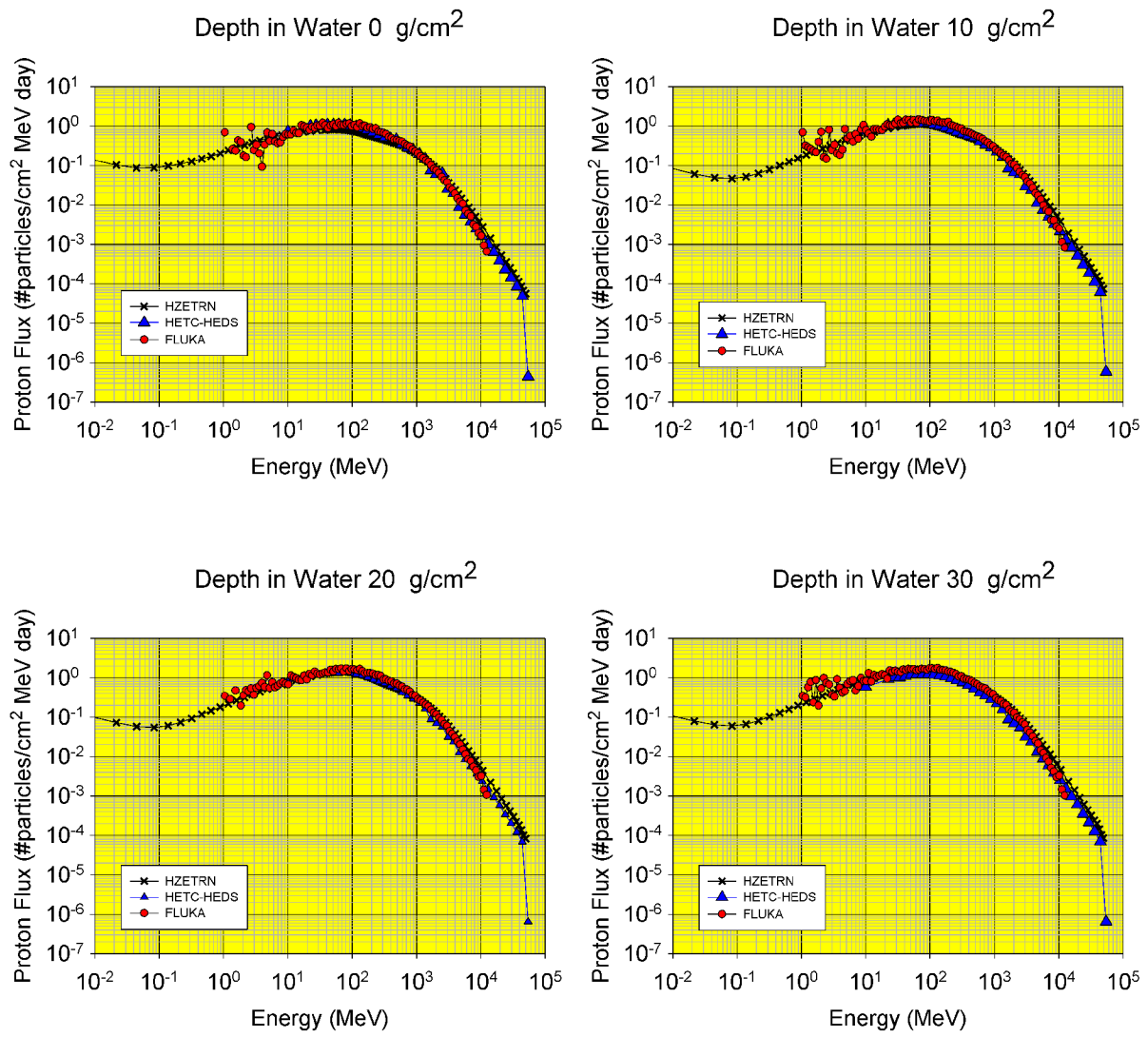


Figure 57: Proton flux for Iron on Aluminum shield.

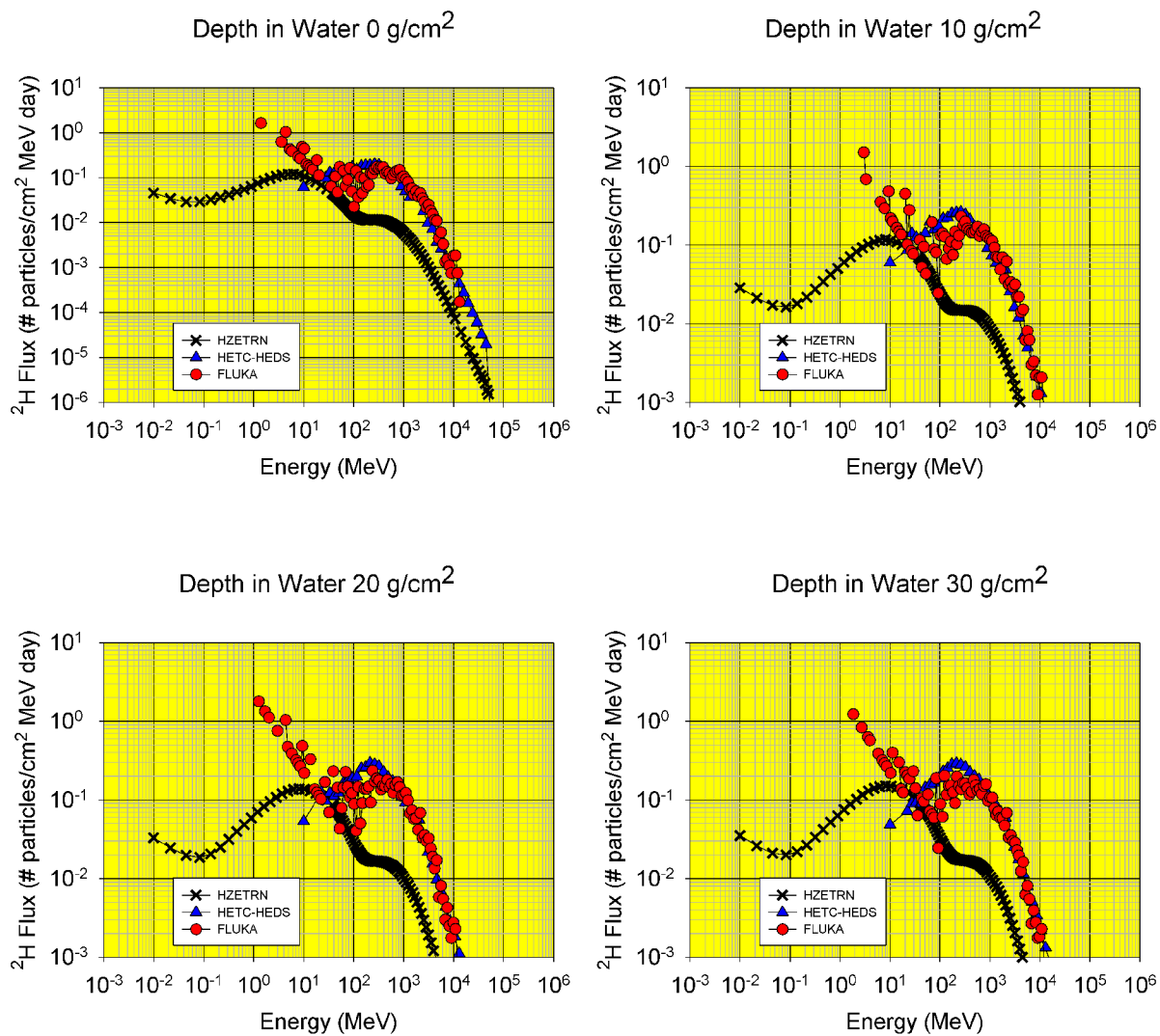


Figure 58:  $^2\text{H}$  flux for Iron on Aluminum shield.

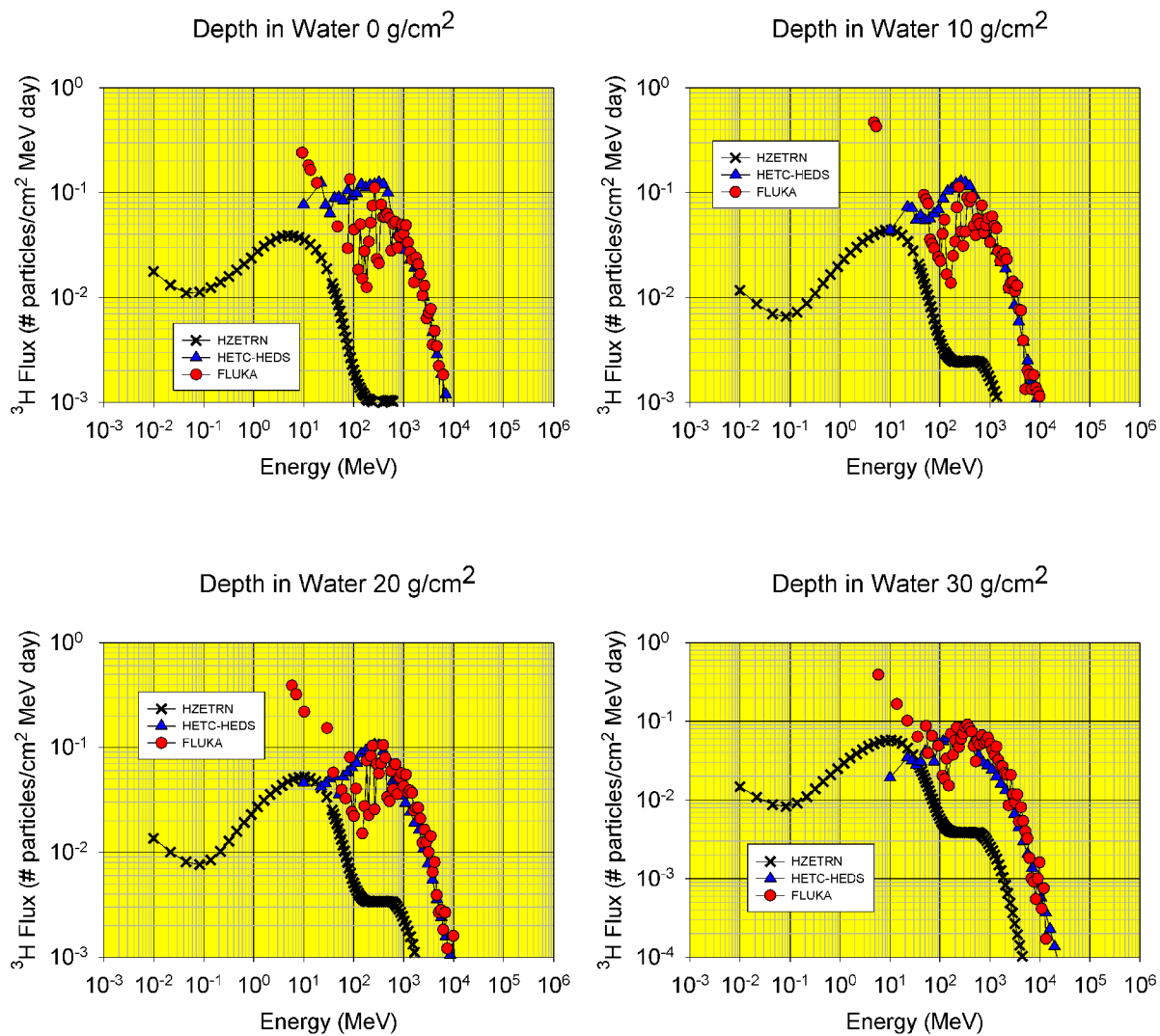


Figure 59:  $^3\text{H}$  flux for Iron on Aluminum shield.

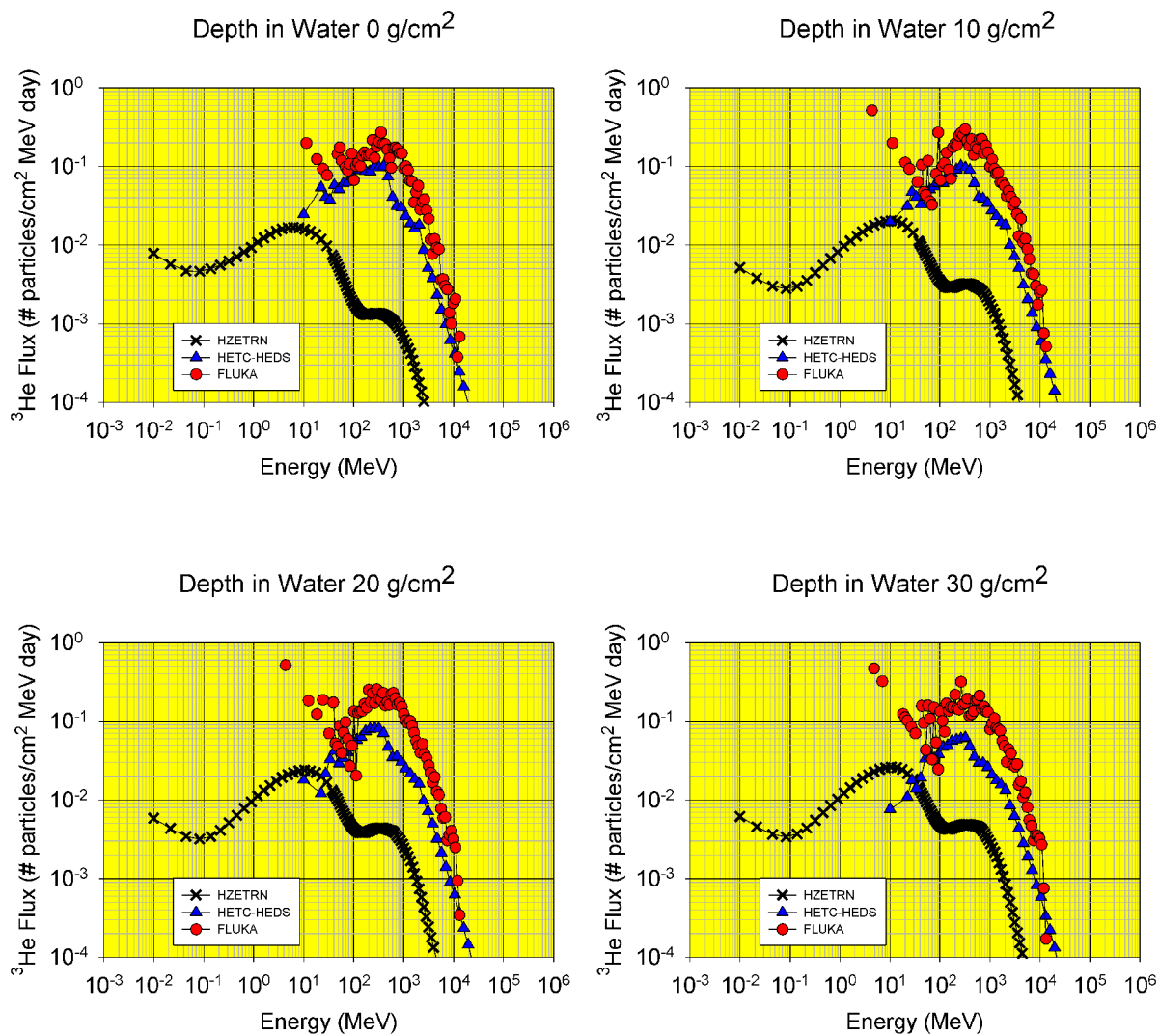


Figure 60:  $^3\text{He}$  flux for Iron on Aluminum shield.

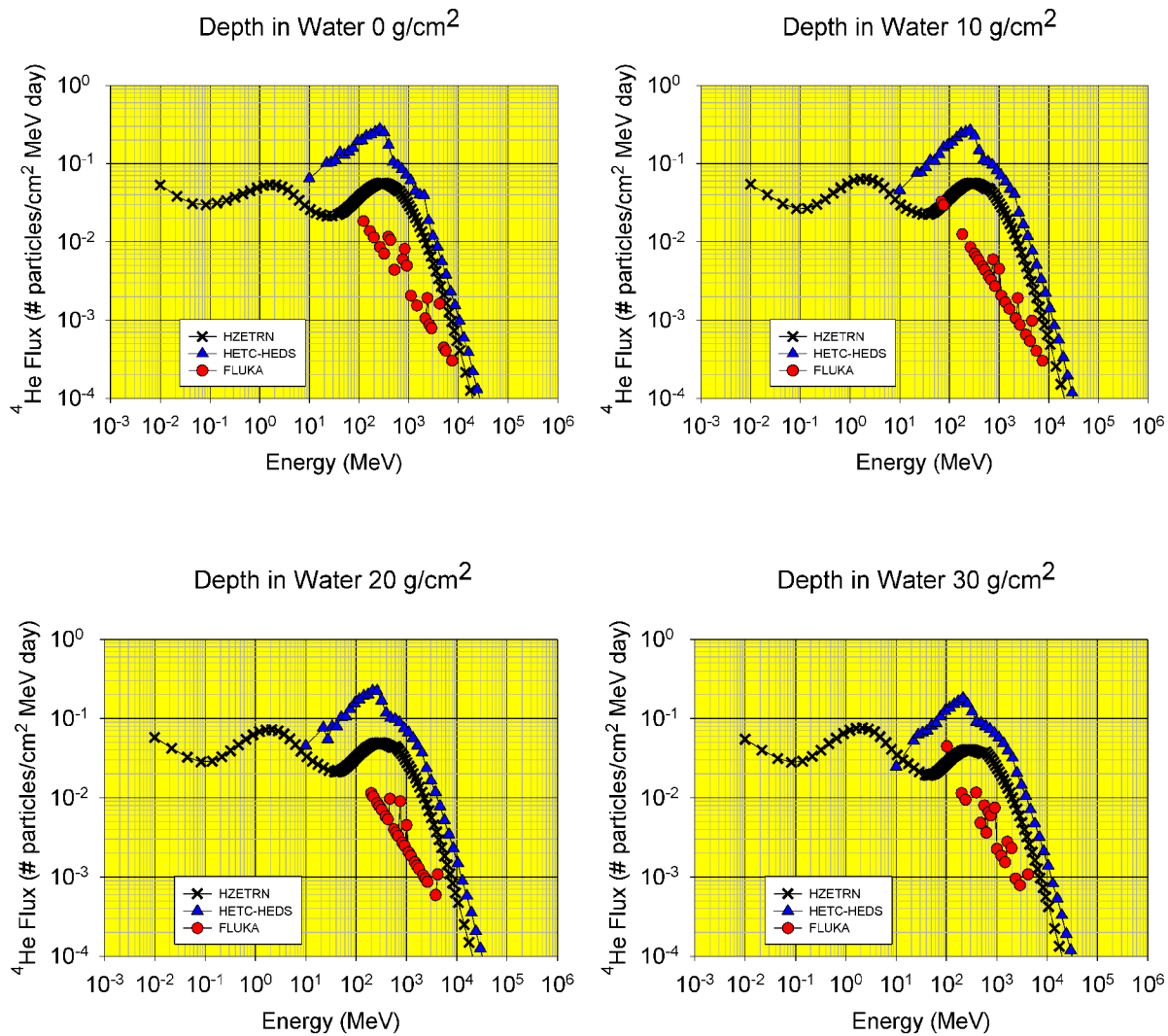


Figure 61:  $^4\text{He}$  flux for Iron on Aluminum shield.

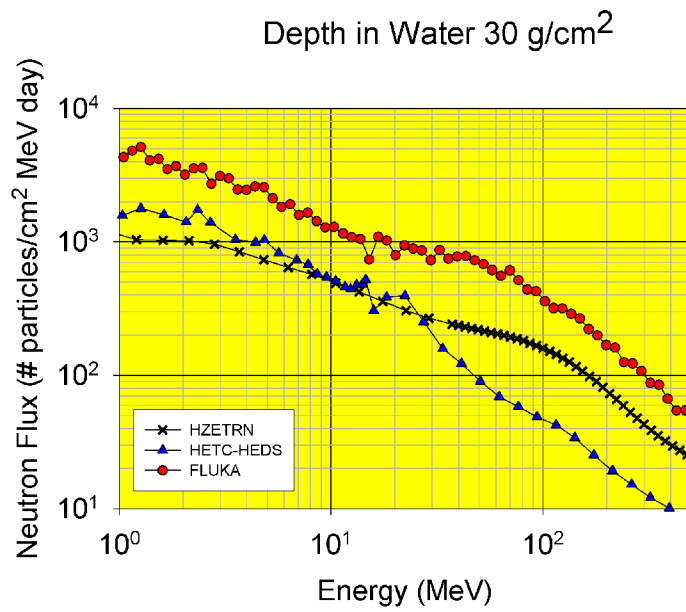


Figure 62: Magnified View of Figure 18 for 30 g/cm<sup>2</sup> depth in water.

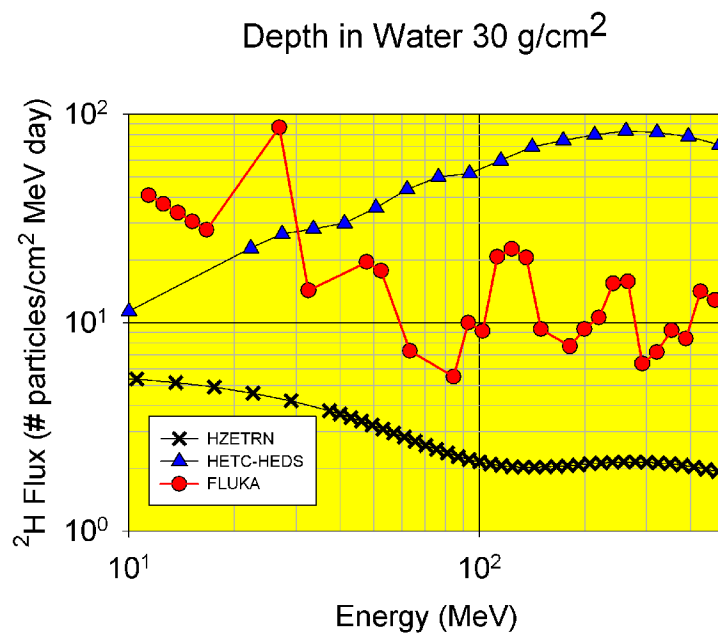


Figure 63: Magnified View of Figure 20 for 30 g/cm<sup>2</sup> depth in water.

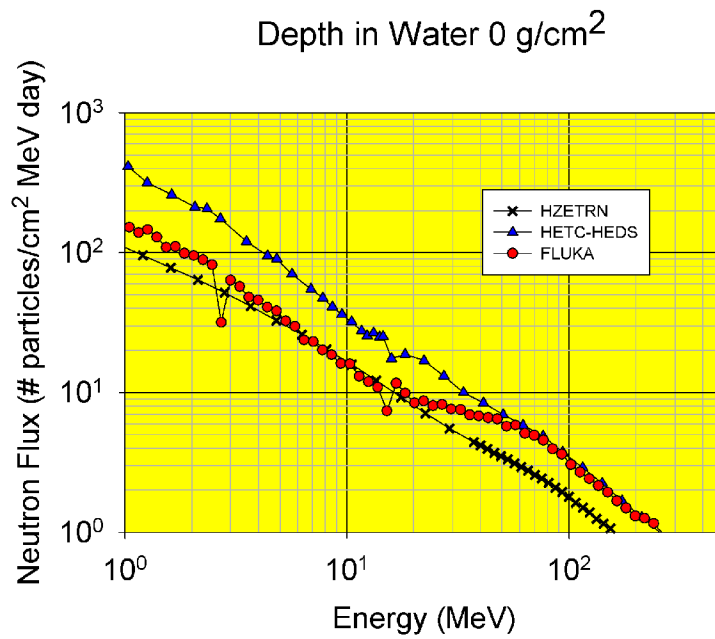


Figure 64: Magnified View of Figure 56 for 0 g/cm<sup>2</sup> depth in water.

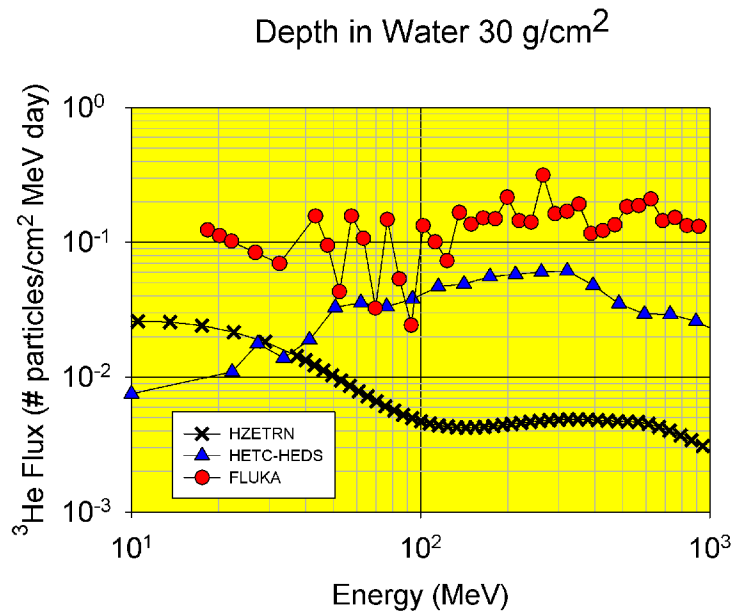


Figure 65: Magnified View of Figure 60 for 30 g/cm<sup>2</sup> depth in water.

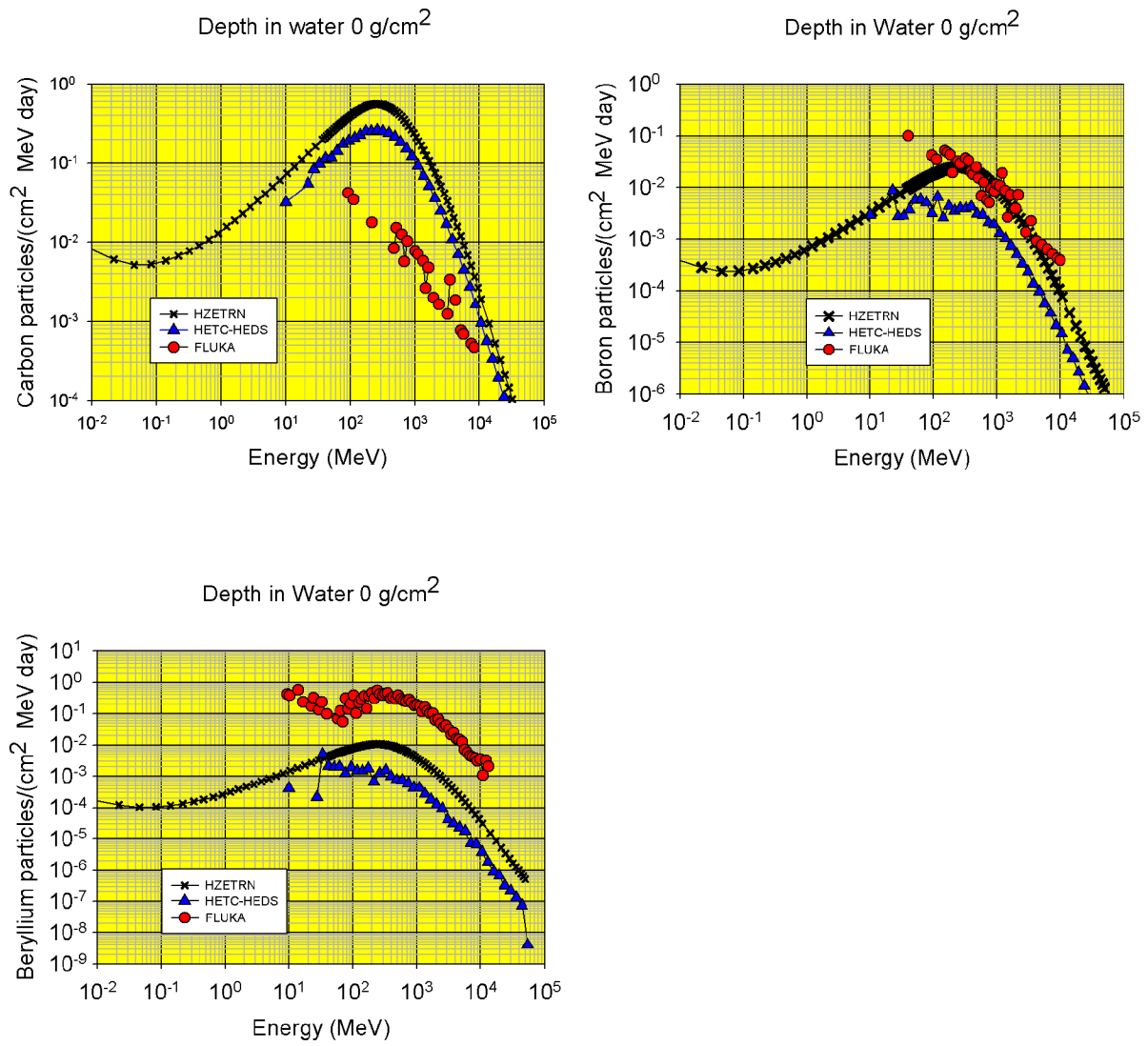


Figure 66: Heavy ion flux associated with Carbon on Aluminum shield.

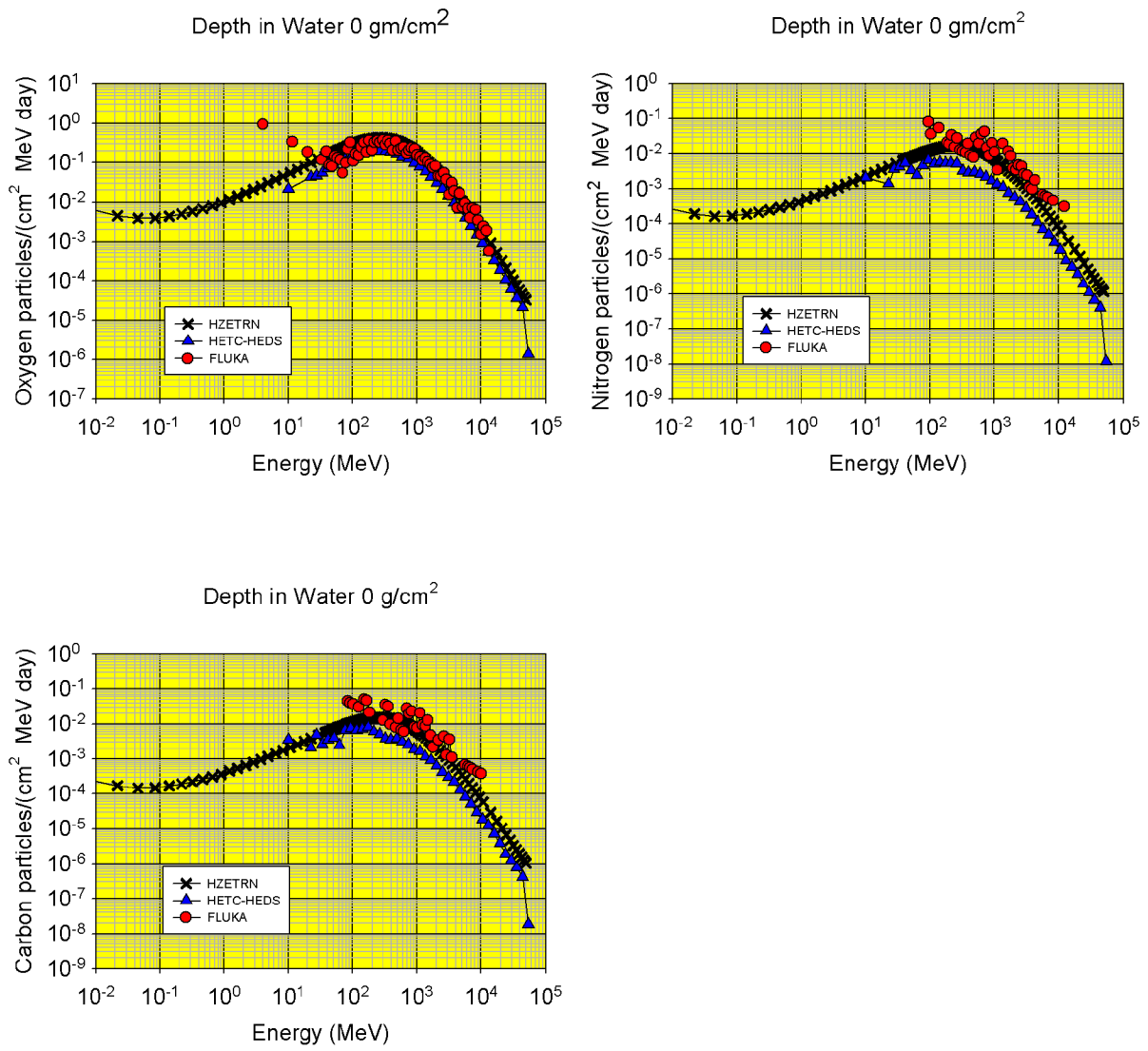


Figure 67: Heavy ion flux associated with Oxygen on Aluminum shield.

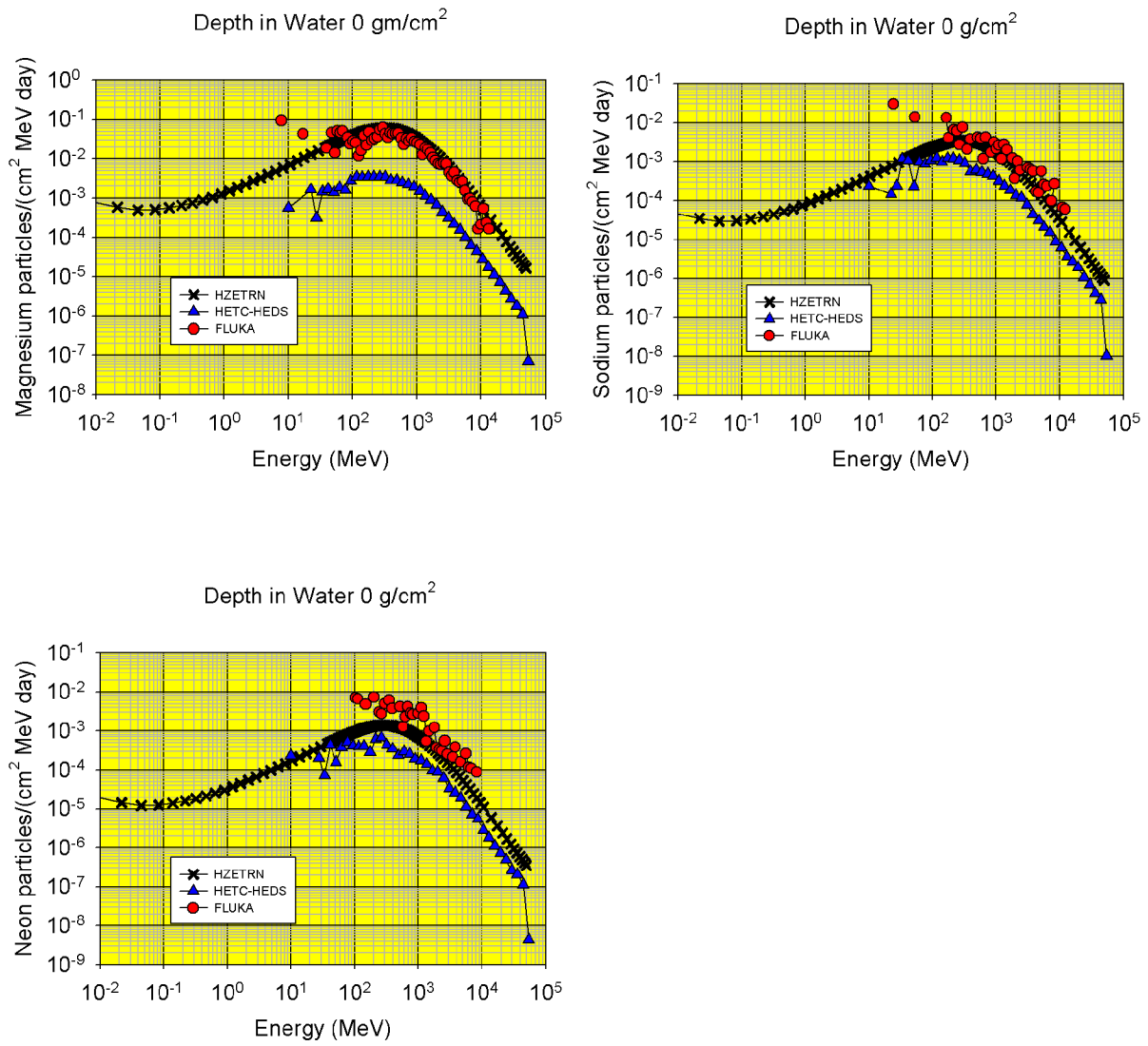


Figure 68: Heavy ion flux associated with Magnesium on Aluminum shield.

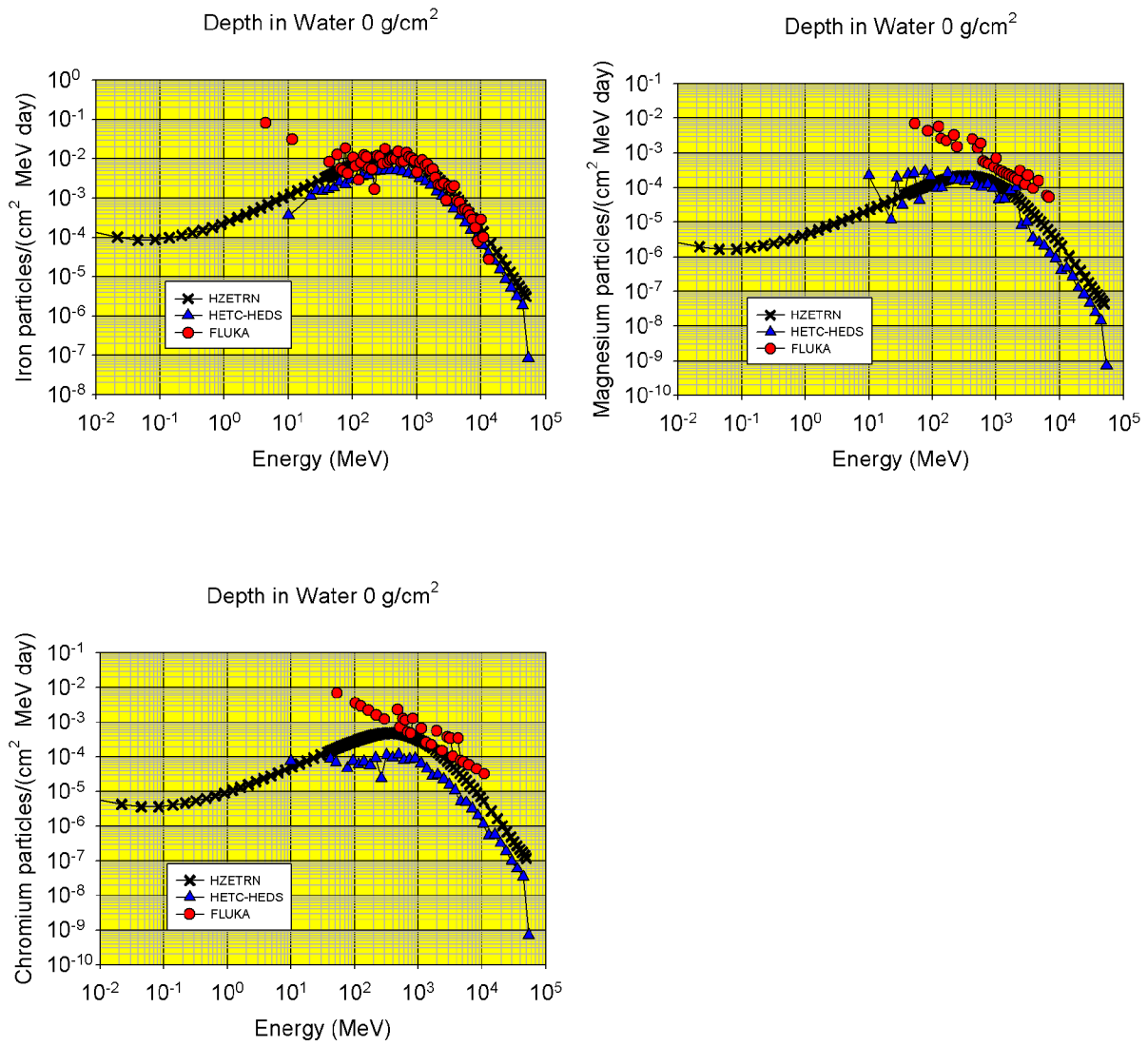


Figure 69: Heavy ion flux associated with Iron on Aluminum shield.

REPORT DOCUMENTATION PAGE				Form Approved OMB No. 0704-0188	
<p>The public reporting burden for this collection of information is estimated to average 1 hour per response, including the time for reviewing instructions, searching existing data sources, gathering and maintaining the data needed, and completing and reviewing the collection of information. Send comments regarding this burden estimate or any other aspect of this collection of information, including suggestions for reducing this burden, to Department of Defense, Washington Headquarters Services, Directorate for Information Operations and Reports (0704-0188), 1215 Jefferson Davis Highway, Suite 1204, Arlington, VA 22202-4302. Respondents should be aware that notwithstanding any other provision of law, no person shall be subject to any penalty for failing to comply with a collection of information if it does not display a currently valid OMB control number.</p> <p><b>PLEASE DO NOT RETURN YOUR FORM TO THE ABOVE ADDRESS.</b></p>					
1. REPORT DATE (DD-MM-YYYY) 01-12-2009		2. REPORT TYPE Technical Publication		3. DATES COVERED (From - To)	
4. TITLE AND SUBTITLE Comparison of Transport Codes, HZETRN, HETC and FLUKA, Using 1977 GCR Solar Minimum Spectra			5a. CONTRACT NUMBER		
			5b. GRANT NUMBER		
			5c. PROGRAM ELEMENT NUMBER		
6. AUTHOR(S) Heinbockel, John H.; Slaba, Tony C.; Tripathi, Ram K.; Blattnig, Steve R.; Norbury, John W.; Badavi, Francis F.; Townsend, Lawrence W.; Handler, Thomas; Gabriel, Tony A.; Pinsky, Lawrence S.; Reddell, Brandon; Aumann, Aric R.			5d. PROJECT NUMBER		
			5e. TASK NUMBER		
			5f. WORK UNIT NUMBER 651549.02.07.01		
7. PERFORMING ORGANIZATION NAME(S) AND ADDRESS(ES) NASA Langley Research Center Hampton, VA 23681-2199			8. PERFORMING ORGANIZATION REPORT NUMBER  L-19753		
9. SPONSORING/MONITORING AGENCY NAME(S) AND ADDRESS(ES) National Aeronautics and Space Administration Washington, DC 20546-0001			10. SPONSOR/MONITOR'S ACRONYM(S)  NASA		
			11. SPONSOR/MONITOR'S REPORT NUMBER(S) NASA/TP-2009-215956		
12. DISTRIBUTION/AVAILABILITY STATEMENT Unclassified - Unlimited Subject Category 93 Availability: NASA CASI (443) 757-5802					
13. SUPPLEMENTARY NOTES					
14. ABSTRACT The HZETRN deterministic radiation transport code is one of several tools developed to analyze the effects of harmful galactic cosmic rays (GCR) and solar particle events (SPE) on mission planning, astronaut shielding and instrumentation. This paper is a comparison study involving the two Monte Carlo transport codes, HETC-HEDS and FLUKA, and the deterministic transport code, HZETRN. Each code is used to transport ions from the 1977 solar minimum GCR spectrum impinging upon a 20 g/cm <sup>2</sup> Aluminum slab followed by a 30 g/cm <sup>2</sup> water slab. This research is part of a systematic effort of verification and validation to quantify the accuracy of HZETRN and determine areas where it can be improved. Comparisons of dose and dose equivalent values at various depths in the water slab are presented in this report. This is followed by a comparison of the proton fluxes, and the forward, backward and total neutron fluxes at various depths in the water slab. Comparisons of the secondary light ion 2H, 3H, 3He and 4He fluxes are also examined.					
15. SUBJECT TERMS Deterministic; Monte Carlo; Radiation transport					
16. SECURITY CLASSIFICATION OF:			17. LIMITATION OF ABSTRACT	18. NUMBER OF PAGES	19a. NAME OF RESPONSIBLE PERSON
a. REPORT	b. ABSTRACT	c. THIS PAGE			STI Help Desk (email: help@sti.nasa.gov)
U	U	U	UU	93	19b. TELEPHONE NUMBER (Include area code) (443) 757-5802